

## Investigation of voltage stability improvement in the distribution network with large amount of induction motors using PSS/E: Load interruption and use of SVCs

*Master of Science Thesis in the Master's Degree Program, Electric Power Engineering*

**Sandra Milena Moreno Castillo**  
**Jagger Hamulili Bwembelo**

Department of Energy & Environment  
Division of Electric Power Engineering  
CHALMERS UNIVERSITY OF TECHNOLOGY  
Gothenburg, Sweden 2014



THESIS FOR MASTER OF SCIENCE

**Investigation of voltage stability improvement in the distribution network with large amount of induction motors using PSS/E: Load interruption and use of SVCs**

**Sandra Milena Moreno Castillo  
Jagger Hamulili Bwembelo**



**CHALMERS**

Department of Energy & Environment  
Division of Electric Power Engineering  
CHALMERS UNIVERSITY OF TECHNOLOGY  
Gothenburg, Sweden 2014

# Investigation of voltage stability improvement in the distribution network with large amount of induction motors using PSS/E: Load interruption and use of SVCs

Sandra Milena Moreno Castillo

Jagger Hamulili Bwembelo

©SANDRA MILENA MORENO CASTILLO, JAGGER HAMULILI BWEMBELO, 2014

Department of Energy & Environment  
Division of Electric Power Engineering  
Chalmers University of Technology  
SE-412 96 Gothenburg, Sweden

Telephone:+46 (0)31-7721000

Fax:+46 (0)31-7721633

Cover: Load interruption of 40% of non-motor loads together with load shedding of 60% of motor loads.

Figure 5.17 (a).

Chalmers Bibliotek, Reproservice  
Gothenburg, Sweden 2014

# Investigation of voltage stability improvement in the distribution network with large amount of induction motors using PSS/E: Load interruption and use of SVCs

Sandra Milena Moreno Castillo  
Jagger Hamulili Bwembelo

Department of Energy & Environment  
Division of Electric Power Engineering  
CHALMERS UNIVERSITY OF TECHNOLOGY

## Abstract

Voltage stability improvement methods following a disturbance and Fault Induced Delayed Voltage Recovery (FIDVR) event are studied with the aim of satisfying a voltage recovery criterion and saving as much load as possible. These methods are temporary load interruption and the use of Static Var Compensators (SVCs). The loads are temporarily tripped and then reconnected. The locations and sizes of SVCs are also determined. The criterion to be met is the recovery of voltages at all buses in the network to 0.9 pu within 1 s following a disturbance. Simulations are done on a typical distribution system with a large number of motor loads using Power System Simulator for Engineering (PSS/E) software with the help of Python programming language for automation and control and the results are analyzed. The results show that load interruption aids and significantly improves the voltage recovery following a disturbance in the network. It is also observed from the results that the use of SVCs also enables the voltage to recover faster with the criterion for voltage recovery at all buses fulfilled. However, the best results are obtained when load interruption is combined with the use of SVCs. The two methods complement each other. When the two methods are combined the amount of load that has to be interrupted is less and the number of SVCs required is also reduced. This results in fewer loads being interrupted. Moreover, the investment cost on SVCs is also reduced.

**Index Terms:** Voltage stability, Fault Induced Delayed Voltage Recovery (FIDVR), load interruption, Static Var Compensator (SVC).



# Acknowledgements

This report would not have been possible without the support of many people. The authors wish to express their gratitude to their supervisor, Dr. Tuan Le who was abundantly helpful and offered invaluable assistance, support and guidance. Special thanks to Prof. Thierry Van Cutsem from University of Liège for his support and provision of network data. Thanks to Pavan Balram for his help and support during the process of this thesis.

Jagger would like to thank his wife Phyllis, his son Joseph and his daughter Lois for their support, encouragement, patience and prayers during the period that he was away undertaking the Master's Degree program. They have been a source of inspiration. He would also like to thank Chalmers and the Chalmers Foundation for awarding him the Avancez scholarship as well as his employers, ZESCO Limited, for granting him study leave which has enabled him to pursue the Master's Degree program.

Esta tesis se la quiero dedicar especialmente a la memoria de mi amado padre Adán Moreno Salamanca, que aunque no este conmigo físicamente, se que él siempre estuvo orgulloso de mí y siempre quiso que esta maestría se hiciera realidad. Gracias Papito te amaré por siempre. Deseo expresar infinitas gracias a mi familia por su apoyo incondicional y ayuda durante estos años de estudios. Muchas gracias a mí amado Eduardo por su amor y comprensión ya que sin él esta maestría no hubiera sido posible. Mil infinitas gracias Mamita Sofía, tu me has enseñado a luchar y perseverar por las cosas importantes de la vida, sin ti y mi papá yo no sería la persona que soy hoy, los amo y me siento afortunada de la familia que construyeron para mí, mis hermanos y mi Eduardo. Muchas gracias a mis queridos hermanos Germán y Edgar por su acompañamiento e incondicional amor, a mi abuelita Tulia que la quiero mucho y a la familia Castillo en especial a mis tíos Carlos, Idelfonso y Edilma a Sandra, Diego, Isabela, María Helena por su amor y acompañamiento.

Muchas gracias a la familia Moreno, gracias primos, tíos, amigos por su apoyo y amor en cada una de los recibimientos y despedidas en Colombia; esos buenos momentos hicieron durante este tiempo, la vida más fácil lejos de mi tierra. Mi querida tía Rosa gracias por

ser tan tierna y linda conmigo de igual manera a mis tías María y Brígida.

Finalmente y no menos importante quisiera agradecer a mi amigo del alma John Carlos Molina por su amistad incondicional y acompañamiento, señora Lucila y Cecilia Aza gracias por el apoyo durante este tiempo.

Sandra Milena Moreno Castillo

Jagger Hamulili Bwembelo

*Gothenburg, Sweden, 2014*



# Contents

<b>Abstract</b>	<b>v</b>
<b>Acknowledgements</b>	<b>v</b>
<b>Contents</b>	<b>v</b>
<b>List of symbols, abbreviations and acronyms</b>	<b>viii</b>
<b>1 Introduction</b>	<b>1</b>
1.1 Project Background . . . . .	1
1.2 Project Objective/Aim . . . . .	2
1.3 Tasks . . . . .	2
1.4 Scope . . . . .	3
1.5 Organization of the thesis . . . . .	3
<b>2 Literature Review</b>	<b>6</b>
2.1 Voltage stability . . . . .	6
2.2 Measures for improving Voltage Stability . . . . .	9
2.3 Undervoltage Load Shedding Using Distributed Controllers . . . . .	13
2.4 Load shedding and Tap Changer Blocking with information from generator Over Excitation Limiters (OELS) . . . . .	14
2.5 Load shedding based on predictive control . . . . .	14
2.6 Load shedding using induction motor kinetic energy . . . . .	15
2.7 A combination of load shedding and the use of SVCs . . . . .	15
2.8 Event based load shedding . . . . .	15
2.9 Static Var Compensator (SVCs) . . . . .	16
<b>3 Induction Motor Model</b>	<b>20</b>
3.1 Induction motor . . . . .	20
3.2 Simulation process of an induction motor as a bus load in PSS/E . . . . .	21
3.3 Equivalent circuit . . . . .	21

3.4	Induction motor models . . . . .	22
3.5	Induction Motor Load Model CIM5BL . . . . .	23
3.6	IMD application tool . . . . .	24
3.7	Motor type 1 . . . . .	25
3.8	The integration time step $\Delta t$ . . . . .	25
<b>4</b>	<b>Load flow and dynamic simulation using PSS/E</b>	<b>26</b>
4.1	Directories and Files Overview . . . . .	27
4.2	Steady-state load flow . . . . .	28
4.3	Dynamic simulation connection of the induction machines (IMD) . . . . .	29
4.4	Python programming language . . . . .	32
<b>5</b>	<b>Improvement of voltage stability by temporary load interruption</b>	<b>34</b>
5.1	Simulations without load interruption . . . . .	36
5.2	Non-motor load shedding . . . . .	37
5.3	Load shedding of various percentages of non-motor and motor loads. . . . .	40
5.3.1	10% load shedding of motors . . . . .	41
5.3.2	20% load shedding of motors . . . . .	43
5.3.3	40% load shedding of motors . . . . .	44
5.3.4	80% load shedding of motors . . . . .	45
5.4	Load interruption of 40%, 60% and 80% of non-motor loads . . . . .	45
5.5	Load interruption of 40%, 60% and 80% of non-motor loads together with load shedding of 60% of motor loads. . . . .	49
<b>6</b>	<b>Improvement of voltage stability by using SVCs</b>	<b>51</b>
6.1	Simulation results . . . . .	56
6.1.1	SVC placed at Node 11C . . . . .	56
6.1.2	SVC connected to Node 11B and 11C . . . . .	60
6.1.3	SVC connected to Node N11AC5 . . . . .	62
6.1.4	SVCs connected to Node 13C, 13B, 11C, 11B, 10C, 10B, 8C, 8B, 7C, 7B, 5C and 5B . . . . .	65
6.1.5	SVC placed at Node N11A . . . . .	67
6.1.6	SVCs placed at Node 11A and 13A . . . . .	69
6.1.7	SVCs placed at Node 4A, 11A and 13A . . . . .	71
6.1.8	SVCs placed at Node 4A, 5A, 11A and 13A . . . . .	73
<b>7</b>	<b>Improvement of voltage stability by combining load interruption with using SVCs</b>	<b>76</b>
7.1	Simulations Results . . . . .	76
<b>8</b>	<b>Improvement of voltage stability by load shedding using the PSS/E Undervoltage Load Shedding Model Relay</b>	<b>80</b>
8.1	Simulation results . . . . .	80

<b>9</b>	<b>Conclusions and Future Work</b>	<b>84</b>
9.1	Conclusions . . . . .	84
9.2	Future Work . . . . .	85
	<b>References</b>	<b>90</b>
<b>A</b>	<b>Distribution Network</b>	<b>91</b>
<b>B</b>	<b>Python Scripts</b>	<b>92</b>

# List of symbols, abbreviations and acronyms

**BUS\_NAME** : Name of the bus to which element is connected.

**MVA** : Mega-Volt-Ampere.

**SBASE** : System MVA base.

**ID** : Element identifier.

**ZONE** : Zone to which the element is assigned.

**AREA** : Area to which the element is assigned.

**OWNER** : Owner to which the element is assigned.

**$\Delta t$** : Integration time step.

## EXCITER

**$T_E$**  : Time constant, in seconds (s).

**$E_{MIN}$**  : Minimum field voltage, in pu [1].

**$E_{MAX}$**  : Maximum field voltage, in pu.

**$K$**  : The gain.

## DOUBLE-CAGE INDUCTION MOTORS

**MBASE** : Machine base power.

**$R_A$** : Armature resistance, in pu on motor base.

**$X_A$** : Armature leakage inductance, in pu on motor base.

**$X_M$** : Magnetizing inductance, in pu on motor base.

**$R_1$** : Resistance of first rotor winding, in pu on motor base.

**$X_1$** : Reactance of the first rotor winding, in pu on motor base.

**$R_2$** : Resistance of second rotor winding, in pu on motor base.

**$X_2$** : Reactance of the second rotor winding, in pu on motor base.

***H*** : Inertia constant, pu motor base.  
***T<sub>nom</sub>***: Load torque at 1 pu speed.  
***D*** : Load damping factor.

## ACRONYMS

**FIDVR**: Fault Induced Delayed Voltage Recovery.  
**SVC** : Static Var Compensator .  
**PSS/E**: Power System Simulator For Engineering.  
**UVLS**: Under Voltage Load Shedding.  
**FACTS**: Flexible AC Transmission Systems.  
**STATCOM**: Static Synchronous Compensator.  
**SVG**: Static VAR Generator  
**SIPS**: System Integrity Protection Scheme.  
**SPS**: Special Protection System (also referred to as System Protection Scheme)  
**OEL**: Over Excitation Limiter.  
**LTC**: Load tap changer.  
**SPS**: Special Protection System.  
**VSA**: Voltage security assessment.  
**AVR**: Automatic Voltage Regulators.  
**PSS**: Power System Stabilizer.  
**EHV**: Extra High Voltage.  
**GENCO**: Generating Company.  
**TSO**: Transmission System Operator.  
**MEL**: Most Effective Load.

# 1

## Introduction

### 1.1 Project Background

**N**OWADAYS, power systems are operated closer to their stability limits due to deregulation and challenges in constructing new transmission lines and power stations [2]. At the same time, there has been an increase in the usage of motors in air conditioners, refrigerators and heat pumps as well as voltage-insensitive loads that have electronic supplies. This makes power systems to be prone to voltage instability problems [3].

Fault-induced delayed voltage recovery (FIDVR) is a trend that has been observed in power systems with a high penetration of induction motor loads following a fault. FIDVR is defined as “*the phenomenon whereby system voltage remains at significantly reduced levels for several seconds after a fault in transmission, sub-transmission, or distribution system has been cleared*” [4]. This problem is mainly caused by motor load re-acceleration after a fault in the nearby transmission system which causes a severe voltage drop. This leads to motor loads drawing high current from the grid which causes even more voltage drop. In the worst case, motors may stall which results in the voltage instability problem [5]. Generators and Load Tap Changers (LTCs) on transformers can sometimes reach their limits of allowed control range following a severe voltage drop. LTC movement can also be too slow[6].

Some of the notable early FIDVR events in North America are the Tennessee Valley Authority (TVA) Service Area cascading voltage collapse in August 1987, Florida Power and Light Company (FPL)’s Miami area in August 1988 and Southern California Edison’s (SCE) network (in 1988 and in SCE’s desert regions in June 1990). During these events motors (pumps and /or air conditioners) either tripped on thermal and overload protection or stalled drawing a lot of current[4]. Some major incidents related to voltage instability are the French system disturbance (December 19, 1978 and January 12, 1987),

Northern Belgium system disturbance (on August 4, 1982), Florida system disturbance (December 28, 1982) and WSCC USA (July 2, 1996) [7]. Other major incidences are NE of USA/Canada blackout (August 14, 2003), blackout in southern Sweden and Eastern Denmark (September 23, 2003) and the Polish system disturbance (June 26, 2006) [3].

Temporary load interruption with load shedding as backup has been proposed in [5] for averting FIDVR or voltage instability. It can aid the recovery of the voltage after a disturbance which helps the motors to re-accelerate and the stalling of some of the motors can also be avoided. The load is switched off and then reconnected after a short time interval or if the voltage recovers above the value that has been set [5]. Load shedding is the last resort to prevent voltage instability when all else fails [7, 8]. It is a cost effective way to mitigate voltage instability[9]. However, the load is not reconnected after being shed therefore it is not saved as is the case with load interruption. Thus, other means of aiding the voltage recovery can also be combined with load interruption so that as much load as possible is saved and load shedding is minimized. One of the methods that can be investigated is the combination of load interruption and the use of FACTS devices such as Static Var Compensators (SVC). SVCs have also been used to aid voltage recovery following disturbances to prevent voltage instability such as in [10].

## 1.2 Project Objective/Aim

The aim of this thesis is to study voltage stability improvement in a distribution network with a large amount of induction motors by a combination of temporary load interruption and using SVCs so as to counteract the problem of FIDVR and save as much load as possible. During this thesis a generic algorithm/approach will be developed in order to determine the amount of load to be interrupted and the time-interval to mitigate the voltage instability problem. In order to establish these, the time-dependent relationship between voltage and power interruption (both active and reactive power) will be derived and utilized in the algorithm. The use of SVCs to aid the voltage recovery and reduce the amount of interrupted load will also be investigated. The size and locations of the SVCs will also be determined. A case study will be done on a test network. Dynamic simulations of the system will be performed in the Power System Simulator for Engineering (PSS/E) software and the performance of the methods/approach will be tested.

## 1.3 Tasks

The main tasks during this thesis revolve around the development of a generic algorithm/approach in order to determine the minimum amount of load to be interrupted and the interruption time as well as investigating the use of SVCs in order to prevent the voltage instability problem. The two methods of preventing voltage instability will then be combined and the results analyzed.

The following are the activities that have been carried out during the period of the thesis,

1. Literature review on voltage stability
2. Literature review on existing system protection schemes for the improvement of voltage stability.
3. Survey of existing algorithms for protection against voltage instability such as under-voltage load shedding, etc.
4. Literature review on SVCs
5. Learning to use PSS/E simulation tool for dynamic simulation.
6. Performing load flow and dynamic simulations of a test-model of a distribution system with a high share of motor loads in PSS/E.
7. Development of an analytical formula or approach for temporally load interruption to determine the minimum amount of load to be interrupted and the interruption time.
8. Implementation of the test-model network and the approach/method developed in Task-7 in PSS/E. Carrying out simulation runs for various scenarios of load interruption.
9. Implementation of the test-model network with SVCs in PSS/E. Determination of sizes and location of SVCs.
10. Implementation of the test-model network with SVCs and the approach/method developed in Task-7 for temporally load interruption for the mitigation of the voltage instability problem.
11. Final thesis report and presentation at Chalmers.

## 1.4 Scope

The thesis covers the development of an analytical formula or approach to determine the minimum amount of load to be interrupted and the interruption time as well as its implementation in PSS/E for the prevention of voltage instability. It also covers the use of SVCs to counteract the voltage instability problem. The location and sizes of the SVCs are also determined. The two methods are combined and studied. Load flow and dynamic simulations of the system are done during this work.

## 1.5 Organization of the thesis

In this thesis different methods of improving voltage stability will be used in order to achieve a fast voltage recovery after a disturbance is introduced in the test network. The criteria used in this thesis is that voltage should recover to 0.9 pu within 1 s. In

order to achieve this target different methods and scenarios will be simulated such as load shedding, load interruption, SVCs and different combinations of these methods will be considered. The organization of the thesis has been made in such a way that the reader finds an introduction, literature review of different methods for improving voltage stability, results of the simulations of different methods and scenarios, conclusion and future work. The layout of the thesis is as follows:

1. Chapter 1: Gives an introduction of the project background.
2. Chapter 2: Provides literature review on voltage stability and different methods that are used to improve voltage stability.
3. Chapter 3: In this chapter it is well explained how the induction machines have been simulated in PSS/E.
4. Chapter 4: Gives an overview on the simulation setup and implementation in PSS/E. A brief description of how to perform load flow and dynamic simulations in PSS/E is also given.
5. Chapter 5: In this chapter the results for improving voltage stability by load interruption are presented.
6. Chapter 6: In this chapter the results for improving voltage stability by using SVCs are presented.
7. Chapter 7: In this chapter the results for improving voltage stability by a combination of load interruption and the use of SVCs are presented
8. Chapter 8: In this chapter the results for improving voltage stability by using an under-voltage relay are presented.
9. Chapter 9: The conclusions of the work are stated as well as the future work.

The methodology of how the voltage stability improvement investigations were carried out is illustrated in Fig. 1.1

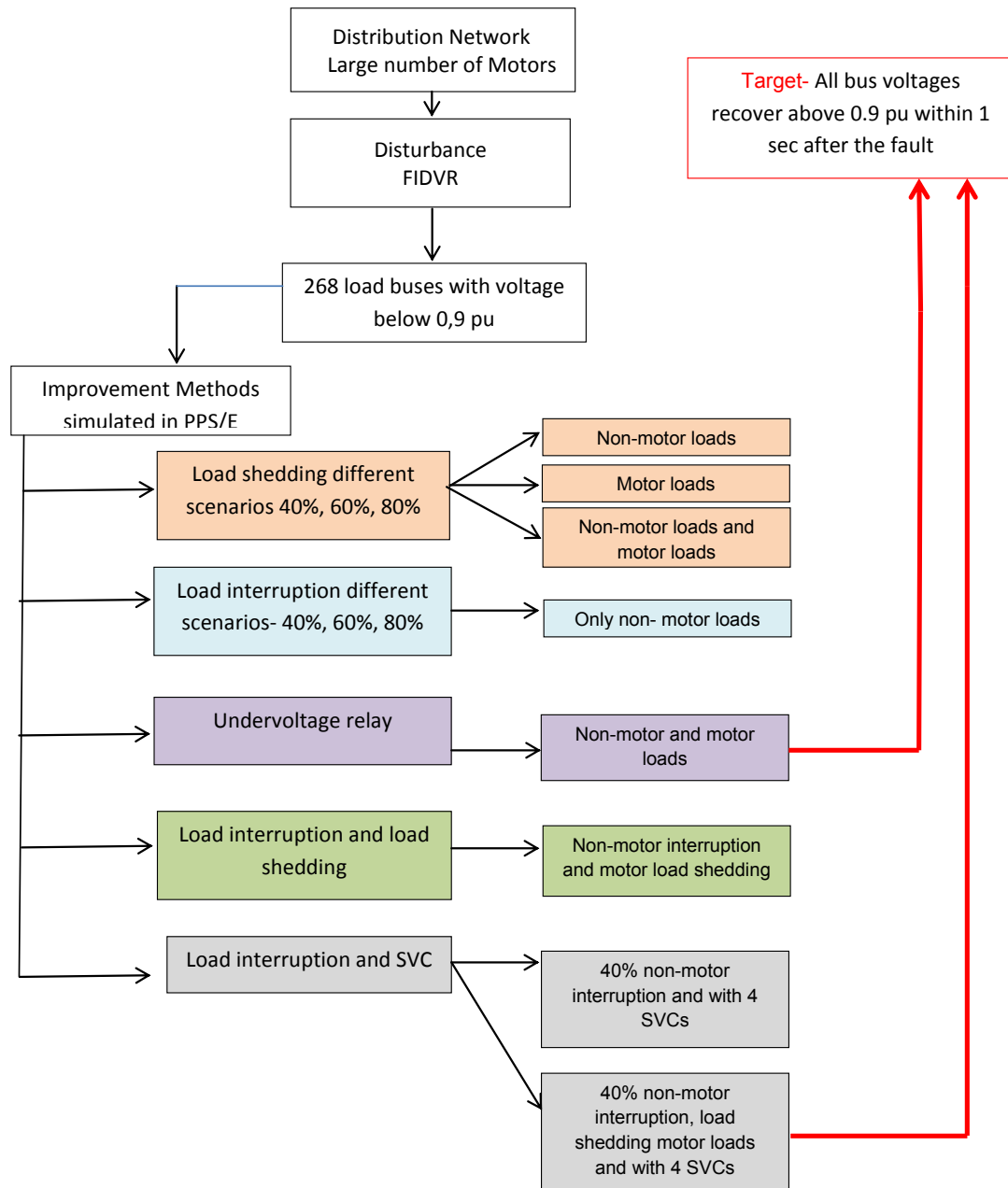


**Figure 1.1:** Methodology of the voltage stability improvement investigations.

# 2

## Literature Review

**T**HIS chapter gives an overview from the literature of voltage stability, the main factors that lead to voltage instability and the measures to improve voltage stability. Literature review on the FIDVR phenomenon is also presented in this chapter. A number of technical papers have been written with various proposals on how to mitigate the FIDVR phenomenon. Research in this field is ongoing. Some of the proposals and schemes currently in use are categorized and highlighted below. The theory behind Static Var Compensators (SVCs) is also presented in this chapter since simulations have been done to study their effect in aiding the voltage recovery following a disturbance.

### 2.1 Voltage stability

Voltage stability is whereby the system is capable of sustaining stable voltages at all buses in a network following a disturbance [11]. Voltage instability is when voltages in a network considerably drop continuously to the point where the system becomes unstable and supply of power to the load is disturbed. This may lead to voltage collapse. The tendency of load dynamics to reinstate the amount of power consumed post-disturbance to a level that cannot be supplied by the generators and transmission system is what brings about the instability. Voltage stability has received a lot of attention in recent years because events such as blackouts attributed to voltage instability have happened around the world and more are likely to occur. Power systems are operating closer to their limits which make them more predisposed to voltage instability [12]. A significant part of this section comes from [12] where voltage instability has been extensively discussed with references from various sources.

A number of issues have led to power systems being more prone to voltage instability. One of the reasons is that it is getting harder to get permission to construct new

power stations and transmission lines. The result is that power stations are being built further away from the load in remote areas thereby increasing the electrical distance. Shunt compensation can increase the amount of power that is transmitted. However, this comes at the expense of bringing the normal operating point nearer to the stability limit. Unplanned outages of generators and transmission lines can also lead to voltage instability. Another contributing issue is that there is economic impetus to operate power systems near their limits due to deregulation of power markets. Establishing the voltage stability limits of a system also becomes necessary as a result of this need [12].

A simple system is shown in Fig. 2.1,

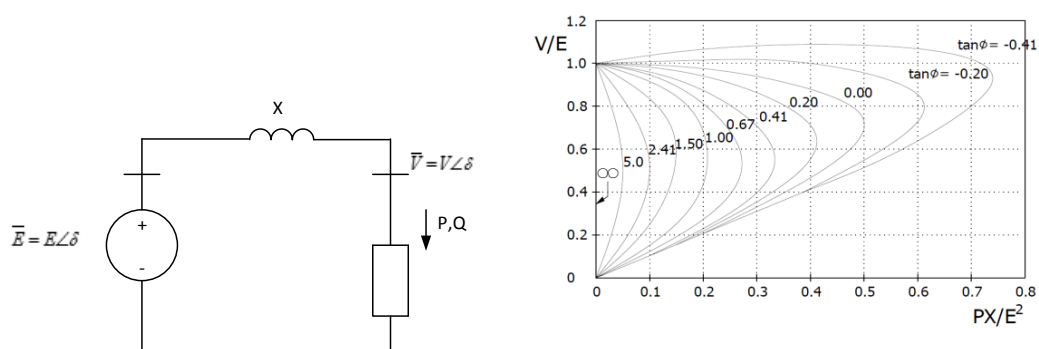


**Figure 2.1:** Simple Two-bus system [8, 12].

For the simple system shown in Fig. 2.1, the power flow equations are expressed as [7, 12],

$$P = -\frac{EV}{X} \sin \delta, \quad (2.1)$$

$$Q = -\frac{V^2}{X} + \frac{EV}{X} \cos \delta. \quad (2.2)$$

In the above equations,  $P$  and  $Q$  are the active and reactive power that the load consumes, respectively. The voltage magnitude at the load bus is denoted as  $V$ , the phase angle between the generator and the specific load bus is  $\delta$ . Finally,  $E$  is the generator voltage magnitude, which is assumed constant.

The PV curves for the system for different power factors are also shown in Fig. 2.1. From the PV curves, it can be seen that there is maximum power at the “nose” of the curves beyond which the system becomes unstable. The instability can be due to a rise in the impedance,  $X$ , or a decrement in the generator voltage  $E$  such that it becomes impossible to supply the load that was there prior the occurrence of a disturbance. It can also be because the load is increased to a point beyond the maximum transferable power of the system in normal operation [12].

Long-term voltage stability comprises of the dynamics of equipment which take long to act such as tap-changing transformers, loads controlled by thermostats and generator current limiters [3]. Some of the causes of long-term voltage instability are the operation of Load Tap Changers (LTCs) of transformers and the action of over-excitation Limiters (OELs) of generators. Long-term voltage instability happens over some minutes [12] usually up to 10 minutes [3]. After a severe disturbance there could be a dramatic drop of voltages at load buses. The LTCs for the transformers supplying these loads would then try to increase the voltages at these buses to be within the dead-band that has been set. This results in the restoration of the load power. LTCs therefore eventually make the load to act like constant power load in the long run. However, this in turn depresses the voltages upstream in the transmission network. The voltages on the low voltage side of the transformers in the distribution network would initially increase but eventually the effect of the LTCs would be minimal or even opposite in that the voltage would actually start to reduce with each LTC operation. This can happen if some of the generators in the area reach the limit of their field current with the result that OELs are activated. The generators whose OELs are activated are not able to provide further reactive power support and so the voltages at their buses drop and the maximum load power also reduces. The system after the disturbance might not be able to satisfy this load restored by the LTCs due to a reduction in the maximum power which could lead to instability [12].

Thermostatically controlled loads can also lead to long-term voltage instability. These types of loads are self-restoring. In this type of electrical heating, the power reduces as the square of the voltage if there is a reduction in voltage. The temperature is regulated by the thermostat which turns the heating resistor on and off to maintain it. However, if there is a significant voltage drop in the network after an event such as a disturbance then the heating resistor is kept on for a longer time to provide the same amount of energy or it is not turned off. If the number of heaters in the network is large then this action becomes similar to self-restoring loads though it can be like impedance load if the drop in voltage is significant. Thermostatically controlled loads can have a considerable effect on a network especially in winter if they constitute a substantial share of the load. The effect can also be pronounced if LTCs do not manage to raise the voltage closer to the dead-band [12].

Short-term voltage stability comprises of the dynamics of elements of the load which act quickly such as induction motors, electronically controlled loads and HVDC converters [3, 13], . Short term instability occurs over some seconds [12] usually up to 10 s [3]. The presence of induction motors can lead to short-term instability. Induction motors are self-restoring loads. The active power of induction motors reduces as the square of the voltage in a similar manner as constant impedance load. This can happen following a disturbance. The load can then return to almost the same level as it was before within 1 s. It can even return to constant power in some cases. The reactive power reduces sort of quadratically to a low point then recovers until motors stall because of depressed voltage. This may happen at a voltage of 0.7 pu for large motors and a higher voltage

for small motors. The effect of induction motors restoring load can be high in summer at peak load in networks with a high penetration of air conditioners [12].

Long-term voltage stability is therefore characterized by the action of LTCs, OELs, switched shunt compensation and the restoration of the composite load as well as secondary control of voltage and frequency [12]. On the other hand, the aspects of short-term voltage stability are generators, SVCs, Automatic Voltage Regulators (AVRs), Power System Stabilizers (PSSs), turbines and governors, induction motors, HVDC links and FACTS devices such as SVCs [12] and STATCOM [14].

## 2.2 Measures for improving Voltage Stability

Certain measures can be undertaken to improve voltage stability. One of the measures is system reinforcement. This can be done in a number of ways. New transmission lines can be built from the power stations to the load centers. New power stations can also be built closer to the load. However, owing to the difficulty of building new lines and power stations close to populous areas where the load is concentrated due to issues to do with protecting the environment as well as political reasons other measures to reinforce the system can also be implemented. Series compensation enables the reduction of the impedance of transmission lines thereby restraining the voltage drop for lengthy lines. In spite of these gains, factors such as cost and increase in complexity of protection have to be checked and taken into account. Shunt compensation is a long-established means of preserving the voltage profile within an acceptable range by the provision of reactive power support [12].

It is well known that reactive shunt compensation enables a larger amount of power to be transmitted in steady-state and the regulation of the voltage profile over a line to a desired level. It is also used to improve the transient stability of a network by increasing the transmittable power of the post-fault system as well as power oscillation damping. The loading of the network on a typical day varies so the objective is to adjust the characteristics of the line to meet the load at a given point of time. The type of compensation used depends on the current status of the system in terms of loading. Fixed or mechanically switched shunt reactors are used to reduce over-voltages that may occur when the system is lightly loaded. Shunt capacitors are used to raise the voltage to a predetermined level when the system is heavily loaded thereby preventing low voltages in the system [15].

Shunt var compensation is used in the middle of a transmission line connecting two AC systems that has more than one source of supply for line segmentation. This concept is illustrated in a two-machine transmission model. The voltage profile along the line is not uniform and the lowest voltage is at the middle point of the line. Therefore, connection of shunt var compensator at this point gives the best result because the line is divided into two equal parts with the same amount of power transfer capability. The longer portion of the line determines the maximum transmittable power if the compensator is

not connected in the middle [15]. Transmittable active power is given by [15],

$$P = \frac{2V^2}{X} \sin(\delta/2). \quad (2.3)$$

Likewise, the reactive power is

$$Q = \frac{4V^2}{X} (1 - \cos(\delta/2)) \quad (2.4)$$

Transmittable power is increased twofold with mid-point shunt compensation. The voltage profile also improves and becomes more uniform along the line. However, this entails the injection of more reactive power, which can increase up to fourfold, by the var compensator and the generators at the ends of the line. Line segmentation for voltage support using SVCs has been used in practice [15].

Shunt var compensation is also used at the end of a radial system. The terminal voltage at the end of the line varies with the load and load power factor as illustrated in Fig. 2.2(a) for the graph of normalized receiving voltage  $V_r$  versus normalized load power  $P$ . This is the case without shunt compensation. The system is also shown in the figure with line reactance  $X$  and load impedance  $Z$ . The nose-point of the plot for each of the curves for the various power factors is the load at which voltage instability commences. As can be seen in the figure, the voltage drop is higher as the load increases. Furthermore, the nose-point increases with capacitive loads and reduces with inductive loads [15].

Fig. 2.2(b) shows the radial system with shunt var compensation at the receiving end of the line where the load is connected. The voltage is maintained at 1 p.u as can be seen in the figure. The curves also show that shunt compensation can improve voltage stability by providing reactive power support. The voltage deviation is highest at the end of the line in a radial system. This is therefore the ideal place to connect the compensator [15].

Shunt compensation at the receiving end of a radial line is used for voltage support in case of the loss of a generator or one of the circuits supplying the load. This can also happen if, for instance, two lines from two different power stations are supplying an area load and one of the lines trips. There would be a deficit of power if the system was stretched prior to the disturbance. This could lead to voltage collapse [15].

Some devices and controllers are also used to improve voltage stability. SVCs can be used to prevent short-term voltage instability because they provide rapid reactive power support. Mechanically switched shunt compensation can be used to prevent long-term voltage instability. The reactors that are used to lower the voltage for long unloaded Extra High Voltage (EHV) transmission lines can also be switched off so as to raise the voltage. AVR set points for generators can be raised as well as using LTCs for generator step-up transformers to raise the voltage. The dynamic reactive power reserve of generators, synchronous condensers and SVCs in a network can be increased by turning on shunt compensation. This leaves enough reactive power reserve available by equipment

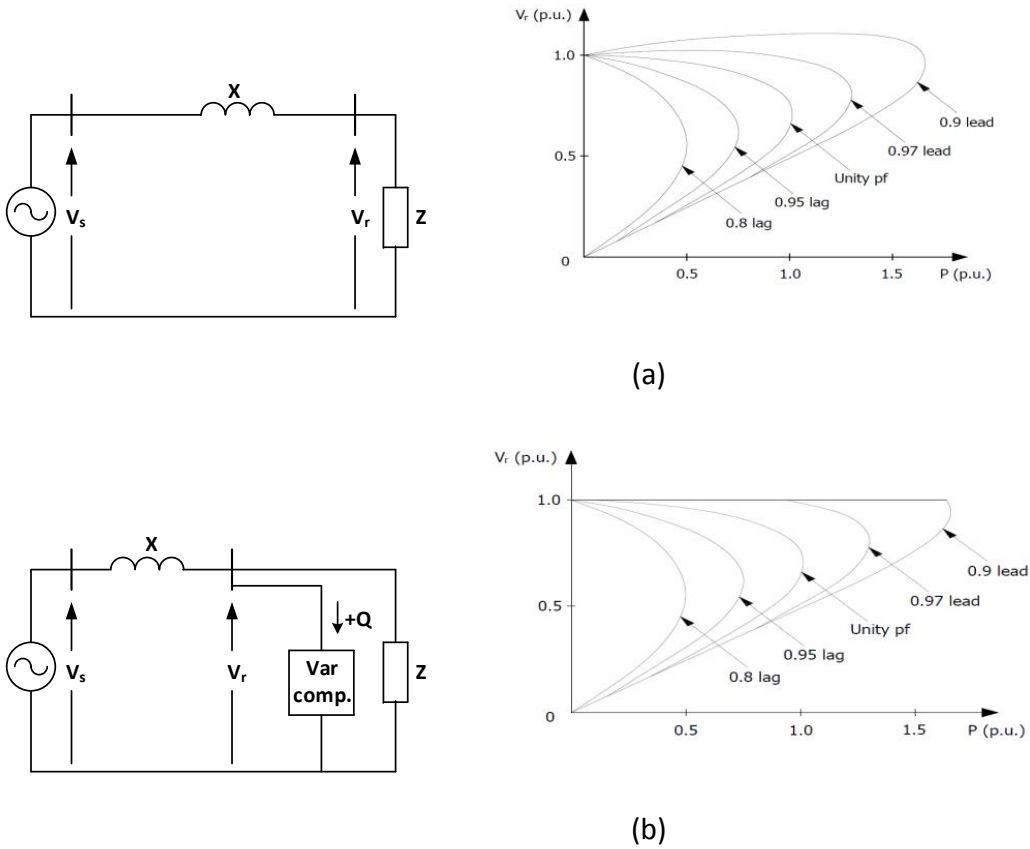


**Figure 2.2:** Changes in voltage stability limit of a radial system with load and power factor (a), and improvement in voltage stability with shunt compensation (b) [15].

which can act quickly to use if needed to prevent voltage instability [12].

Operational planning can also be used to prevent voltage instability. The system can be checked to see if it is secure in terms of voltage stability. Transmission System Operators (TSOs) and Generating Companies (GENCOs) assess the security margins so as to prevent congestion. Contracts may have to be altered to suit the prevailing situation in the network. Real time monitoring of the network can also be done apart from planning. Power stations that are closer to the load can be switched on even if using these plants might be more expensive than cheaper ones located far away. Machines that act more rapidly such as gas turbines and hydro power stations can also be started up. If the margins are still not enough load shedding can be used as a last resort [12].

System Protection Schemes (SPSs) can also be used to avoid voltage instability. These are also called Special Protection Schemes. Companies are more inclined to operate sys-

tems closer to their limits with the aim of maximizing profits because of deregulation. With this status quo the most likely scenario is to use security margins to take care of contingencies while SPSs can be used for more serious disturbances which do not often happen. SPSs operate automatically to avert instability. SPSs can combine a number of measures such as LTC blocking, decrease of LTC set points to decrease the voltage, returning the tap positions of transformers to prearranged points or load shedding. Distribution voltages can be lowered so as to reduce the load but sub-transmission voltages can be raised so as to lower the losses and also take advantage of shunt compensation. Load shedding of small induction motors to improve short-term voltage stability is supposed to be rapid. Large motors have under-voltage protection so they trip relatively faster than smaller motors such as those found in air conditioners which use thermal protection [12].

Power blackouts due to, for example, faults at power stations, damage to transmission lines, short circuits and overloading in the generation or transmission systems (to name but a few situations), can lead to the shedding of loads in selected parts of the electric network in order to provide power flow at critical feeders such as hospitals, mines, treatment plants, etc. Different load shedding schemes are in use and proposed and some of them are mentioned hereafter.

When it comes to load shedding schemes, the system operator usually makes decisions based on concerns about the security of the system. Such concerns include voltage [16, 17], current, power, frequency limitations [18], and customer interruption costs [19]. Taking into account the above mentioned factors, several articles addressed their research in developing an efficient method to minimize the load curtailment. To achieve that, in [20], the authors proposed a scheme based on static optimization (Kuhn-Tucker theorem) for a 26-node example problem. Similarly, based on optimization, but using instead a Newton based dynamic algorithm, [21] presents a reformulated optimal load shedding. Furthermore, linear and quadratic programming models have also been used in [22, 23], as well as strategies based on genetic algorithms [24].

One article that studies dynamic load shedding including the load characteristics in a highly interconnected and loaded electrical power system is [25]. This paper introduces a load shedding policy for generation load imbalances and formulates the problem in terms of nonlinear programming problem. A recent proposal based on time optimal load shedding is discussed in [21]. Concerning load shedding on a specific feeder, [26] analyses the application of the Everett optimization scheme for value-based load shedding in a naval-ship power system. Adaptive load shedding to regulate unacceptable frequency deviation is described in [27]. In this case, an islanded area consisting of one lumped generator and turbine model is used. In case of load shedding for power systems with multiple distributed generation, paper [28] tackles this problem. Based on the role of distributed generation in emergency state, the authors identified three scenarios in order to study static and dynamic models. A combination of adaptive and intelligent shedding techniques for load shedding is the main topic of [29]. In this paper, the authors

described a new under-frequency load shedding method for an islanded distribution network. For a review about the main problems of load shedding concerning the integration of wind turbines into power systems, the reader is referred to [30] and references therein for more details. Optimal load shedding in smart electric power grids is studied in Ref. [31]. Finally, concerning the economic aspects of load shedding, different articles can be found in the scientific literature among them we refer to [32]. As mentioned before this review is not complete or exhaustive.

To maintain power system security, it is advantageous to use and develop measures to improve voltage stability. Indeed, during this thesis load interruption, load shedding, under-voltage relays, SVCs and a combination of load interruption and using SVCs will be implemented in order to investigate the improvement in voltage stability. These measures will be done in order to facilitate the machines that are still connected to the network to re-accelerate after fault clearing.

### 2.3 Undervoltage Load Shedding Using Distributed Controllers

Load shedding schemes using distributed controllers have been proposed in [6]. The extent and rate at which the voltage drops determines the amount of load to interrupt. No communication is required between controllers since they are distributed and operate based on the status and progression of voltage drop in their zone. The amount of load that is shed is proportional to the rate of voltage drop [6]. This load shedding scheme falls under the classification of SPSs against long term voltage instability [33]. The voltages at some transmission buses are monitored by individual controllers which act on the respective load in the distribution network. The notable features of the proposed protection scheme are that it is response-based, rule-based, works on closed-loop operation and uses a distributed scheme. The characteristics of these features are [6]:

- Response-based: activation of load shedding is based on measurement of voltage. The source of the disturbance is not identified. The operation of other controllers is also taken into consideration.
- Rule-based: Load shedding is initiated if voltage drops below a threshold value for a certain period of time. The rate of voltage drop determines the amount of load to shed.
- Closed-loop operation: The controllers check the voltage in their zone after their initial activation and determine whether to shed more load or not until the voltage goes back to normal (above the threshold value). This enables them to adjust to the significance of the disturbance.
- Distributed: The controllers are distributed so that those closest to the disturbance are activated first because that's where the voltage drop is more significant.

Another approach that is proposed in Ref.[34] is the combination of load interruption and shedding using a System Integrity Protection Scheme (SIPS). The local controllers act on a distribution bus by first temporarily interrupting load (mainly non motor) connected to the same bus. Load shedding (of mainly motor load) is then initiated if the voltage does not recover above a time-varying threshold voltage or the limit of load available for interruption is reached. The load is just disconnected and not reconnected back in the second case (for motor load). The time-varying threshold voltage for load interruption is different from the one for load shedding and there is a time delay between the activation of the two [34].

## **2.4 Load shedding and Tap Changer Blocking with information from generator Over Excitation Limiters (OELS)**

A load shedding scheme that is proposed in [6] is used in combination with switching shunt compensation, the raising of generator voltages and the blocking of Transformer LTCs in [35] to mitigate long-term voltage instability. The tap changer blocking is activated in a distributed manner only where it is required which is an improvement of the proposal in [6] according to [35]. This proposal was demonstrated on a real-life model of the Western region of the RTE system located in France.

Another proposal aimed at improving the local distributed under-voltage load shedding scheme of [6] is a wide area scheme as suggested in [36] for prevention of long-term voltage instability. Information is sent to the controllers from neighboring generators that have reached their over excitation limits for a pre-set period of time regarding the status quo. The controllers then initiate the load shedding at a much quicker time if the voltage drops below the threshold value than would normally be the case if the field currents of the generators did not exceed the limits of their over excitation limiters OELS [36].

Further, a continuation of the wide area UVLS scheme proposed in [36] is done in [37] where the protection scheme prevents both short-term and long-term voltage instability. A comparison between the shedding of motor and non-motor load is also done.

## **2.5 Load shedding based on predictive control**

A new relay algorithm is proposed in [38] for Under-Voltage Load Shedding (UVLS) to aid in the recovery of voltage after a FIDVR event. The information that is used to forecast the time it would take the voltage to recover above the threshold value is the rate of recovery of the voltage. Load is shed in the distribution system if the prediction is that the disturbance would lead to instability. This scheme is now implemented in some substations in Georgia Power Company [38].

## 2.6 Load shedding using induction motor kinetic energy

In [39], a new online load shedding strategy against FIDVR that utilizes the kinetic energy deviation of induction motors is proposed. It can distinguish kinetic energy deviation which is similar to the integral of power imbalance and can thus identify motor stalling using online measurements. The most effective loads (MEL) to be shed is also identified and is the first one to be shed.

## 2.7 A combination of load shedding and the use of SVCs

FACTS devices have also been proposed and installed to address the issue of FIDVR so as to aid fast voltage recovery. Proposals were made in [10] for the use of SVCs in the Saudi Electricity Company network in the North West Region (SEC) to support the recovery of the voltage following FDVR events. Under-voltage Load Shedding is used as back protection for severe disturbances such as three phase faults (which would be too expensive to mitigate using SVCs). The load model (CIM5BL) in PSS/E that was used has a provision for under-voltage load shedding using an embedded relay. The per unit voltage for activation of the relay and time delay in cycles before tripping can be set. The model that was used for the SVCs in PSS/E is CSVGN1. Simulations showed a great improvement of the recovery of the voltage without motor stalling to within the criteria of 1 second that had been set with the use of SVCs for single phase faults. Voltage recovery within one second was aided by SVCs and undervoltage load shedding in the case of three phase faults [10].

An SVC rated 0 to +260 Mvar was installed and connected to the 230kV bus of the Winder substation through a transformer by the Georgia Transmission Corporation (GTC) in America in June 2008 in order to prevent FIDVR due to a high penetration of air conditioner loads [40]. The SVC mitigates voltage collapse and reduces the amount of load that is shed by UVLS in case of severe faults such as three phase faults with breaker failure. The criteria set by GTC is for voltage to recover to 0.8 pu within 2s following the commencement of a fault. Studies carried out using PSS/E with the complex load model (CLODAR) showed the effectiveness of the SVC for various scenarios with the set criteria being met where it had previously not been met if SVCs are not used. A user written model of the SVC was used. Since being installed the SVC has operated during severe disturbances and prevented FIDVR in the Northern Atlanta area network [40].

## 2.8 Event based load shedding

The load shedding schemes that have been discussed are response based. An event based scheme that was designed and implemented in the Hellenic system in Greece is presented in [41] to prevent voltage collapse. The two protection schemes are designed to be activated if two specific critical contingencies happen in the system. The design

of other load shedding schemes such as one meant to restore load-ability margin using a Voltage Security Assessment (VSA) on-line tool, a decentralized scheme and three centralized wide-area protection schemes are also discussed in the paper.

## 2.9 Static Var Compensator (SVCs)

Radical changes in power electronics resulted in the use of Flexible AC Transmission System (FACTS) devices in electrical power systems [44]. The reliability and efficiency of power systems is enhanced by FACTS devices. Semiconductors are used to control reactive power resulting in an increase in the maximum transmittable power [15, 42]. There are different classes of FACTS devices. These are shunt-connected, series-connected and a combination of both. Series-connected devices change the characteristics of the lines because they have an adjustable reactance which in turn varies the overall reactance of the line thereby reducing the electrical distance between generation and loads. Shunt-connected devices such as SVCs and Static Synchronous Compensators (STATCOM) are used to control bus voltages or provide reactive power support [42].

An SVC is a shunt-connected device that can supply or absorb variable capacitive or inductive current so as to regulate certain characteristics of a network mostly voltage [43]. SVCs were developed at the beginning of the 70s [15, 44]. They are used for applications such as voltage regulation, dynamic stability improvement and to lessen voltage flicker [48]. SVCs are increasingly being used in distribution systems. This trend started in the late 80s [42, 45, 46]. The range of the rating of these compact SVCs is 1-10 Mvar. One of the applications is the reduction of voltage fluctuations in distribution networks with fast load changes, which leads to fast voltage variations. Examples of such loads are motors (due to motor startups), electric furnaces and welders [45, 46]. An SVC is made up of shunt capacitors and reactors. Thyristor switching is used to control its output and the response is rapid. The equivalent reactance of the SVC automatically varies according to the prevailing conditions of the system. This leads to either a capacitive or inductive equivalent reactance with the SVC output current being capacitive or inductive respectively. The voltage is controlled by controlling the equivalent reactance [44]. The most commonly used configuration of a continuously controlled SVC is a Fixed-Capacitor (FC) connected in parallel with a Thyristor Controlled Reactor (TCR) [42]. This configuration of the FC-TCR SVC is shown in Fig. 2.3. Another configuration consisting of a Thyristor Switched Capacitor (TSC) and a TCR is also widely used [44, 47].

The adjustable equivalent reactance,  $X_{Leq}$ , of the TCR for an FC-TCR SVC can be represented as [44],

$$X_{Leq} = X_L \frac{\pi}{2(\pi - \alpha) + \sin 2\alpha}, \quad (2.5)$$

where  $\alpha$  is the thyristor firing angle.

The effective reactance of the SVC,  $X_{eq}$ , is obtained by combining  $X_C$  and  $X_{Leq}$  in

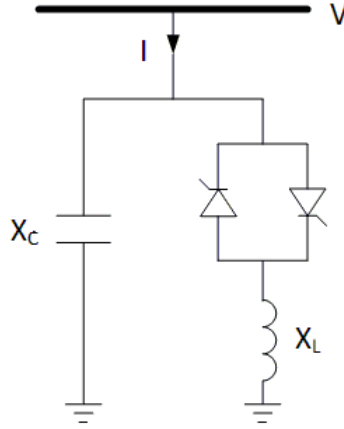


**Figure 2.3:** Structure of the SVC [44]

parallel. It is given by [45],

$$X_{eq} = \pi \frac{X_C X_L}{X_C(2(\pi - \alpha) + \sin 2\alpha) - \pi X_L}, \quad (2.6)$$

where

$$X_C = \frac{1}{W_C}, \quad X_L = \frac{1}{W_L}.$$

The equivalent susceptance of the SVC is as follows,

$$B_{eq} = -\frac{\pi X_L - X_C(2(\pi - \alpha) + \sin 2\alpha)}{\pi X_C X_L}. \quad (2.7)$$

There are three major SVC steady-state models that are used in load flow studies. These are the generator-fixed susceptance model, the total susceptance model and the firing angle model [42, 44]. The last two models were proposed and developed by [45].

The generator-fixed susceptance model is an early model recommended by IEEE [47] and CIGRE [48]. This model represents the SVC as a generator behind an inductive reactance. The reactance is adjustable which enables the regulation of the voltage. The reactive power limits have to be specified. The steady-state V-I characteristic of this model is shown in Fig. 2.4.

The slope portrays the reactance and thus the voltage regulation characteristic. The system load characteristics for various conditions such as light loading (upper characteristic) and heavy loading (bottom characteristic) are also portrayed. This model works well as long as it is within the reactive power limits. Outside these limits, it is modeled as a fixed susceptance. However, the voltage dependence of the fixed susceptance is not captured by this model unlike the total susceptance model [44].

In the total susceptance model, the SVC is portrayed as a variable susceptance as shown in Fig. 2.5. Limits are applied to the susceptance to represent the rating [42, 44]. From Fig. 2.5, the current in the SVC and reactive power are, respectively, [44]

$$I = jBV_k, \quad (2.8)$$

$$Q_k = -V_k^2 B. \quad (2.9)$$

The linearized equation of the SVC can also be obtained from Fig. 2.5 and is expressed as [44],

$$\begin{bmatrix} \Delta P_k \\ \Delta Q_k \end{bmatrix} = \begin{bmatrix} 0 & 0 \\ 0 & Q_k \end{bmatrix} \times \begin{bmatrix} \Delta \delta_k \\ \Delta B_{svc}/B_{svc} \end{bmatrix}. \quad (2.10)$$

This equation, with susceptance taken as the state variable is needed for the Newton-Raphson power flow. The value of the susceptance is found using an iterative process which is given by [44]

$$B_{SVC}^{i+1} = B_{SVC}^i + (\Delta B_{svc}/B_{svc})B_{SVC}^i. \quad (2.11)$$

The susceptance changes according to the compensation that is required. The total susceptance that is found is the one that is needed to sustain the voltage at the desired level. This susceptance is then used to determine the firing angle. This is also done by iteration.

In the firing angle model, the equivalent susceptance of the SVC depends on the firing angle,  $\alpha$ , of the thyristors and the representation is as shown in Fig. 2.4. The model is portrayed by a thyristor controlled reactor in parallel with a fixed capacitor. The linearized SVC equation is expressed as [44],

$$\begin{bmatrix} \Delta P_k \\ \Delta Q_k \end{bmatrix} = \begin{bmatrix} 0 & 0 \\ 0 & \frac{\partial Q_k}{\partial \alpha} \end{bmatrix} \times \begin{bmatrix} \Delta \delta_k \\ \Delta \alpha \end{bmatrix}, \quad (2.12)$$

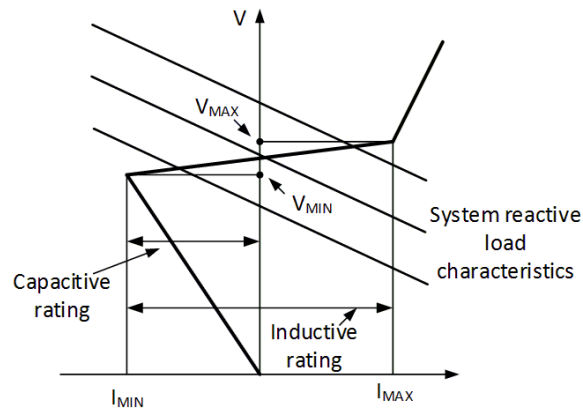


**Figure 2.4:** SVC steady-state V-I characteristic [44].

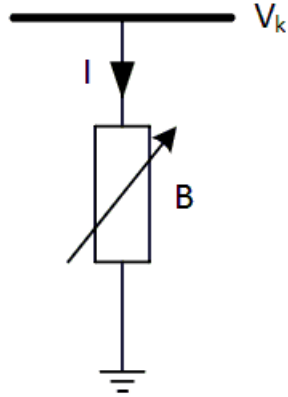


**Figure 2.5:** SVC variable shunt susceptance

where

$$\frac{\partial Q_k}{\partial \alpha} = \frac{2V_k^2}{\pi X_L} (\cos 2\alpha - 1)$$

In this case, the firing angle is the state variable. The new value of the angle is given by [44],

$$\alpha^{i+1} = \alpha^i + \Delta \alpha^i. \quad (2.13)$$

Then, Eq. (2.7) is used to find the SVC susceptance  $B_{eq}$  that follows.

In this thesis, an algorithm/approach for temporally load interruption that can be used in a protection relay to mitigate FIDVR will be proposed. The algorithm/approach that is used in combination with SVCs determines the amount of load to interrupt and the duration of the interruption.

# 3

## Induction Motor Model

**D**UE to the fact that this thesis is dealing with induction machines, the purpose of the present chapter is to provide to the reader a simple introduction to them. For it to be a complete treatment, the main goal is to explain the behavior of induction machines and the manner in which they can be exclusively modeled using PSS/E.

The first part of the chapter is devoted to defining an induction motor by describing its components, explaining the physical principles that govern its functioning and, by setting the set of mathematical expressions that model the system. The second part introduces the modeling of induction motors in PSS/E. The problems faced during the simulation process are highlighted and described. Similarly, the solution to those problems are very well documented. It is hoped that the material included in the thesis can serve as a useful guide for future users of PSS/E.

### 3.1 Induction motor

An AC induction motor is an electromechanical system that converts electrical energy into mechanical one. The main feature of an induction motor is the mechanism by which the electric current in the rotor is generated. For an AC electric motor the current on the rotor is generated by electromagnetic induction, in this case, from the magnetic field of the stator winding. As a consequence, an induction machine does not require any kind of mechanical commutation, separate-excitation or self-excitation for all or part of the energy transferred from the stator to the rotor. This is one of the major differences when compared to dc electrical machines.

In the above framework, the physical principle that leads to the functioning of an AC machine is the Induction law of Faraday. In this case, an external AC current is supplied to the stator, but no external DC field current is provided to the rotor. The resulting

AC currents in the rotor are the result of electromagnetic induction [49], [50] [51].

In this section, the protocols and procedures for setting up simulations of induction machines in PSS/E are described in detail. The document is mainly based from the experience acquired from the authors during the completion of the thesis and from Siemens Power Technologies International's (PTI) program manuals.

There are two ways of modeling induction machines in PSS/E. The first one consists of connecting the induction machine directly to the bus through an induction machine icon. In this case, at least one induction machine data record must be specified at each network bus at which an induction machine is to be represented. Multiple induction machines may be represented at a bus by specifying more than one induction machine data record for the bus, each with a different machine identifier. It is important to highlight that the induction machine simulation icons are available in version 33.4 and 33.5. The second one consists of representing the induction machine as a bus load in the load flow simulation and incorporating this load into one of the pre-defined load models available in PSS/E for dynamic simulations (see descriptions of the models below). During the execution of this thesis the second way was chosen due to initialization problems in the load flow studies and the lack of load models for dynamic simulations with the first way. Independent of the choice, the results coming from both ways should provide the same results. The following paragraphs are devoted to analyzing the simulation process using the second method.

## **3.2 Simulation process of an induction motor as a bus load in PSS/E**

As one of the main purposes of this thesis was to implement the model used by Professor Cutsem, see [5], the initial step of this work was to determine the kind of model that best fits the physical behavior of this system within PSS/E. After discussion with Professor Cutsem, and due to the characteristics of the system: rotating load dynamics, it was determined that the induction motor load in the system can be classified under the umbrella of the CIM5BL model, double cage type 1 motor in PSS/E. The purpose of the following paragraphs is to explain this terminology and clarify the way of reasoning that led the authors to this assertion.

## **3.3 Equivalent circuit**

In the manual of PSS/E [1], the simulation process starts by developing a simplified mathematical model that captures the main physical features of the electromagnetic phenomena while allowing the user flexibility during the simulation process. As a result of this modeling process, the following figure (Fig. 3.1) is a schematic representation of the positive sequence steady state equivalent circuit for the induction machine.

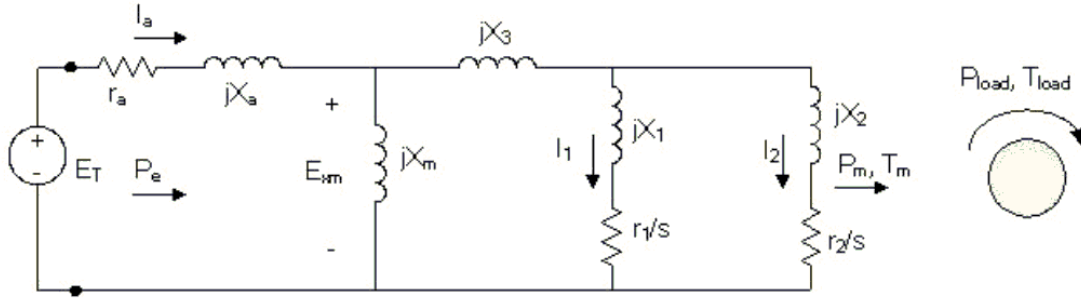


**Figure 3.1:** Induction Machine Equivalent Circuit [1].

Where the left side of the circuit is the machine armature and the right side is the rotor.  $R_a$  is the armature resistance and  $X_a$  is the armature Leakage reactance. The armature and the rotor are linked through the magnetizing reactance  $X_m$ . The rotor side consists of two parallel resistance and reactance branches,  $r_1$ ,  $X_1$  and  $r_2$ ,  $X_2$ , that represent the “cages (windings in the rotor)”. The reactance  $X_3$  is not included in the model of all the induction machines in this thesis because the motors were modeled as double rotor winding machines. Once the mathematical and physical modeling process is done, the computer simulation in PSS/E can be initiated. In order to control the simulation flow, the first step is to realize that each induction machine data record has the following format: I, ID, AREA, ZONE, MBASE, H, A, B, D, E, RA, XA, XM, R1, X1, R2, X2, X3, E1, SE1, E2, SE2, IA1, IA2, XAMULT, Tnom, Type. The definition of these parameters and values are presented in list of symbols and abbreviations

### 3.4 Induction motor models

In order to perform simulations of Induction motors and their driven loads, PSS/E contemplates three different models for different scenarios. It is recalled that the approach used in the thesis is to simulate induction machines as bus loads in the load flow and introduce them into one of these pre-defined models for dynamic simulations in PSS/E.

The first level of detail is normally used when the data for individual loads is either not available or difficult to obtain. Models such as LDFRBL are used to replicate the voltage/frequency/load characteristics of the load. This level of detail does not enable the study of the effects of the characteristics of motor loads on bus voltages and the system [52].

The second level of detail is normally used when the main interest is to model the rotating load and the steady state behavior of the motor. The electromagnetic dynamics of the motor are not taken into account. The CMOTOR model is used for this level of detail. Only operation at fixed slip is possible to be modeled with this model. The voltage decay is not taken into account after tripping [52].

The third level of detail takes into account the motor electromagnetic dynamics and rotating load dynamics. These are thoroughly represented at this level. The models that are used for this level are the CIM5BL, CIM6BL, CIMWBL, CIMTR2 and CIMTR4. CIM5BL has been selected because it best suits the network that is being studied. In this level of detail, the transient component starts from zero but responds to changes in the network conditions such as voltage to reflect rotor flux linkages. The transient and sub-transient time constants of the rotor winding determine the decay.

From the above description, due to the fact that the modeling of an induction machine with rotating loads is of primary interest, it is concluded that the model studied by [5] can be classified by approach number 3. What is remaining now, is to determine the specific model and the type of motor to which it belongs. These questions will be the topic of discussion for the next sections.

### 3.5 Induction Motor Load Model CIM5BL

The CIM5BL model can be used to model either single-cage or double-cage induction motors including rotor flux dynamics. In addition, the effects of rotating load dynamics can be included. These features makes it a promising candidate to the studied system [5].

In the power flow, the motor is modeled as a bus load where the entire load at a specific load ID is taken as constant power load. These models may be applied to an individual load or a subsystem of loads. The data input for the model are the equivalent circuit impedances for Type 1 equivalent circuit model. These can be seen in Fig. 3.2. The Model Type is specified in  $ICON(M+1)$ .

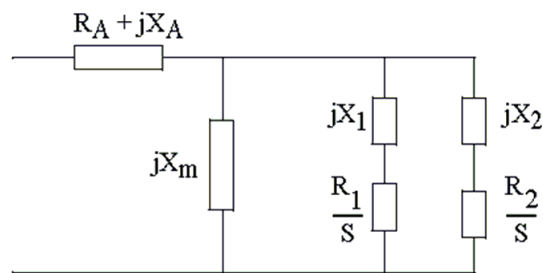


**Figure 3.2:** CIM5 Type Model [1].

The CIM5 models translate the equivalent circuit parameters into transient parameters (flux linkage components) for use in the actual model calculations, according to the equations in Fig. 3.3.

The equivalent circuit impedances are specified in per unit on motor MVA base. The user has two choices for the specification of motor MVA base:

CONS	Description
J	$R_A$
J+1	$X_A$
J+2	$X_m > 0$
J+3	$R_1$
J+4	$X_1 > 0$
J+5	$R_2$ (0 for single cage) 1"
J+6	$X_2$ (0 for single cage)
J+7	$E1 \geq 0$
J+8	$S(E1)$
J+9	$E2$
J+10	$S(E2)$
J+11	MBASE 2"
J+12	PMULT
J+13	H (inertia, per unit motor base)
J+14	$V_l$ (pu) 3"
J+15	$T_l$ (cycles) 4"
J+16	TB (cycles)
J+17	D (load damping factor)
J+18	$T_{nom}$ , Load torque at 1 pu speed (used for motor starting only) $\geq 0$ )
1	To model single cage motor: set $R_2 = X_2 = 0$ .
2	When MBASE = 0, motor MVA base = PMULT x MW load. When MBASE > 0, motor MVA base = MBASE.
3	$V_l$ is the per unit voltage level below which the relay to trip the motor will begin timing. To disable relay, set $V_l = 0$ .
4	$T_l$ is the time in cycles for which the voltage must remain below the threshold for the relay to trip. TB is the breaker delay time cycles

ICON	Description
M	IT, motor type (1 or 2)

VARs	Description
L	Admittance of initial condition Mvar difference
L+1	Motor Q
L+2	Telec (pu motor base)
L+3	T (pu on motor base)1, 2
L+4	IQ
L+5	ID
L+6	Motor current (pu motor base)
L+7	Relay trip time
L+8	Breaker trip time
L+9	MVA rating
1 Load torque, $T_L = T (1 + D33)D$	
2 For motor starting, $T = T_{nom}$ is specified by the user in CON (J+18). For motor online studies, $T = T_o$ is calculated in the code during initialization and stored in VAR (L+4).	

**Figure 3.3:** Induction Motor Load Model CIM5BL[53]. Model of CIM5BL general description.

1. When  $CON(J+11) > 0.$ , the motor MVA base is specified as  $CON(J+11)$ .
2. When  $CON(J+11) = 0.$ , the motor MVA base is specified as  $CON(J+12)*MW$  load.

### 3.6 IMD application tool

During the simulation process, one major problem that was faced was to determine the appropriate nominal torque  $T_{nom}$ . During the course of this thesis the values for all the parameters of the machine were tested in the (IMD) application tool from PSS/E utilities.  $T_{nom}$  was determined (and specified in  $CON(J+18)$  from motor data.  $T_{nom}$  was calculated through motor parameters (IMD) tool. It is important to mention that the motor nominal rating was used to specify MVA base in  $CON(J+11)$ , MBASE. In addition, the simulation integration time step should be reduced in order to prevent instability of the system during dynamic simulations.

### 3.7 Motor type 1

During the simulation process all the motors were simulated as type 1. All the time constants were done based on the equations shown in Table 3.1. The equivalent model is shown in Fig. 3.2. During this thesis all the motors were modeled using the CIM5BL double cage model and type 1 equivalent circuit was used and stored in ICON(M).

**Table 3.1:** Mathematical expressions to determine the different parameters for Motor type 1. Where  $\omega_0 = 2\pi * 50 \text{ rad/s}$  for a 50 Hz system;  $X$  and  $L$  are in the per-unit system [52].

Type 1
Double Cage
$T_0' = L_1 + L_M / \omega_0 R_1$
$T_0'' = L_2 + (L_1 L_M / L_1 + L_M) / \omega_0 R_2$

### 3.8 The integration time step $\Delta t$

As indicated in the previous section, an important parameter to determine during the simulation process is the integration time step,  $\Delta t$ . The values for  $\Delta t$  should be lower than 1/4 or 1/5 of the shortest time constant in the system. In the test network the equipment with the smallest time constant are the motors. Thus, the time constants for motor type 1 of the CIM5BL model had to be determined. The formulas that are used for this are well described in Eqs. (3.1) and (3.3) below.

It is highlighted in the program application guide that typical time constant values for 50 Hz is 0.01 s and for 60 Hz is 0.0083 s. Therefore, the integration time step for 50 Hz becomes 0.002 s and for 60 Hz becomes 0.00166 s when the time constant is divided by 5. For the case analyzed in this thesis, the calculation of the principal time constant was computed as (see Table 3.1.)

$$T_0' = (L_1 + L_m / \omega_0 R_1) = 0.5712 \text{ s.} \quad (3.1)$$

Therefore,

$$\Delta t = T_0' / 5 = 0.11424 \text{ s.} \quad (3.2)$$

Similarly, the second time constant reads,

$$T_0'' = \frac{L_2(L_1 + L_m) + L_1 * L_m}{L_1 + L_m} / \omega_0 R_2 = 0.0599 \text{ s.} \quad (3.3)$$

As a consequence,

$$\Delta t = T_0'' / 5 = 0.012 \text{ s.} \quad (3.4)$$

# 4

## Load flow and dynamic simulation using PSS/E

**I**N this chapter the simulation setup and implementation in PSS/E is described. The simulations were done on a typical distribution network with a large amount of induction motors. The data for the test network was kindly provided by Professor Thierry Van Cutsem. The test network is composed of the following:

- One infinite bus – slack bus.
- One generator.
- High voltage network – 36 kV.
- Medium voltage network – 15 kV.
- One 36/15 kV and seven 15/0.4 kV transformers.
- 14 LV feeders.
- 286 loads connected to 286 buses (motor and non-motor).
- 3×100 kVA motors and 140×6 kVA motors (double-cage rotor).

The smaller motors are connected to the 0.4 kV load buses while the larger motors are connected to 15 kV load buses. Part of the test network is shown in Fig. 4.1. The figure shows the slack bus, the generator, the 36/15 kV transformer, two of the seven 15/0.4 kV transformers and four of the fourteen LV feeders. Feeder N4AC and N4AB are the first two LV feeders in the network and feeder N13AB and N13AC are the last two that are furthest from the source of supply. The complete single line diagram as implemented in PSS/E is shown in the Appendix A in Fig. A.1

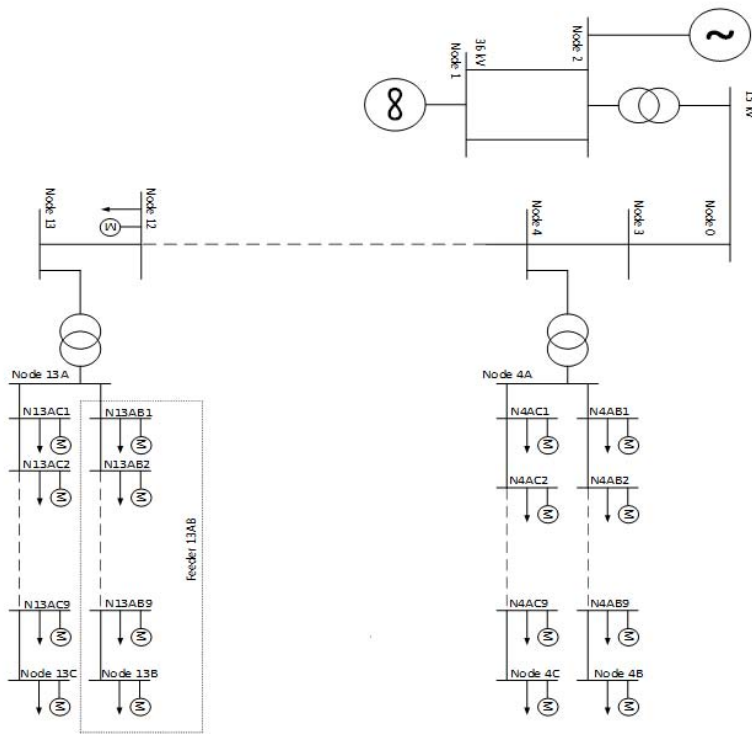


Figure 4.1: Single line diagram showing part of the test system [5].

## 4.1 Directories and Files Overview

During the simulation process a folder with an unlimited number of files was created for PSS/E. Two subfolders were created one for load flow and the second one for dynamic simulations. It is important to mention that PSS/E always runs out of a working folder [1]. PSS/E uses two types of files, input files and output files. These types of files can be seen by PSS/E as:

1. Input files. Data required by PSS/E. All the files are created by the user.
2. Output files. This type of file includes results and files generated automatically by PSS/E.

PSS/E uses three different types of files. These are source, binary and both source and binary. Source files can be used by PSS/E and the user. Binary files are used by PSS/E. Source and Binary can be used by PSS/E and other programs [1].

File formats used during the load flow and dynamic simulations are:

1. Slider diagram file (.sld). Containing all the data for the line diagram and it is linked with save case file.

2. Save case file (.sav). Binary file containing the power flow data, [1].
3. Power flow data file (.raw). Containing the power flow data for the initial working case [1]
4. Dynamic data file (.dyr). File containing all the machine data necessary to perform dynamic simulations, [1].
5. Snapshot file (.snp). Binary file containing all the data at an exact instant during dynamic state.
6. Output file (.out). File containing all the information saved after the dynamic simulation.

## 4.2 Steady-state load flow

The parameters used to run the load flow simulation during this thesis are also the ones that were used in [5]. However, the fraction of motor load used in this thesis is 50% while 60% was used in [5]. All the loads were modeled as constant power loads in the load flow analysis. Full Newton-Raphson method was used for the load flow solution in this thesis. For load flow simulation all the parameters of the transmission lines and transformers used are in pu. The parameters were obtained as shown below

$$Z_{Base} = \frac{V_{Base}^2}{S_{Base}}, \quad (4.1)$$

$$Z_{pu} = \frac{Z_{real}}{Z_{Base}}, \quad (4.2)$$

$$X_{pu}^{new} = X_{pu}^{old} \times \frac{V_{old}^2}{S_{old}} \times \frac{S_{Base}^{new}}{V_{Base}^{2new}}. \quad (4.3)$$

From the above equations, line and transformer parameters are calculated.

In PSS/E load flow simulation can be performed as follows:

1. In the toolbar click new.
2. Network case and diagram.
3. Build new case.
4. Draw the diagram with the aid of the toolbar. Use the load icon to represent the static and induction machine loads. Therefore, two load icons are connected to each load bus. The induction machine icon is not used in this project.
5. Enter all the parameters of the machines (total machine load for each bus), buses, branches and transformers.

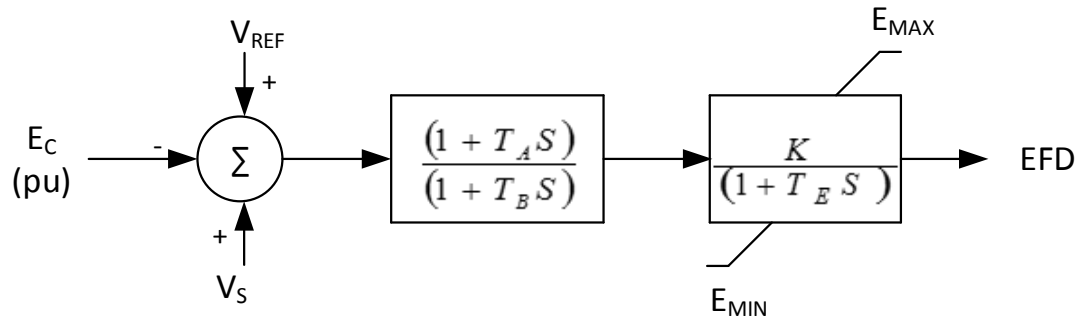
6. Save in the format of (.sav and .sld).

Below is an explanation of how to run the load flow:

1. On the toolbar click Power flow.
2. Followed by solution.
3. Then click solve (NSOL/FNSL/FDNS/SOLV/MSLV).
4. In the window displayed (load flow solutions) select the type of solution required. Full Newton-Rhpson (FNSL) was used in this thesis.
5. Click Solve.
6. Then Close.

### 4.3 Dynamic simulation connection of the induction machines (IMD)

After running the load flow simulation it is possible to start the dynamic simulation. A saved case file of the load flow simulation is used as the basis for starting the dynamic simulation. This is used in conjunction with a dynamic data file. Dynamic models of the generator and the exciter were used. The PSS/E model that was used for the generator is Genrou which is a round rotor generator model. It is a model of a solid rotor generator. It models the generator at the sub-transient level as stated in [52]. The parameters and characteristics of this generator model match the data that was given for the test system generator. The model that was used for the exciter is SEXS. It is a broad model and is not explicit to a particular type of exciter according the software manual [52]. It encompasses the features of a diverse range of excitation systems [52]. The SEXS exciter model was used because it is a close representation of the type of exciter in the data that was provided for the test system. The block diagram of the SEXS exciter is shown in Fig. 4.2. In the figure  $K$  is the gain. The time constant  $T_E$  and the boundaries  $E_{MAX}$  and  $E_{MIN}$  portray the power source. The time constants  $T_A$  and  $T_B$  enable the use of a high steady-state gain but still being able to get an acceptable dynamic performance. The CIM5BL models were used for the motors. The parameters for the models are entered in the dynamics data (DYRE File) file. The loads were converted to the form that takes into account the voltage dependence in a more appropriate way as is also stated in [45]. The constant power load that was used in the load flow was converted to 100% constant current for active power and 100% constant admittance for reactive power.



$$V_S = V_{OTHSG} + V_{UEL} + V_{OEL}$$

**Figure 4.2:** Generator exciter model block diagram [53].

The simulation setup for running dynamic simulations can be performed as follows:

1. Open the .sav and .sld files previously created in the power flow
2. Run the load flow.
3. Connect an extra load to each bus in order to simulate it as an IMD.
4. In toolbar click view.
5. Click dynamic tree view.
6. Click device models then machines and click on one of the machines.
7. Dynamic data will be displayed.
8. Insert machine parameters. For this simulation GENROU model was selected for the generators since the generators are for a thermal power station.
9. For this simulation the exciter model that was selected is SEXS.
10. At the lower flange of the window click on Load Bus. This is done with the objective of connecting the induction machine models.
11. In Load Characteristic Model (double click to see the induction machine models on each bus) CIM5BL was selected for all the buses. It is important to mention that  $T_{nom}$  was calculated from the PSS/E utility for motor parameters (IMD).
12. Save the dynamic data (.dyr) , (.raw) , (.snp) file format.

Below is an explanation of how to run dynamic simulations:

1. On toolbar click Power flow.
2. Then click convert loads and generators.
3. On the toolbar click power flow again and then click solution.
4. Then click order network for matrix operations (ORDR). Assume all the branches are in service was selected on the window that pops up.
5. Then click power flow/solution then factorize admittance matrix (FACT)
6. Then click power flow/solution then solution for switching studies. Select use voltage vector as start point and select factorize before performing solution (FACT) checkbox before clicking ok.
7. On the toolbar click Dynamics
8. Click on channel setup wizard and then select the check-boxes for the quantities that you want to be included in the output such as voltage, speed, flow (P & Q), etc.
9. Click finish in the channel setup wizard.
10. On the toolbar click Dynamics. Click on solution parameters and enter the integration time step, DELT. The integration time step  $\Delta t$  was calculated in previous Chapters. See Fig.4.3.
11. On the toolbar click on Dynamics.
12. Click on simulation and then click on perform simulation (STRT/RUN).
13. In the perform dynamic simulation window specify a name for the channel output file (.out)
14. Click on Initialize.
15. Run for a certain period of time (pre-disturbance time) for instance a time of 1 s.
16. On the toolbar click on disturbance.
17. Create a disturbance by selecting the element where the fault will be applied. A fault was applied on one of the circuits between bus Node 1 and Node 2 for this case.
18. And run for a certain period of time such as 0.2 s.
19. Click on disturbance/clear fault.

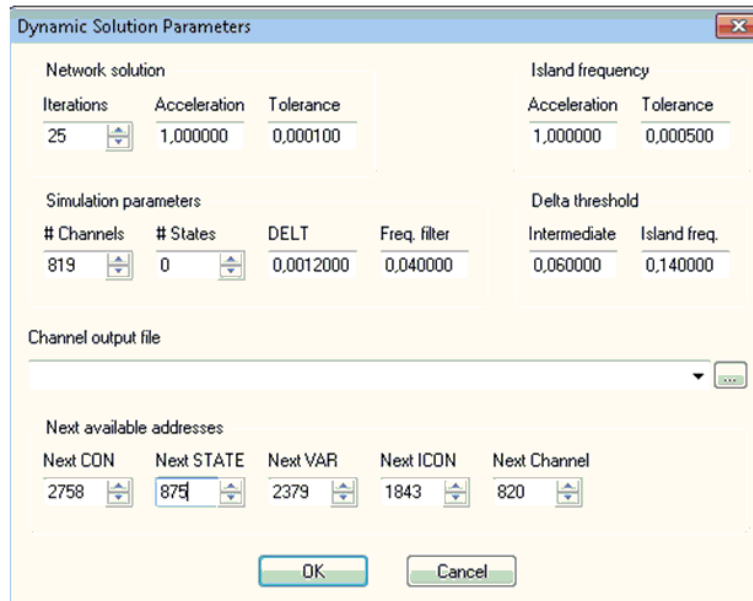


**Figure 4.3:** Setting the integration time step in PSSE

20. Run for a certain period of time such as 1 or 2 seconds.
21. Click on close.
22. On the toolbar click open.
23. Open the OUT. File that was saved previously.
24. The graphics of the results for the dynamic simulations can then be analyzed.

## 4.4 Python programming language

Python was used in this thesis to control PSS/E. Python is a generic programming language which is extensively in use [54]. It is an interpreted language. It is one of the program automation processors used to control PSS/E. Any type of program can also be written using python [1]. The Application Program Interface (API) was used to access PSS/E functionality. The psspy python extension module was used to access the API. Python syntax was used when doing simulation runs for load interruption. It was used for load flow, dynamic simulations, tripping loads and then reconnecting them in steps to automate the process. It was also used to automate the dynamic simulations for voltage stability improvement using SVCs. Dynamic simulations with the undervoltage load shedding relay were also automated using python. The methodology that was used for the various simulation cases is illustrated in Fig. 4.4.

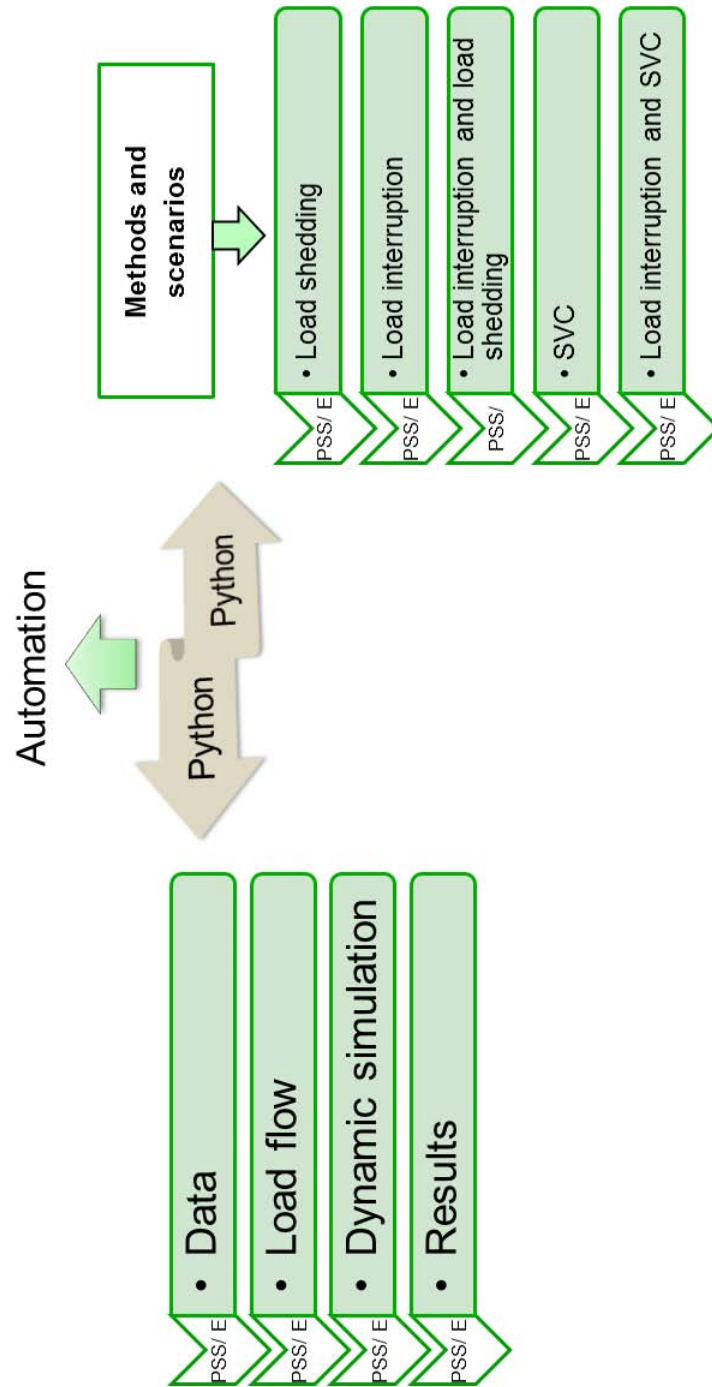


**Figure 4.4:** Methodology of the simulation setup and implementation.

# 5

## Improvement of voltage stability by temporary load interruption

IN this chapter, different scenarios of improving voltage stability by the load interruption method which was introduced in [5] are simulated. Simulations have been done in PSS/E on a test network of a typical distribution system that has a large share of motor loads. Python was used to run and control PSS/E. The Python syntax in the API was used. The simulation was therefore automated. However, the recovery of the voltage had to be checked after every simulation run and then more load earmarked for interruption and included in the Python script until the desired outcome is obtained. There is currently no API Python syntax for PSS/E to directly interrupt the load that is to trip and then reconnect the load at a bus. The only means to trip the load is through the Under-voltage Load Shedding (LVSH type) relay model or by creating a user written model. However, the LVSH relay model only trips the load when the voltage is below a given threshold but it does not reconnect the load. Creating a user written model would have also meant a different programming language (Fortran). Therefore, two additional buses were created and connected to each load bus via zero impedance lines. The non-motor load was connected to one of the new buses and the motor load was connected to the other bus. This arrangement can be seen in the Appendix A in Fig. A.1. This is essentially the same as splitting the bus which is done by activity split (Activity SPLT) in PSSE. Initially, the simulation was run in steady state within the acceptable voltage range of 0.9 pu to 1.1 pu. The dynamic simulation was then initialized with the pre-disturbance steady state normal conditions. The dynamic simulation was run with these conditions for 1 second. Thereafter, a three phase fault was applied on one of the lines between Node 1 and Node 2 in order to create a disturbance. The fault was applied for 200 ms (10 cycles). According to the criteria that has been used in this thesis, the voltage should recover to 0.9 pu within 1s following a disturbance. This is the criteria that was used in [5] were the network data was obtained. This criteria is

shown in Fig. 5.1

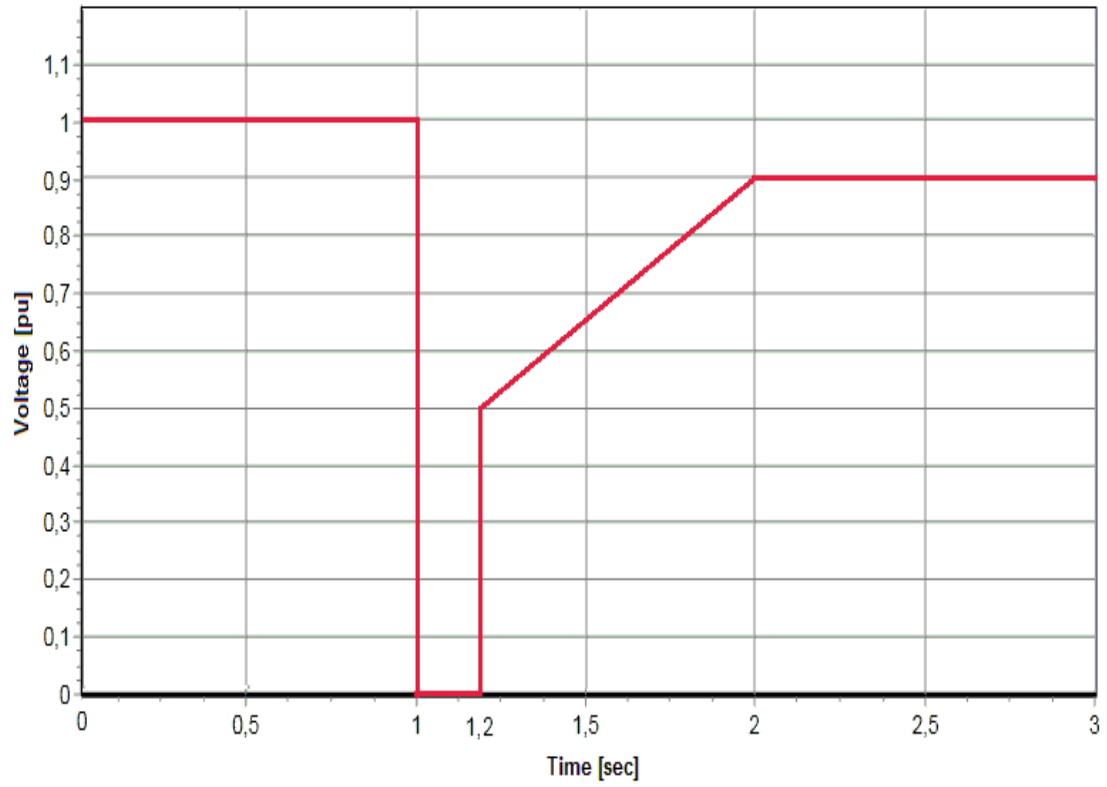


**Figure 5.1:** Criteria for voltage recovery after a disturbance [8].

Load was then interrupted following the clearing of the fault to aid the voltage recovery. The various scenarios that were investigated are presented in the following subsections.

## 5.1 Simulations without load interruption

In this case, there was no interruption or load shedding of the loads. In most of the feeders especially the ones furthest from the source of the MV feeder (Node 0), all the voltages at buses were below 0.9 pu 1 second after the commencement of the fault. In Fig. 5.2, which shows the voltages at buses on feeder N13AC, all the voltages do not recover to 0.9 pu within 1 second following the disturbance. This is the furthest feeder from the source of supply.

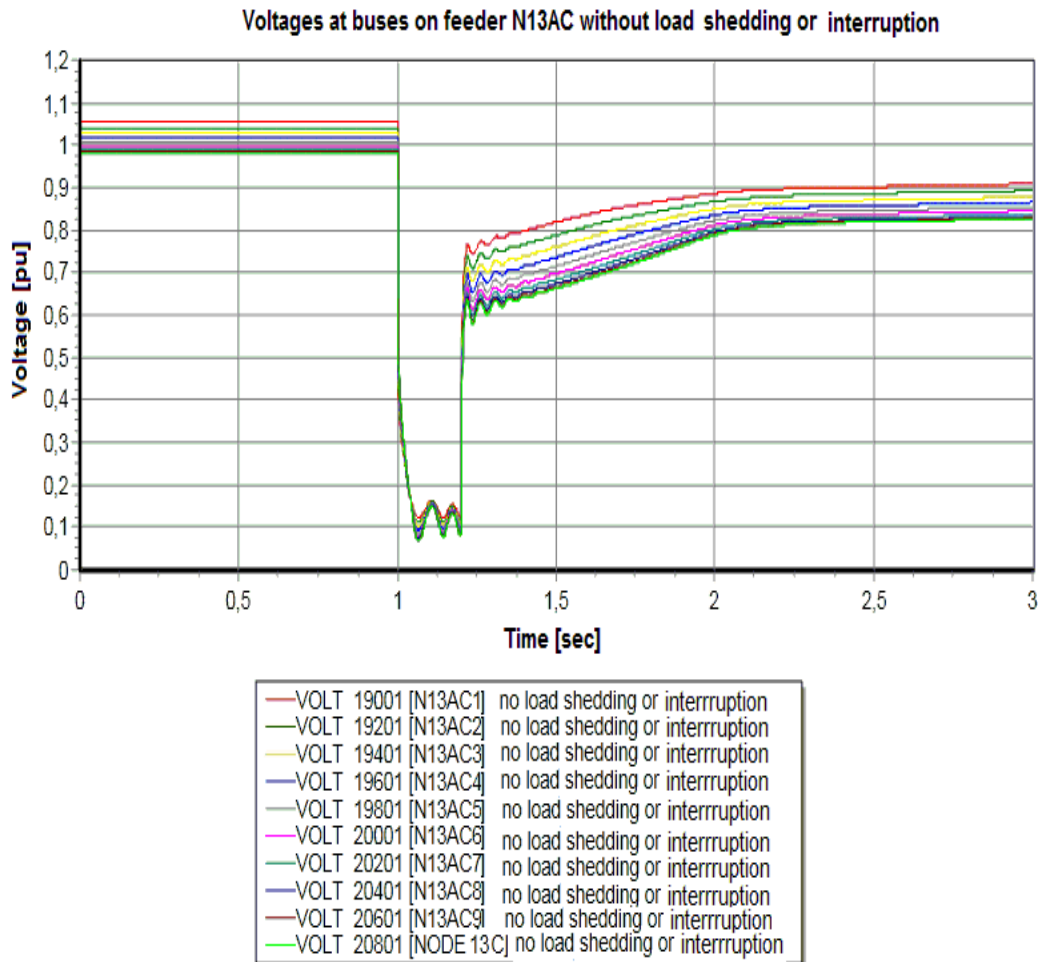


**Figure 5.2:** Voltages at buses on feeder N13AC without load interruption or shedding

Figure 5.3 shows the number of load buses with voltage below 0.9 pu before the fault and 1 second after the fault is applied. It can be seen from the figure that 268 buses have voltage below 0.9 pu after the fault whereas none of the buses had voltage below 0.9 pu prior to the disturbance. This shows the need for load interruption so as to aid

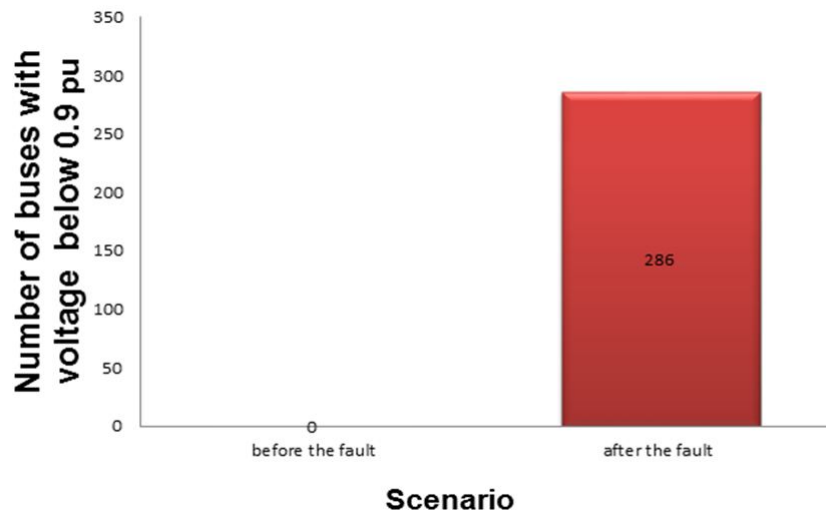


**Figure 5.3:** Number of load buses with voltage below 0.9 p.u 1 second after the fault.

the voltage recovery after fault clearance. The total number of load buses is 286.

## 5.2 Load shedding of 40%, 60% and 80% of non-motor load

In this scenario, the recovery of the voltage for load shedding of 40%, 60% and 80% of non-motor load is simulated. From Fig. 5.4 and Fig. 5.5 it is clear that the voltages at the buses recover faster as the amount of load that is shed is increased. For instance, in Fig. 5.4, it can be seen that the voltages at the buses on feeder N13AC recover faster as the percentage of load that is disconnected is increased. For load shedding of 80% of the non-motor load the majority of the voltages at the load buses recover above 0.9 pu at 2 s (1 s after the initiation of the disturbance). It can also be observed from Fig. 5.5 that the voltage at Node 13C recovers faster as the percent of load that is shed is increased. Node 13C is the furthest bus from the source of supply in the system.

According to Fig. 5.6, the number of buses with voltage below 0.9 pu at 2 s with load shedding is significantly lower than the case without load shedding. It is important to mention that at furthest points on feeders N13AC, N13AB, N11AC N11AB (the furthest feeders from the source) the voltage recovers faster due to the shedding than the case without load shedding but still the voltage on some load buses are not able to reach 0.9 pu at 2 s even for load shedding of 80% of the load. It is also important to mention that although most of the voltages recover to 0.9 pu at 2 s, load shedding is not the best option due to the fact that several loads are off for a long period of time. This is an inconvenience to consumers and can also result in lost revenue. It is also a cost to the grid company as customers would have to be paid for being off supply. For this reason, another improvement method has been simulated.

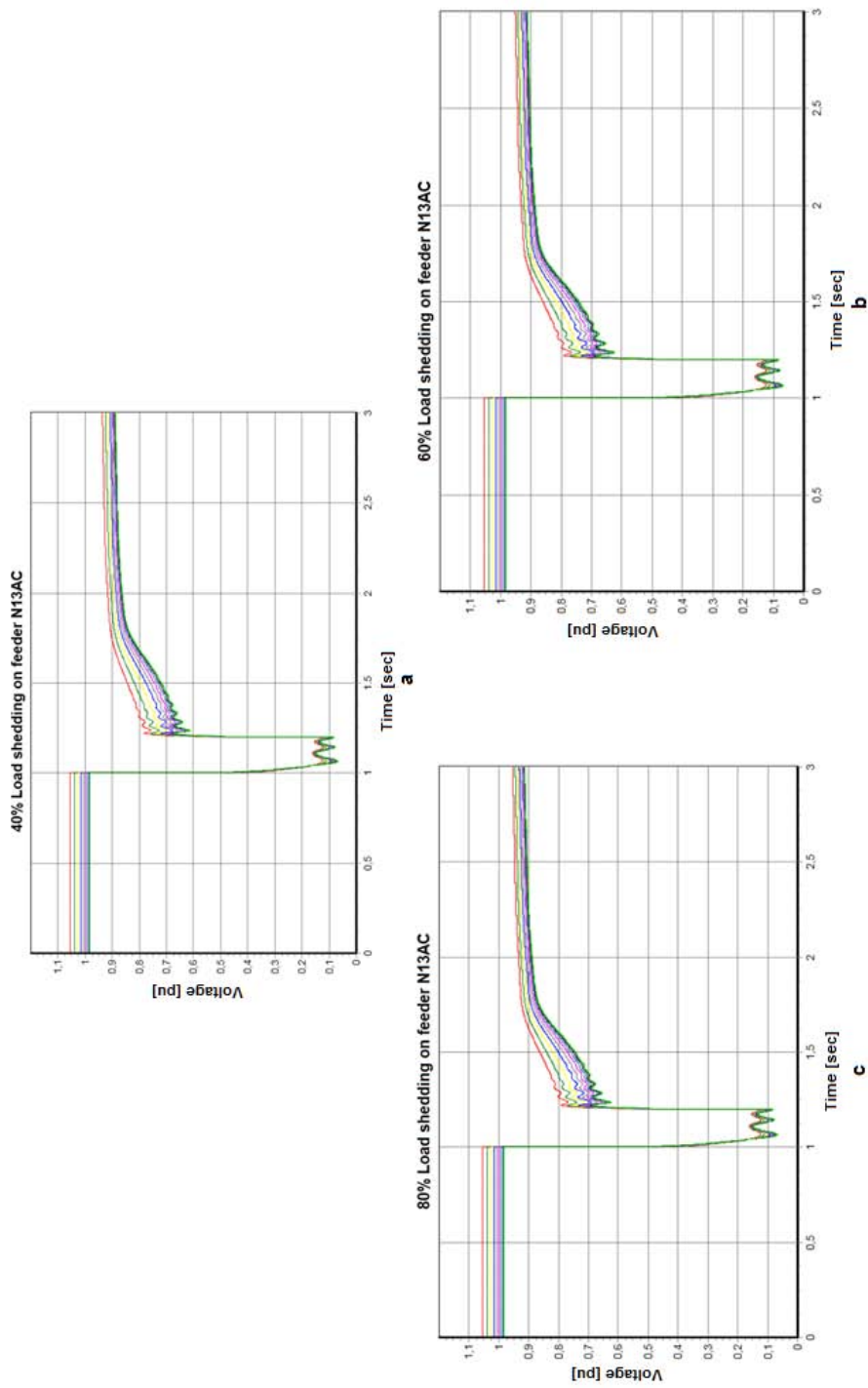


**Figure 5.4:** Voltages at buses on feeder N13AC for various load shedding scenarios (40% (a), 60% (b) and 80% (c)).

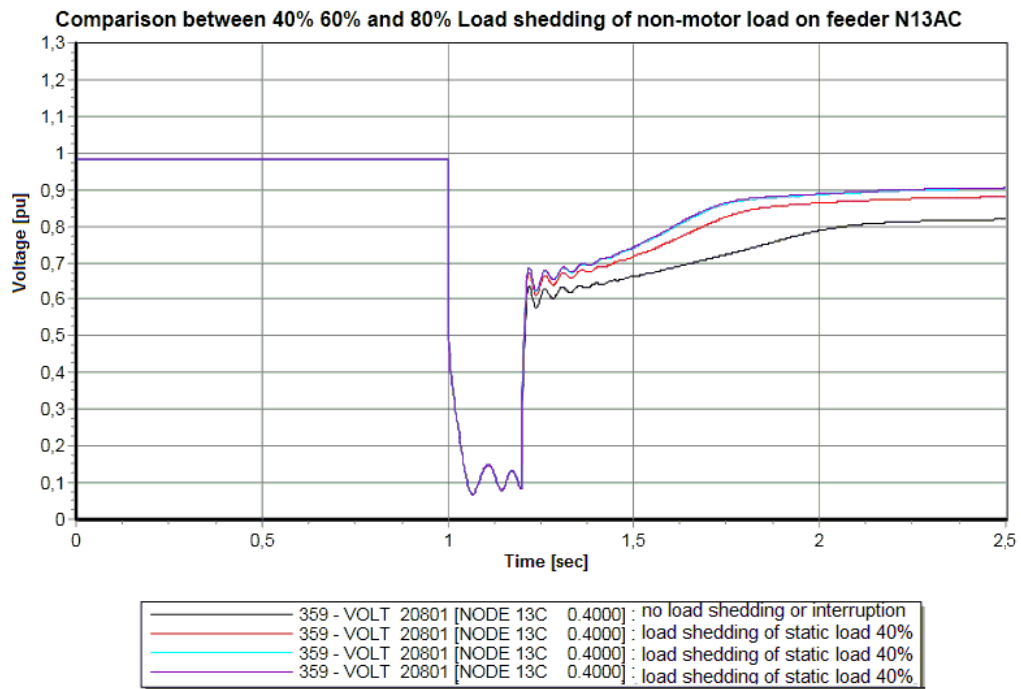


**Figure 5.5:** Voltages at Node 13C for 40%, 60% and 80% load shedding of non-motor loads

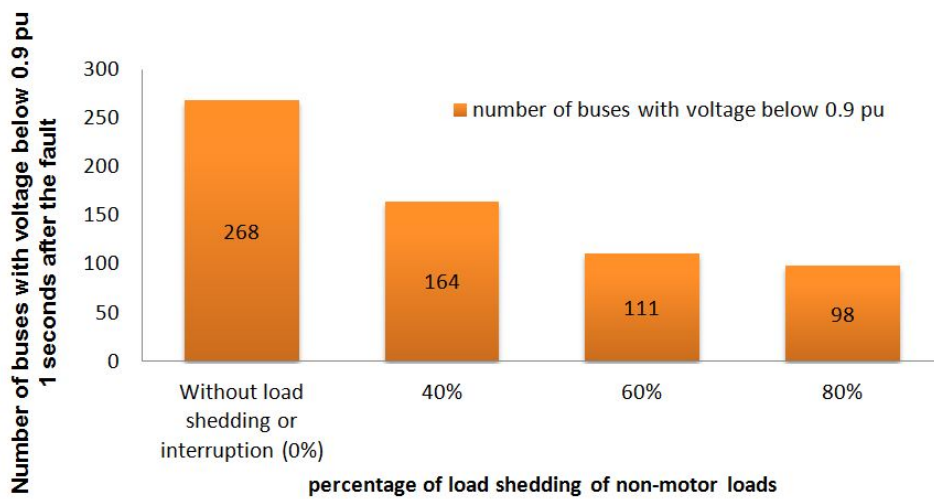


**Figure 5.6:** Number of load buses with voltage below 0.9 pu at 2 s.

### 5.3 Load shedding of various percentages of non-motor and motor loads.

In this scenario, the recovery of the voltage to 0.9 pu 1 s after the disturbance with the disconnection of non-motor and motor loads is studied. From an economical point of view, it is important to say that the shedding of motor loads causes considerable expenses and further inconvenience for industries or customers who use a large share of the motors.

A considerable improvement in the recovery of voltages at buses in the system can be seen when non-motor and motor loads are disconnected. For instance, instead of having 164 load buses with voltages below 0.9 pu at 2 s as is the case with 40% load shedding of just non-motor loads the simulations show that with load shedding of 40% of non-motor and 10% of motor loads the amount of load buses with voltage below 0.9 pu at 2 s reduces to 95. This can be seen by comparing Fig. 5.6 with Fig. 5.9.

The recovery of the voltage for the cases where load shedding of 40%, 50%, 60% and 80% of non-motor loads is combined with shedding of motor loads was studied. Four cases were investigated. These are the shedding of 10%, 20%, 40% and 80% of motor loads. Each of these four cases of shedding of motor loads was done together with load shedding of 40%, 50%, 60% and 80% of non-motor loads. The results for the evolution of the voltages are shown in Figs. 5.7, 5.10, 5.12, and 5.15. The voltages at Node 13C for the cases where 10% and 40% of motor load is shed are shown in Figs. 5.8 and 5.13, respectively. Figs. 5.9, 5.11, 5.14 and 5.16 show the number of buses with voltage below 0.9 pu at 2 s. As can be seen from the figures, the higher the percentage of motor loads that are shed the faster the voltage recovers. In the case where a combination of shedding of 80% of non-motor and 80% of motor loads is studied, the number of buses with voltage below 0.9 pu is only 26. However, as earlier stated the disadvantage with load shedding is that the load is not saved. The load is just disconnected and not reconnected so consumers remain off supply.

The results of the simulations for this specific case are shown below in the next subsections.

### 5.3.1 10% load shedding of motors

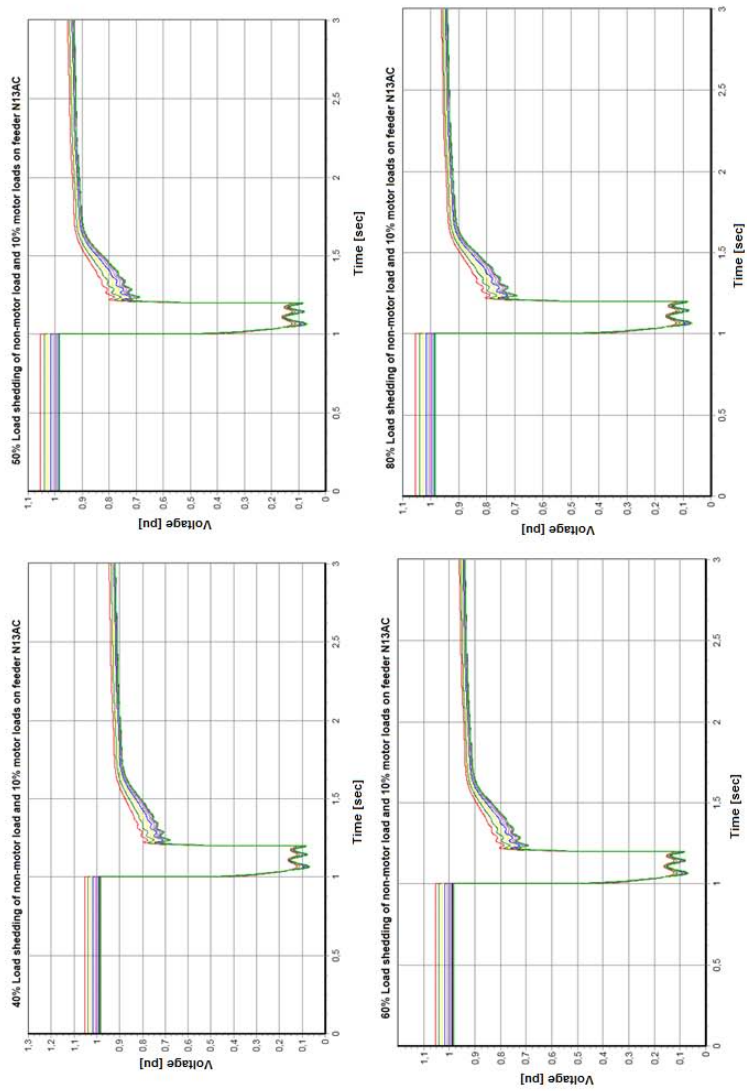


**Figure 5.7:** Load shedding of 10% of motor loads together with various percentages (40%, 50%, 60% and 80%) of non-motor loads.

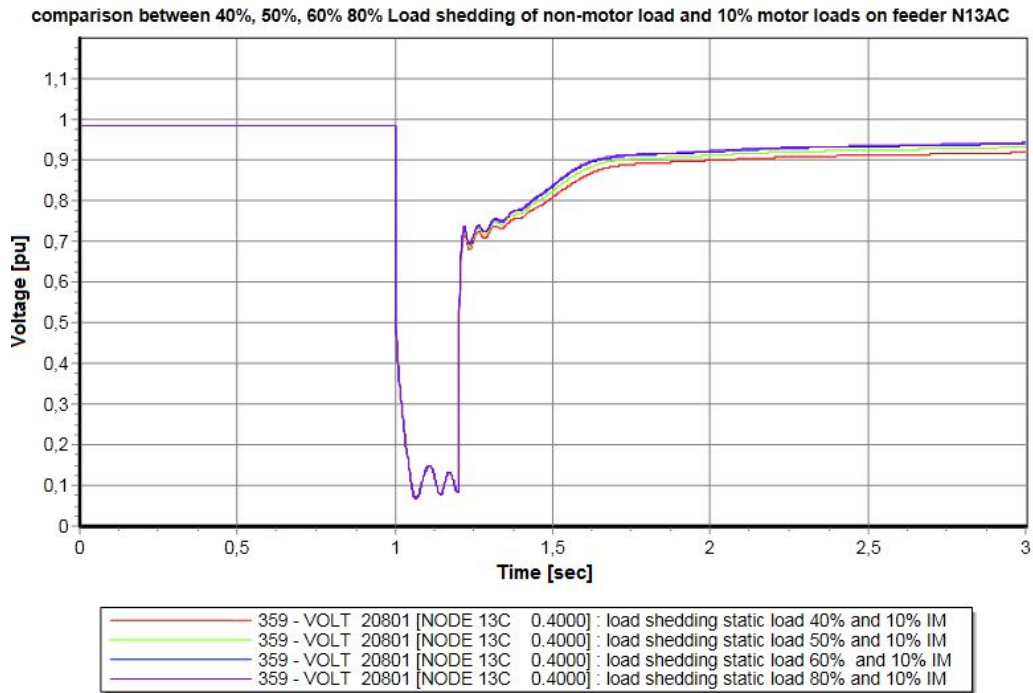


**Figure 5.8:** Voltage at Node 13C for load shedding of 40%, 50%, 60% and 80% of non-motor loads together with the shedding of 10% of motor loads for each case.

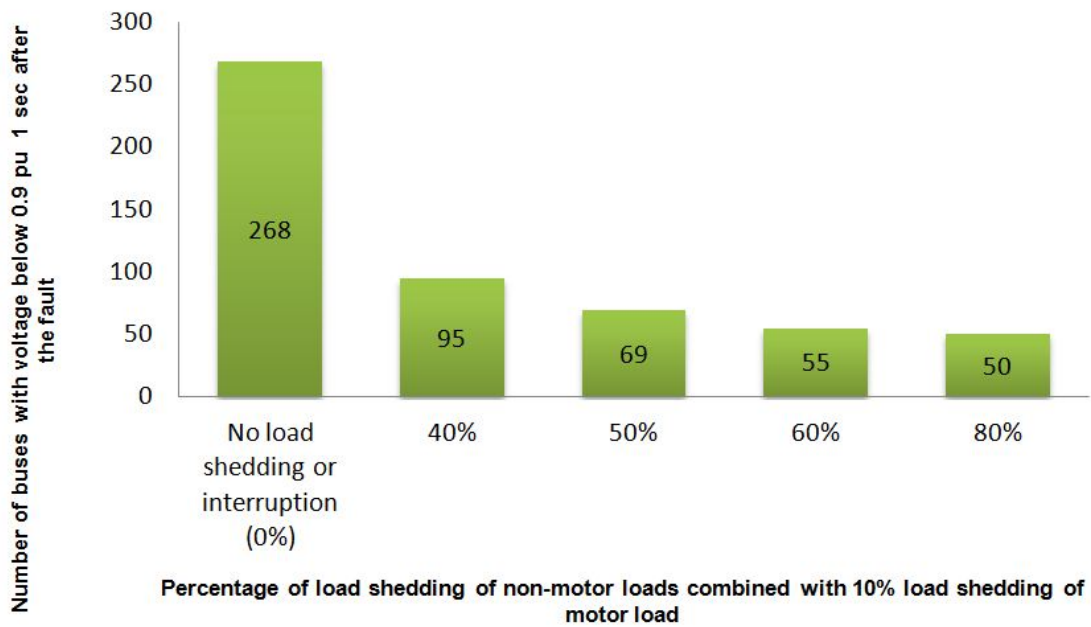


**Figure 5.9:** Total number of load buses with voltage below 0.9 pu at 2s for load shedding various percentages of non-motor loads together with 10% of motor loads.

### 5.3.2 20% load shedding of motors

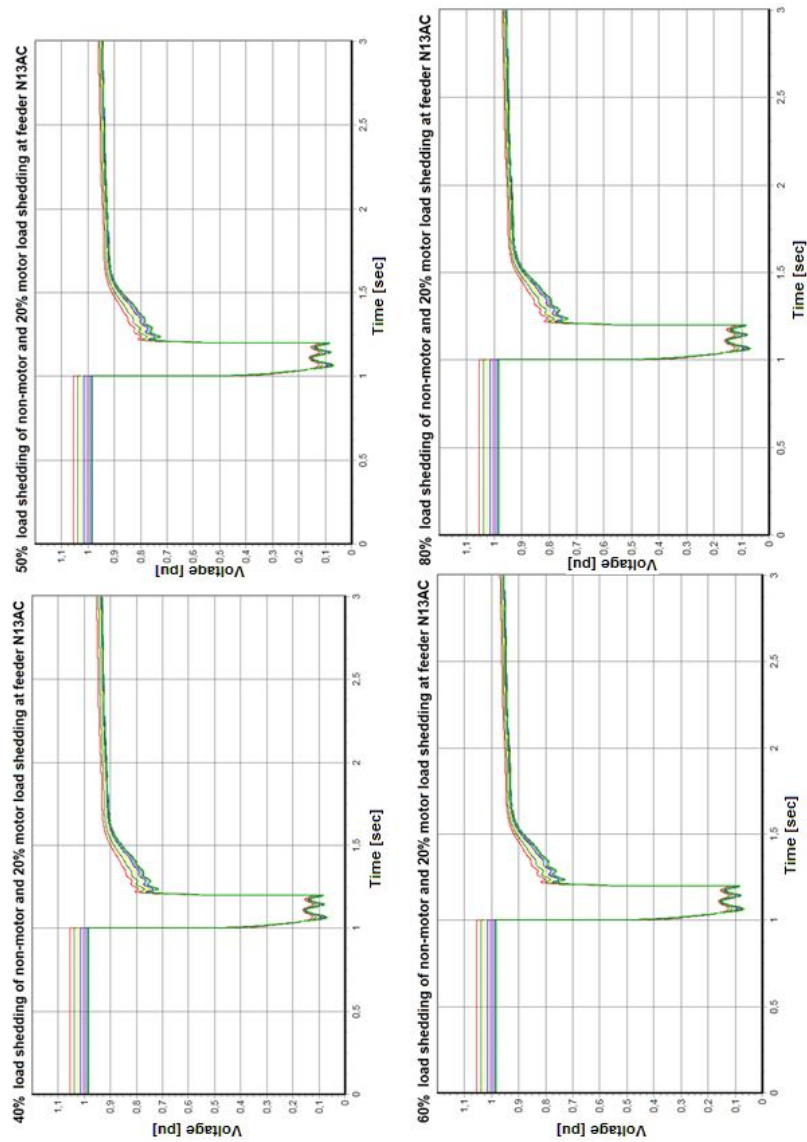


**Figure 5.10:** Load shedding of 20% of motor loads together with various percentages (40%, 50%, 60% and 80%) of non-motor loads.

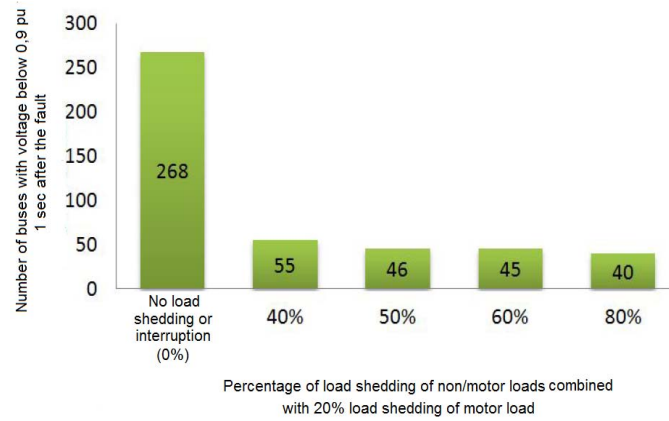


**Figure 5.11:** Total number of load buses with voltage below 0.9 pu at 2 s for load shedding various percentages of non-motor loads together with 20% of motor loads.

### 5.3.3 40% load shedding of motors

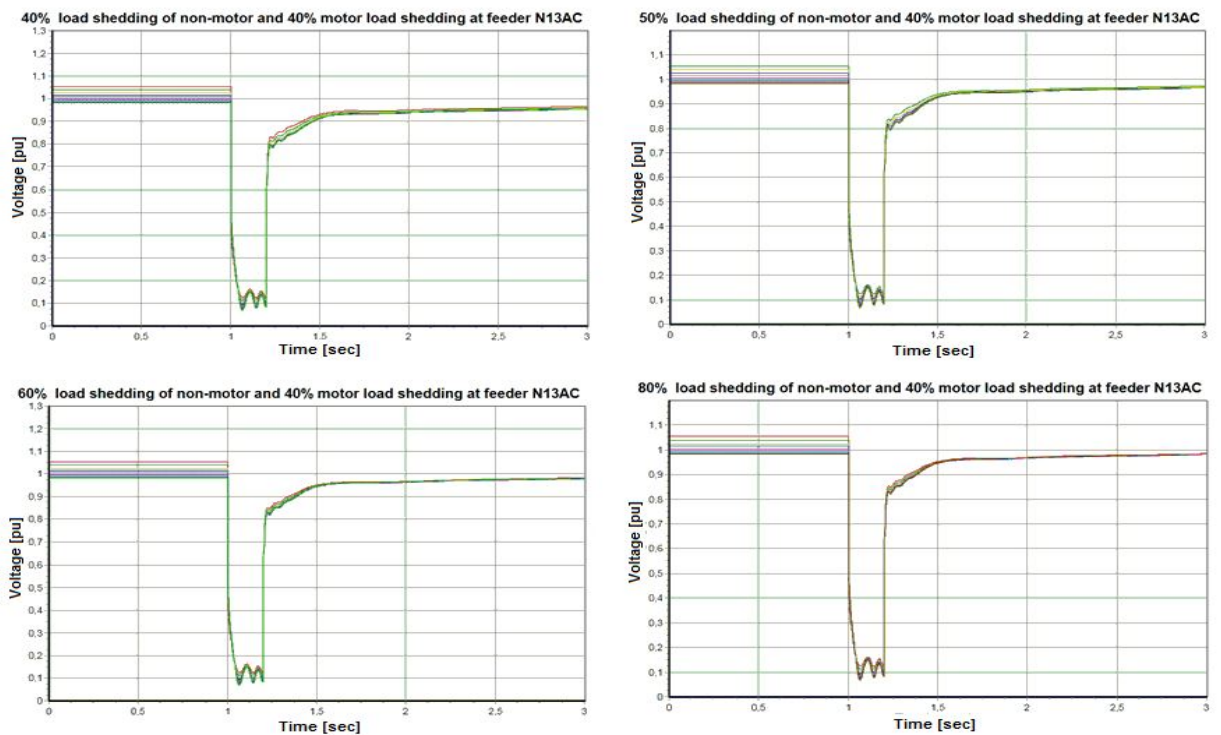


**Figure 5.12:** Load shedding of 40% of motor loads together with various percentages (40%, 50%, 60% and 80%) of non-motor loads.

### 5.3.4 80% load shedding of motors

## 5.4 Load interruption of 40%, 60% and 80% of non-motor loads

In this scenario load interruption of non-motor loads is tested in simulations. The results found in this method for improving voltage stability show that it is possible to reconnect back the load in the network. An interval of 1 second was used for all the reconnections. This criterion was used so as not to introduce a big disturbance during reconnection. This also ensures that there is no big step or steep drop in the voltage during reconnection. The reconnection was first done at buses where the voltage was higher. This was done progressively till load was reconnected to the bus with the lowest voltage. From Figs. 5.17 and 5.18, the recovery of the voltage one second after the disturbance for the various cases can be observed. Fig. 5.19 shows the number of buses with voltage below 0.9 pu at 2 s.

A positive result of this method is the fact that the entire load can eventually be reconnected to the system in 1 s intervals. Four loads were reconnected at a time. The load was therefore saved. It is important to highlight the fact that a combined method of load interruption and using SVCs should be implemented as it has been done in the next Chapter in order to investigate the possibility of all voltages in the entire system recovering above 0.9 pu within 1 second after the fault.

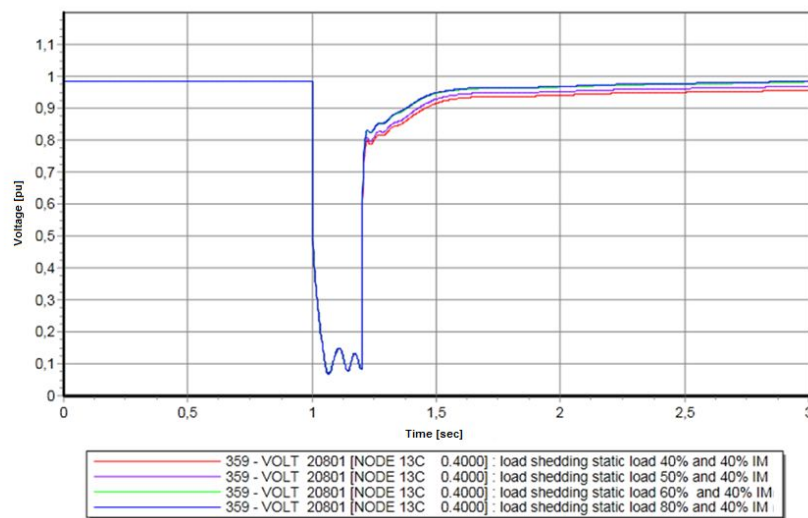


**Figure 5.13:** Voltage at Node 13C for 40%, 50%, 60% and 80% load shedding of non-motor loads with shedding of 40% of motor loads for each case.

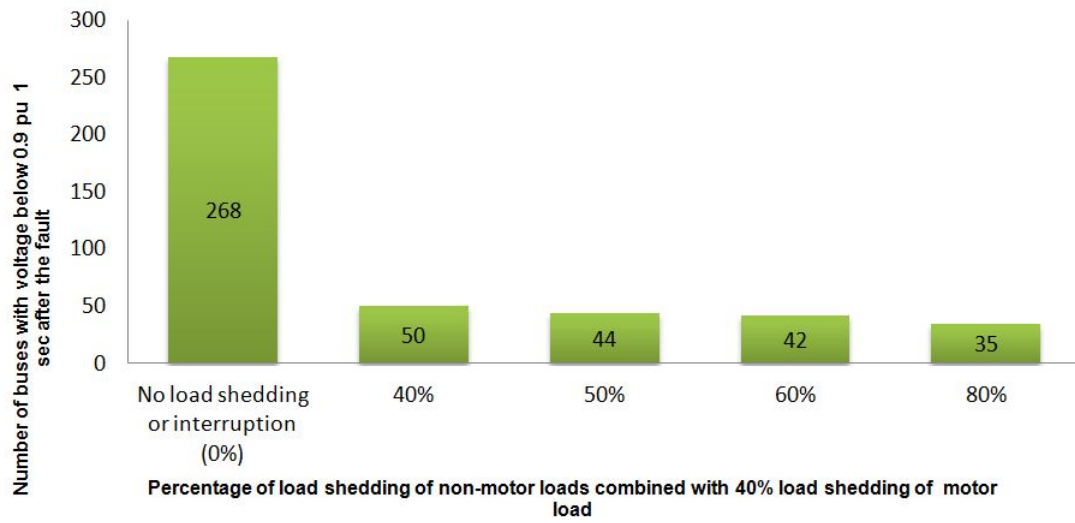


**Figure 5.14:** Total number of load buses with voltage below 0.9 pu at 2 s for load shedding various percentages of non-motor loads together with 40% of motor loads.

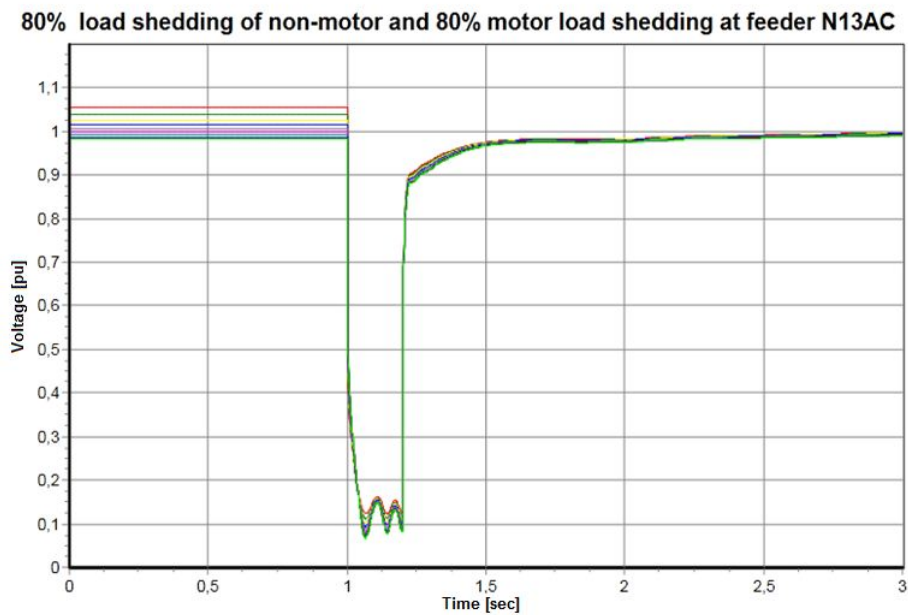


**Figure 5.15:** Load shedding of 80% of motor loads together with 80% of non-motor loads.

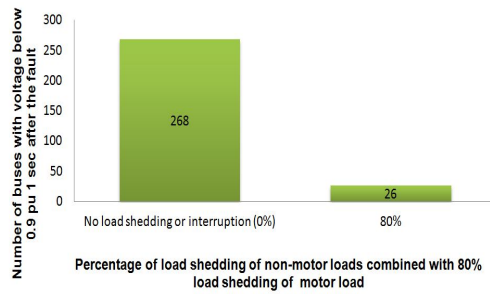


**Figure 5.16:** Total number of load buses with voltage below 0.9 pu at 2 s for load shedding of 80% of non-motor loads together with shedding of 80% of motor loads.

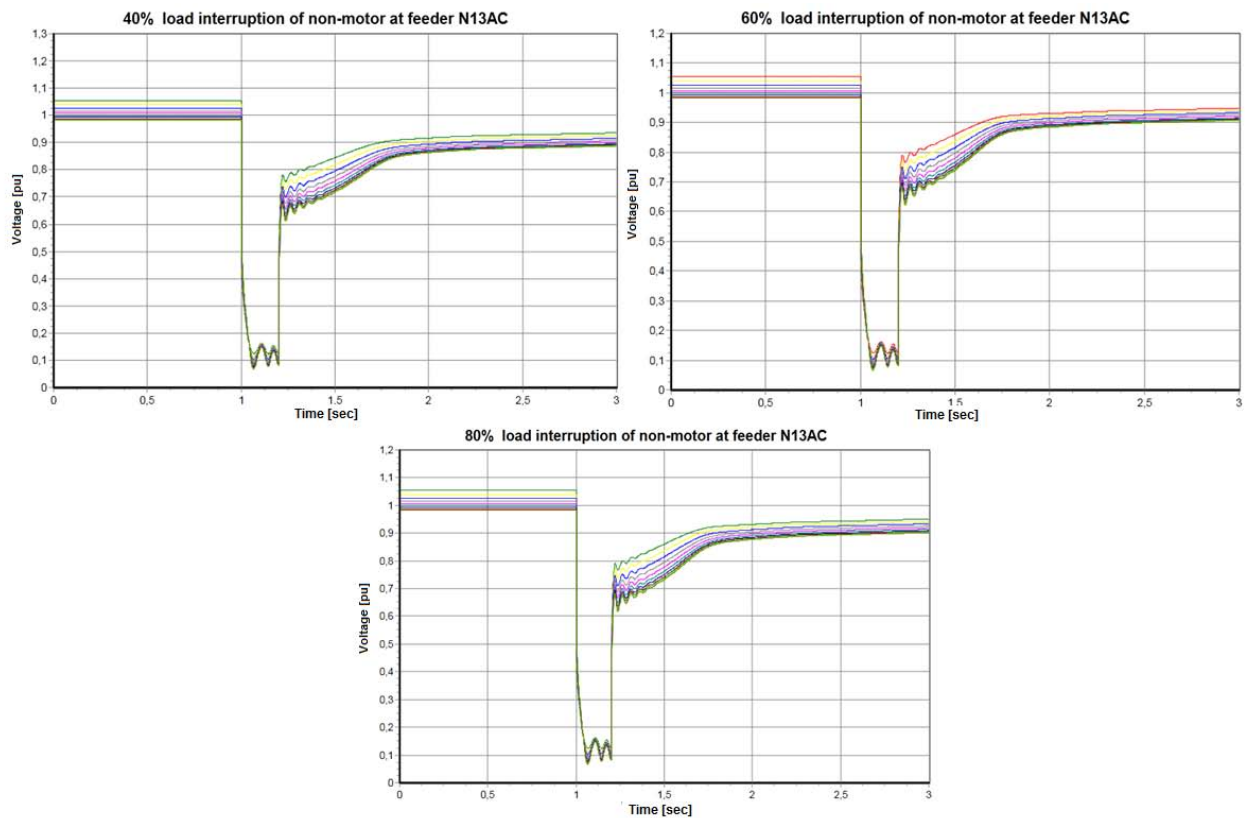


**Figure 5.17:** Voltages at buses on feeder N13AC for various percentages (40%, 60% and 80%, respectively) of interruption of non-motor loads.

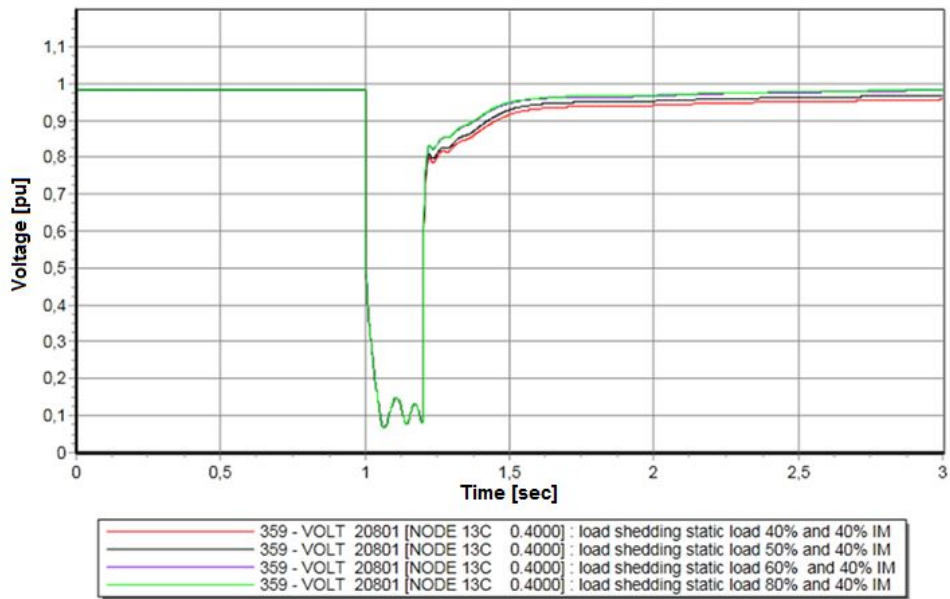


Figure 5.18: Voltage at Node N13C for various percentages (40%, 60% and 80%) of interruption of non-motor loads.

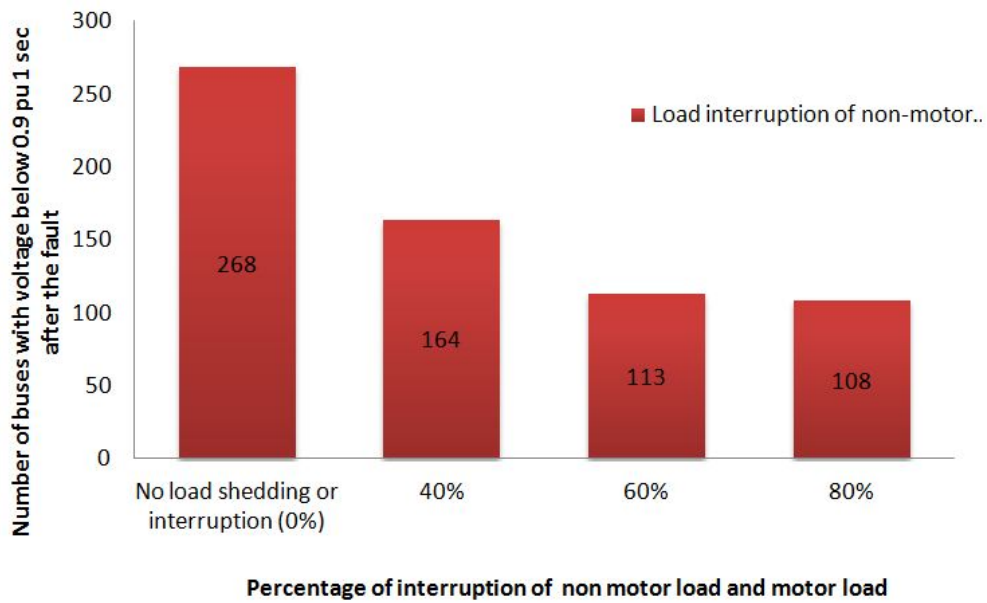
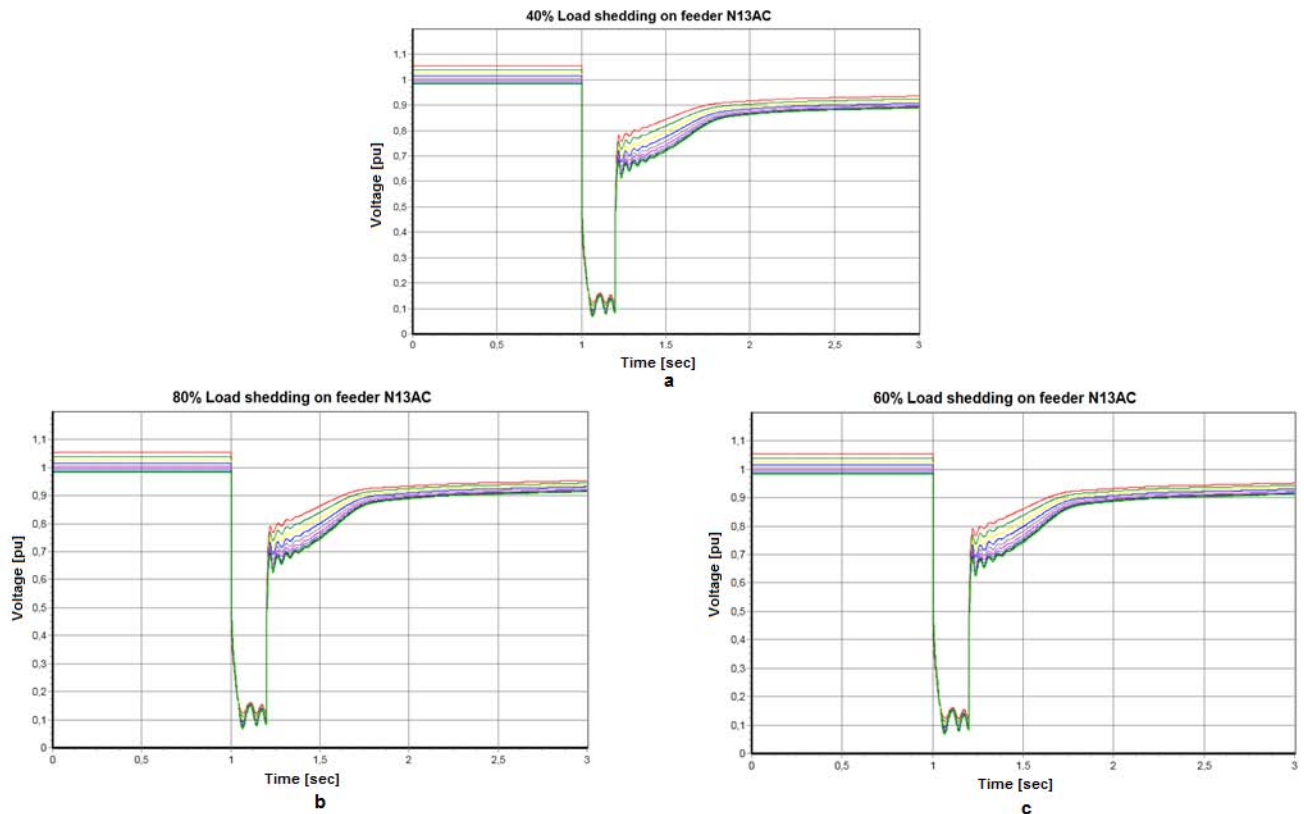


Figure 5.19: Total number of load buses with voltage below 0.9 pu at 2s for the various cases of load interruption of non-motor loads.

## 5.5 Load interruption of 40%, 60% and 80% of non-motor loads together with load shedding of 60% of motor loads.

In this scenario, load interruption of non-motor loads (40%, 60% and 80%) combined with load shedding of motor loads (60%) have been tested. From Fig. 5.20, it is clear to see how the voltage recovers faster with load shedding done as well. An important result that should be highlighted in this scenario is the fact that the voltage recovers faster but a considerable amount of motors are disconnected from the system causing significant economic losses.



**Figure 5.20:** Voltages at buses on feeder N13AC (a, b, c) for various percentages (40%, 60% and 80%) of interruption of non-motor loads and load shedding (60%) of motor loads

In Fig. 5.21, the total amount of buses with voltage below 0.9 pu at 2 s reduces when load shedding is also done apart from load interruption. However, even though 80%

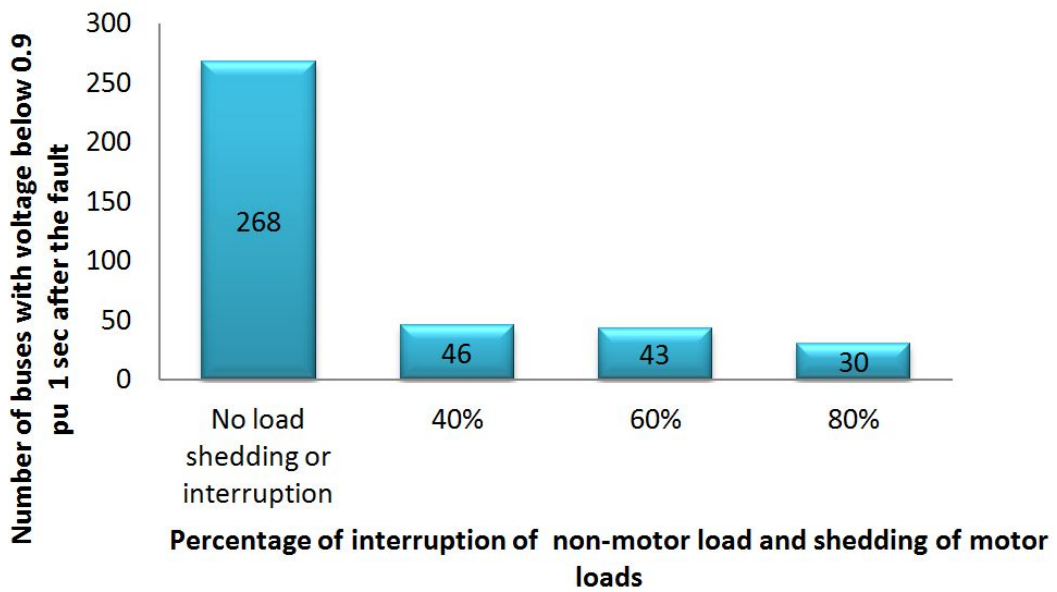


**Figure 5.21:** Total number of load buses with voltage below 0.9 pu at 2 s for various cases of load interruption of non-motor loads with load shedding of 60% of motor loads

of non-motor load is interrupted and 60% of motor load is shed voltages at all buses in the entire system cannot recover above 0.9 pu at 2 s. It is therefore necessary to investigate the scenario where load interruption is combined with the use of SVCs. The main advantage of this scenario compared to the one where load interruption is combined with load shedding is that the load is saved because it is not just disconnected.

# 6

## Improvement of voltage stability by using SVCs

**I**N this chapter, SVCs are used to aid the voltage recovery following the disturbance and the effect is studied. The location in the network and sizes of the SVCs are determined. The duration of the voltage support is also investigated. The same criteria (shown in Fig. 5.1) of voltage recovering to 0.9 pu at 1 s following a disturbance is used. Python scripts were used to automate the dynamic simulations for each one of the various cases.

In PSS/E in order to use the SVC dynamic models in dynamic simulations the SVC should be portrayed as either a switched shunt or a generator in the load flow. The thyristor controlled reactor of the SVC can be put in parallel with an optional capacitor which can be specified in a generator SVC dynamic model such as CSVGN1. The reactive power limits of the generator specified in the power flow should take into account the combined admittance of the inductor and capacitor or only the inductor if the capacitor is not present [52]. This unique treatment of boundary conditions is not needed for the switched shunt. Hence, the recommendation in the PSS/E manual [52] is to portray the SVC as a switched shunt in the load flow. The switched shunt contains both reactors and capacitors [55]. The SVC was modeled as a switched shunt in this project.

Initially, the limits for reactive power output of the switched shunt were set to -9999/9999 Mvar in the power flow. The negative sign indicates inductive admittance in PSS/E. This was done in order to assess the amount of reactive power output that is required to attain a specified voltage at a bus in the initial power flow. This is the procedure that is recommended in the PSS/E manual [55] if such an assessment is to be done. The voltage that was specified for the switched shunt is the same value as the one obtained in the power flow at that particular bus before the switched shunt was connected. This was done so that the pre-disturbance voltage magnitude at the initialization of the dynamic

simulation for the case with and without the SVC is the same. This makes it easy to compare the results of the voltage evolution for the case with and without the SVC during dynamic simulations since the initial conditions are the same. After running the power flow the initial aggregate inductive or capacitive admittance needed to maintain the voltage is obtained. The output of the switched shunt was very low in the power flow in most cases. The control mode of the switched shunt was set to continuous as per instruction in the software manual [52]. This gives a variable shunt inductance and thus variable effective shunt admittance within the rating of the shunt components to regulate the voltage [55]. The dynamic model of the SVC regulates the steps and blocks of the switched shunt during dynamic simulations [52].

The parameters for the maximum and minimum rating of the SVC in Mvar were adjusted in the SVC dynamic model starting with small values and gradually increased until there was no significant improvement in the recovery of the voltage at the bus where the SVC is connected and other nearby buses. The size of the network and the amount of active and reactive power consumed by the load were taken into consideration when determining the initial estimate of the rating of the SVCs. The final rating of each of the SVCs that were connected to the buses at the end of the LV feeders is -0.1/0.3 Mvar (such as Node 13C) and the rating of the ones at the beginning of the LV feeders (such as Node 13A) is -0.25/1 Mvar. Dynamic simulations were run for various scenarios with SVCs located at various points in the network until the recovery of the voltages at all buses in the network met the voltage recovery criterion.

The PSS/E dynamic model of the switched shunt that was used is CSSCST. The block diagram of the model is shown in Fig. 6.1. The parameters of the model were obtained from [10] with a bit of tuning for some of the parameters. The parameters for the models that were used for the lower (-0.1/0.3 Mvar) and higher (-0.25/1 Mvar) rated SVCs are shown in Tables 6.1 and 6.2 respectively. The time constant  $T_5$  estimates delays in the reactor's response to control signals. The time constants  $T_1$  to  $T_4$  enable the transient gain to be reduced and thus a bigger number for the steady-state voltage control gain,  $K$ , can be used. Likewise,  $V_{OV}$  is the set point of the voltage deviation from nominal which results in the reactor being gated all the way on or off (depending on whether the deviation is for voltage rise or voltage drop).  $V_{MAX}$  and  $V_{MIN}$  give the rating of the SVC in Mvar. The description of the parameters is found in [52]. A check to see that the parameters are within the typical limits listed in PSS/E for this model was done using the data checking mode (docu check) function. The reactive power output of the SVCs was plotted by assigning the SVC output admittance (Y) variable of the CSSCST model to an output channel. The channel number was obtained by running the list models and data (docu) function which lists the channels for the models. The admittance is given in pu on system base so it has to be multiplied by the system base (in this case 50 MVA in order to get the actual output admittance of the SVC.

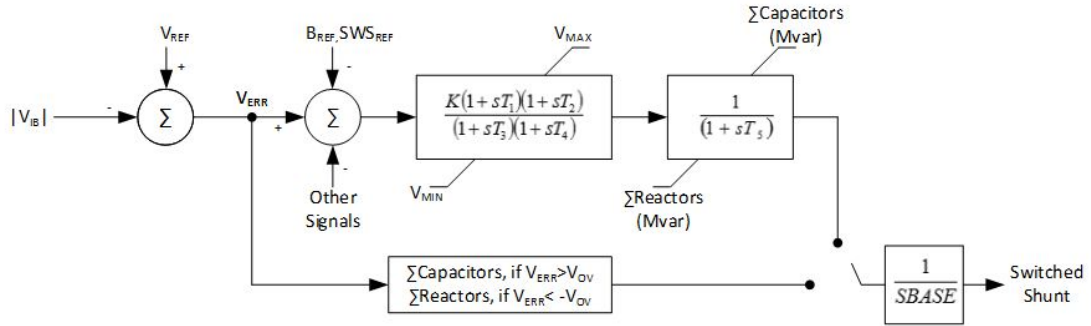


**Figure 6.1:** Block diagram of CSSCST SVC for Switched Shunt model [52].

**Table 6.1:** Parameters for the Switched Shunt SVC model for the SVC rated -0.1/0.3 Mvar

S/N	Description	Value
1	K	10
2	$T_1(s)$	0
3	$T_2(s)$	0
4	$T_3(s)$	0.04
5	$T_4(s)$	0.001
6	$T_5(s)$	0
7	$V_{Max}, MVARs$	0.3
7	$V_{Min}, MVARs$	-0.1
7	$V_{ov}$	0.5

**Table 6.2:** Parameters for the Switched Shunt SVC model for the SVC rated -0.25/1 Mvar

S/N	Description	Value
1	K	10
2	$T_1(s)$	0
3	$T_2(s)$	0
4	$T_3(s)$	0.04
5	$T_4(s)$	0.001
6	$T_5(s)$	0
7	$V_{Max}, MVARs$	1
7	$V_{Min}, MVARs$	-0.25
7	$V_{ov}$	0.5

Initially, the dynamic simulation was run without any SVC connected in the network. A voltage scan was done using the API Python syntax `set_vltscn(status, vhi, vlo)` that checks for voltages which are below and above given thresholds when running the dynamic simulation. `vhi` and `vlo` are the high and low voltage thresholds, respectively. The threshold that was used to check the recovery of the voltage is 0.9 pu and thus this was set as the low voltage threshold. This is in line with the criterion that is used in this thesis of voltage recovering to 0.9 pu within 1 s from the initiation of a disturbance. The voltage scan enabled the number of buses with voltage below 0.9 pu 1 s second after the fault to be determined as well as getting the actual values of the voltage magnitudes. The graphs plotted from the dynamic simulation show a visual presentation of the evolution of the voltages at various buses on the feeders and were also used to check the number of buses with voltage below 0.9 pu 1 s after the fault. Figure 6.2 shows the number of buses with voltage below 0.9 pu at 2 seconds (1 second after the fault is applied) following a disturbance that is applied on one of the lines between Node 1 and Node 2. It was observed that the LV feeders that are furthest from the source of supply of the MV feeder (Node 0) have a larger number of buses with voltage below 0.9 pu 1 s after the disturbance as can be seen in Fig. 6.1. SVCs were placed at various locations in the network following a voltage deviation analysis so as to aid the recovery of the voltage. The voltage deviation analysis was used to locate the feeder with the highest voltage deviation.

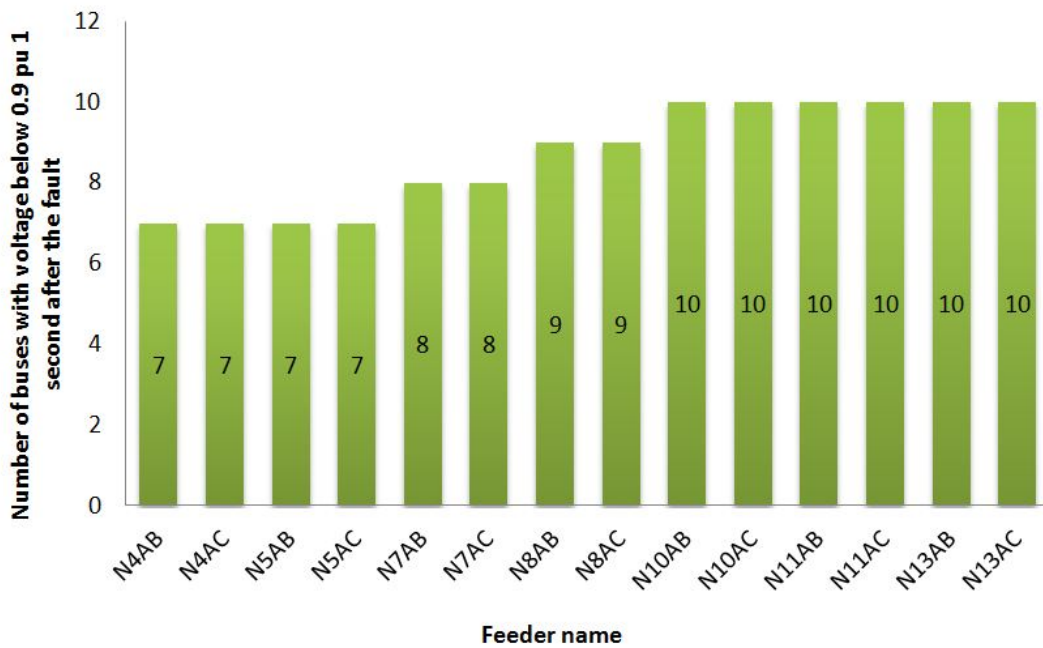


**Figure 6.2:** Number of buses on the various feeders with voltage below 0.9 pu 1 s after the fault (without SVCs).

There are a number of voltage stability indices in the literature. Some of the indices indicate the critical line whilst others show the critical bus in a network which is likely to cause voltage instability or collapse. Indices can also be used to determine the voltage stability margin of a system. The indices predict when voltage instability is likely to occur. In most cases, the values that are used for the indices are in the range of 0 to 1 representing the state of the system from no load to voltage collapse, respectively. There are also indices which can indicate both the critical line and critical bus in a network such as the Fast Voltage Stability Index (FVSI) line stability index developed by [56]. The weakest bus is determined by using the FVSI index to find the maximum allowable load at each bus [56]. Some of the bus voltage stability indices are the Local Indicator (L index) that can show the weakest bus [57], the Voltage Stability Index (VSI) that changes approximately linearly with load [58] and the Stability Index (SI) for radial distribution systems [55]. Some of the line stability indices are the Line Stability Index  $L_{mn}$  [59], Line Stability Index LQP [60] and the Voltage Collapse Proximity Index VCPI [61]. P-V or Q-V curves can also be used as criteria for assessing voltage stability and the margin to instability [62]. The formula for the voltage deviation index that was used in this project is

$$\Delta V = \frac{1}{N} \left[ \sum_{i=1}^N \sqrt{(1 - V_i)^2} \right]. \quad (6.1)$$

A voltage scan was done using the same API Python syntax for checking voltages during dynamic simulations. In this case, a lower voltage threshold of 1 pu was used so as to compare the voltages at the buses on the various feeders with the nominal value as can be seen in the voltage deviation formula. This was initially done without any SVCs in the network. The first SVC was placed on the feeder with the highest voltage deviation then a dynamic simulation was run to check the improvement in voltage recovery that has been achieved. The voltage scan was done again with the first SVC connected then the next SVC was placed on the feeder with the highest voltage deviation and so on.

The results of the voltage deviation calculations for the first case without SVCs are shown in Table 6.3 It can be seen from the table that feeder N11AC has the highest voltage deviation index.

**Table 6.3:** Voltage Deviation on the various LV feeders

Feeder Name	Voltage Deviation
N4AB	0.1136
N4AC	0.1136
N5AB	0.1165
N5AC	0.1177
N7AB	0.1316
N7AC	0.1316
N8AB	0.15
N8AC	0.15
N10AB	0.1635
N10AC	0.1635
N11AB	0.1777
N11AC	0.1804
N13AB	0.1751
N13AC	0.1751

## 6.1 Simulation results

The objective of using SVCs is to ensure that the voltage recovers to 0.9 pu within 1 s after the fault is applied. The voltages at the buses on the various feeders were therefore checked to see if they meet this criteria after connection of SVCs at different points. The results of the simulations are shown in the subsections that follow.

### 6.1.1 SVC placed at Node 11C

The first connection point of the SVC was at Node 11C, which is the furthest bus from the source on feeder N11AC. This is because calculations of the voltage deviation index showed that feeder N11AC had the highest deviation 1 second after the fault was applied as can be seen in Table 6.3. The results of the simulation are shown in Fig. 6.3 below. It can be seen from the figure that all the bus voltages on feeder N11AC recover to 0.9 pu within the stipulated time of 1 s whereas non of them had recovered without the SVC as shown in Fig. 6.2. However, the effect on the other feeders is minimal. This could be due to the small size of the SVC, which is rated -0.1/0.3 Mvar and the fact that the SVC is connected at the end of the feeder. The faster recovery of the voltage is mainly at buses that are in close proximity to the bus where the SVC is connected. On feeders 10AB and 10AC the voltage on one of the buses recovers to 0.9 pu within 1 second on each feeder compared to non without the SVC as can be seen in Figs. 6.2 and 6.3. Increasing the size

of the SVC any further did not provide any significant improvement in the recovery of the voltage and the number of buses with voltage recovering to 0.9 pu within one second did not increase.

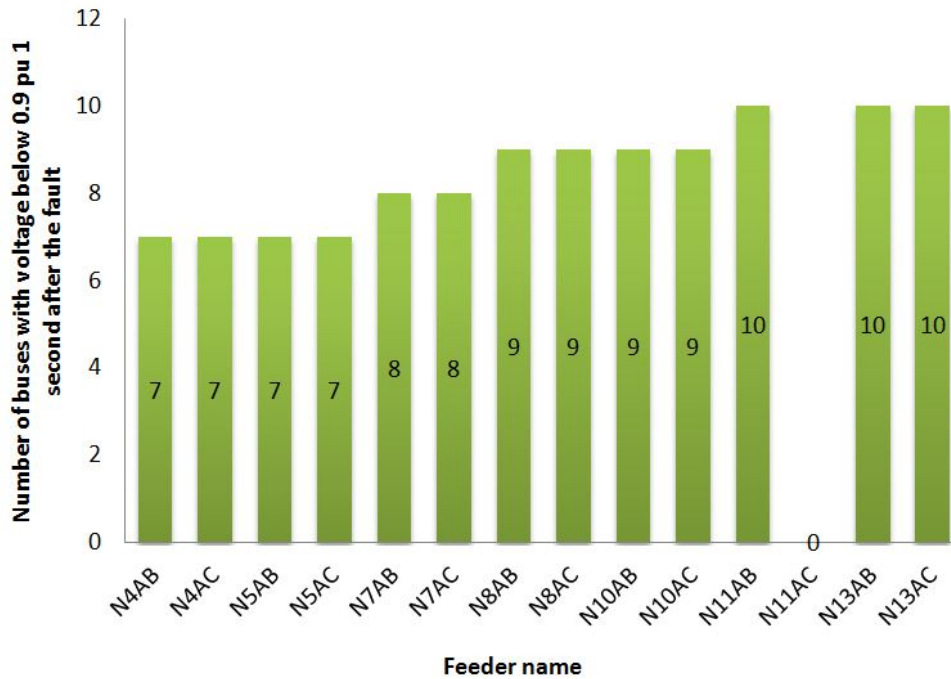
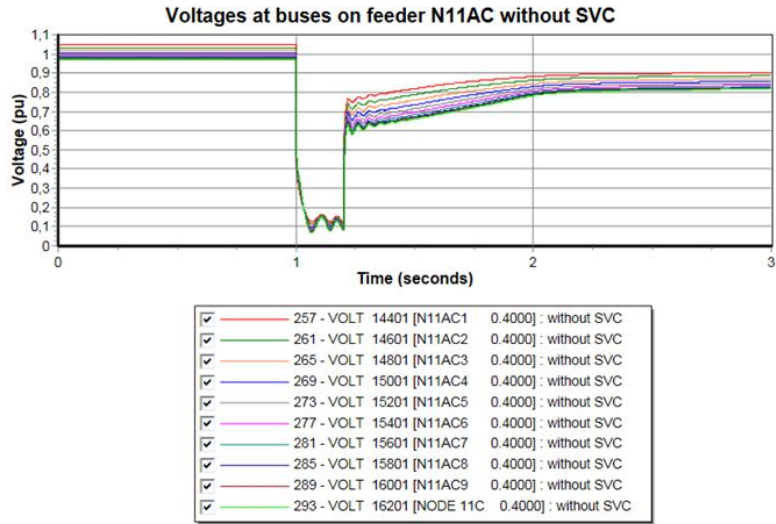


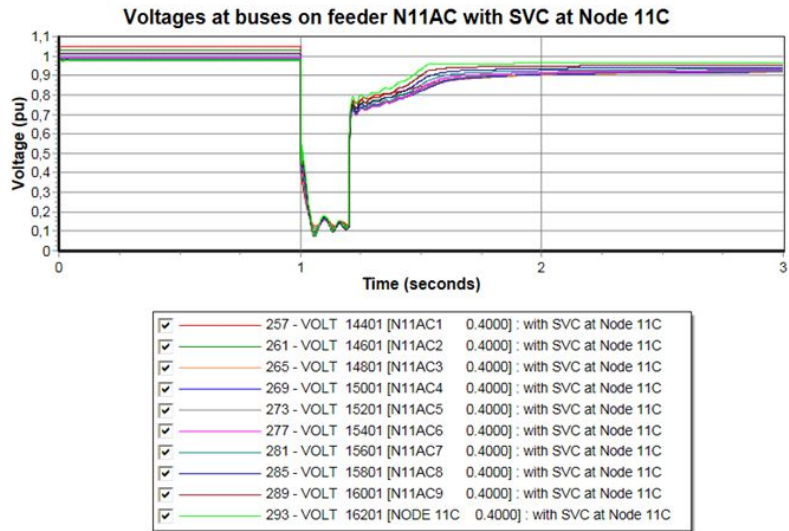
**Figure 6.3:** Number of buses with voltage below 0.9 pu on the various feeders 1 s after initiation of the fault (with SVC at Node 11C)

The evolution of the voltages at the buses on feeder N11AC with and without the SVC at Node 11C is shown in Figs. 6.4 and 6.5. The voltages at the buses drops to almost zero at 1 s when the fault is applied and starts to recover at 1.2 s after the fault has been cleared by tripping of the line between Node 1 and Node 2 where the fault is located. As can be seen in the figure all the voltages on feeder N11AC recover above 0.9 pu within 1 s after the fault is applied with the SVC connected at Node 11C as opposed to non without the SVC. The bus with the slowest voltage recovery without the SVC (Node 11C) which is at the end of the LV feeder has the fastest recovery with the SVC. This is so because the SVC is connected to that bus.



a)

Figure 6.4: Voltages at buses on feeder N11AC without SVC (a) at Node 11C



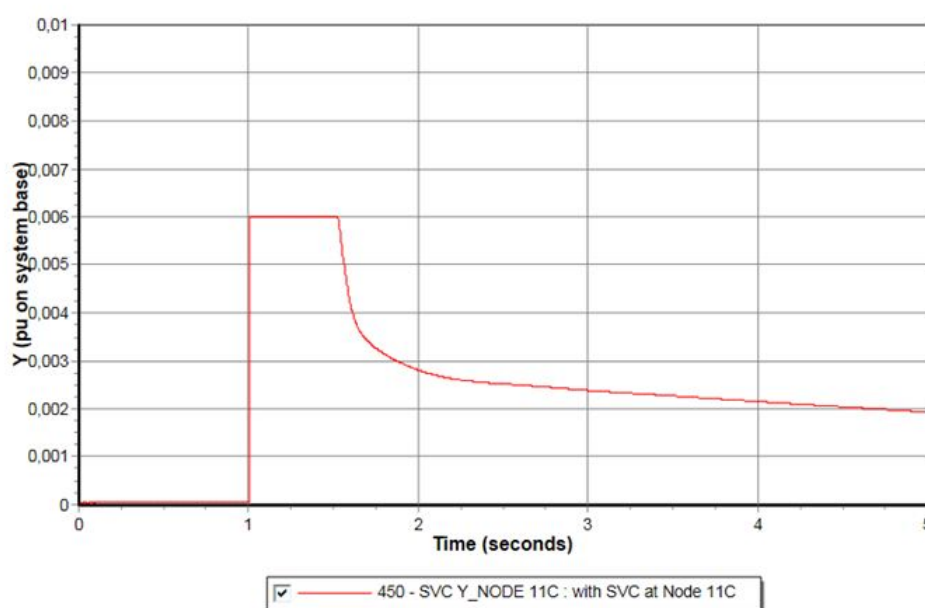
b)

Figure 6.5: Voltages at buses on feeder N11AC without with SVC (b) at Node 11C

The SVC output admittance is shown in Fig. 6.6. The admittance is given in pu on system base. It has to be multiplied by the system base to get the actual output admittance of the SVC. In this case, the maximum output admittance of 0.006 pu on system base during the fault shown in the figure gives a maximum output of

$$Y_{SVC} = Y_{system\ base} \times S_{base} = 0.3Mvar, \quad (6.2)$$

where  $Y_{system\ base}$  is the output admittance of the SVC in pu on system base and  $S_{base}$  is the system base (50MVA).



**Figure 6.6:** SVC output admittance (with SVC at Node 11C)

As can be seen in Fig. 6.6 there is almost no reactive power output from the SVC up to 1s when the fault is applied. The output before the disturbance is the same as the one obtained in the load flow solution. At 1s following the fault the reactive power output increases immediately and reaches a maximum value where the output admittance is 0.006 pu on system base. This gives an output admittance of 0.3 Mvar as shown in Eq. (6.2) which essentially corresponds to the SVC maximum capacitive rating of 0.3 Mvar. This could be due to the presence of an extra controller in the CSSCST SVC model which checks for voltage deviation beyond a given threshold value (override voltage,  $V_{OV}$ ). If the voltage magnitude diverges from nominal by  $V_{OV}$  per unit then the SVC injects or absorbs its maximum rated reactive power. This can happen, for instance, if there is a disturbance and severe voltage drop or if the disturbance is near the bus where the SVC is connected. The override voltage is one of the parameters that have to be specified in the SVC model as can be seen in Tables 6.1 and 6.2. The range

that is given in the PSS/E manual is  $0.1 \geq V_{OV} \leq 0.5$  pu [52]. In this case, it was set to 0.5 pu. When the fault is applied the voltage goes down to slightly below 0.1 pu as can be seen in Figs. 6.4-6.5 and so the deviation is more than 0. pu. The fault is cleared at 1.2s so the fault is for 0.2s. The maximum output admittance is sustained until a few ms after the fault is cleared. The output then starts to decrease until it eventually reaches the pre-disturbance level.

### 6.1.2 SVC connected to Node 11B and 11C

The nodes with the highest voltage deviation index are Node 11B and Node 11C as shown in Table 6.3. Two SVCs each with a rating of -0.1/0.3 Mvar were thus connected to Node 11B and 11C respectively instead of only one at Node 11C as is the case in the previous subsection so as to assess and compare the effect. The results are illustrated in Fig. 6.7. The improvement in voltage recovery is mostly limited to the two feeders were the SVCs are connected as can be clearly seen in the figure. There is a marginal improvement on the adjacent and nearby feeders (feeder N13AB, N13AC, N10AB, N10AC, N8AB, N8AC, N7AB and N7AC) where voltage recovers above 0.9 pu on one more bus on each of the feeders with the SVCs connected compared to the case without them.

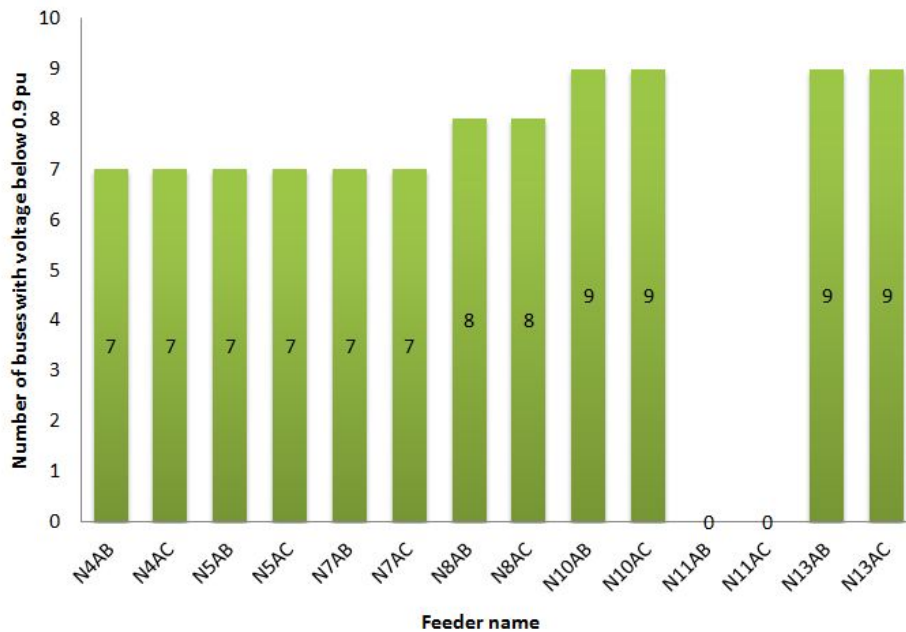


**Figure 6.7:** Number of buses with voltage below 0.9 pu on the various feeders 1s after initiation of the fault (with SVCs at Nodes 11B and 11C)

The evolution of the voltages at the various buses on feeder N11AB and N11AC with and without the SVCs is shown in Figs. 6.8 - 6.10. As can be seen in the figures, all the voltages on the two feeders recover above 0.9 pu 1 s after the disturbance with the SVCs connected to bus N11AB and N11AC whereas non do so without the SVC.

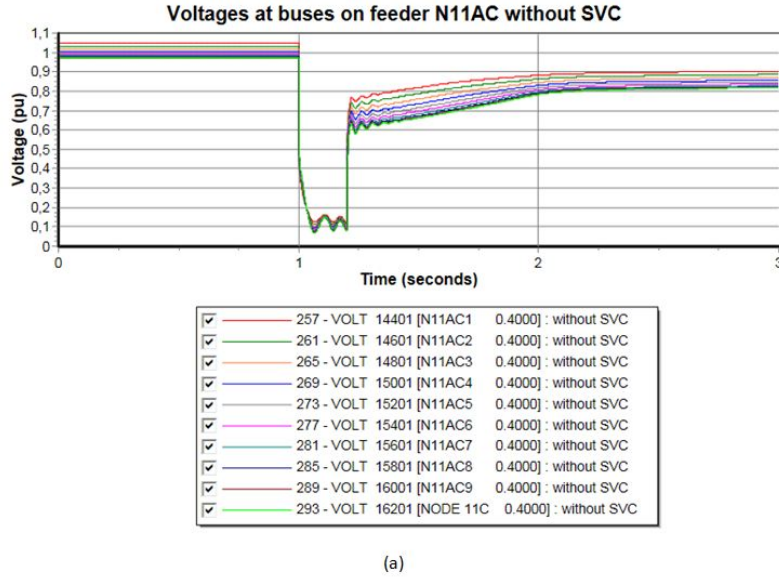


**Figure 6.8:** Voltages at buses on feeder N11AC without SVC (a)

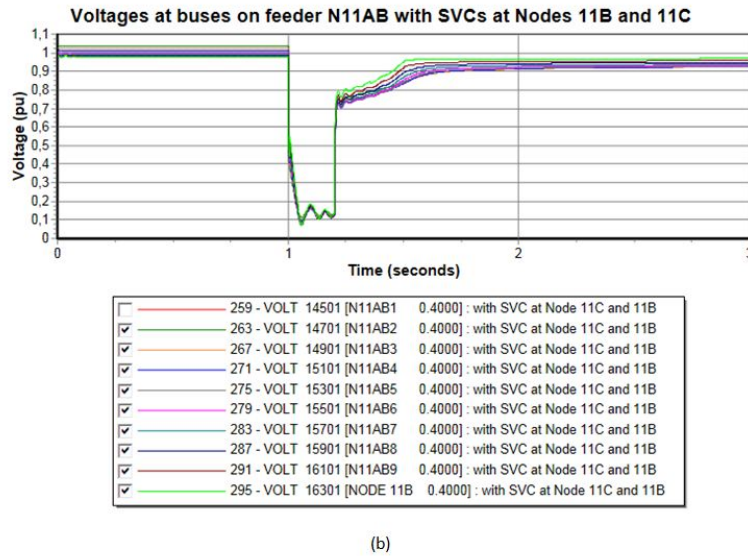
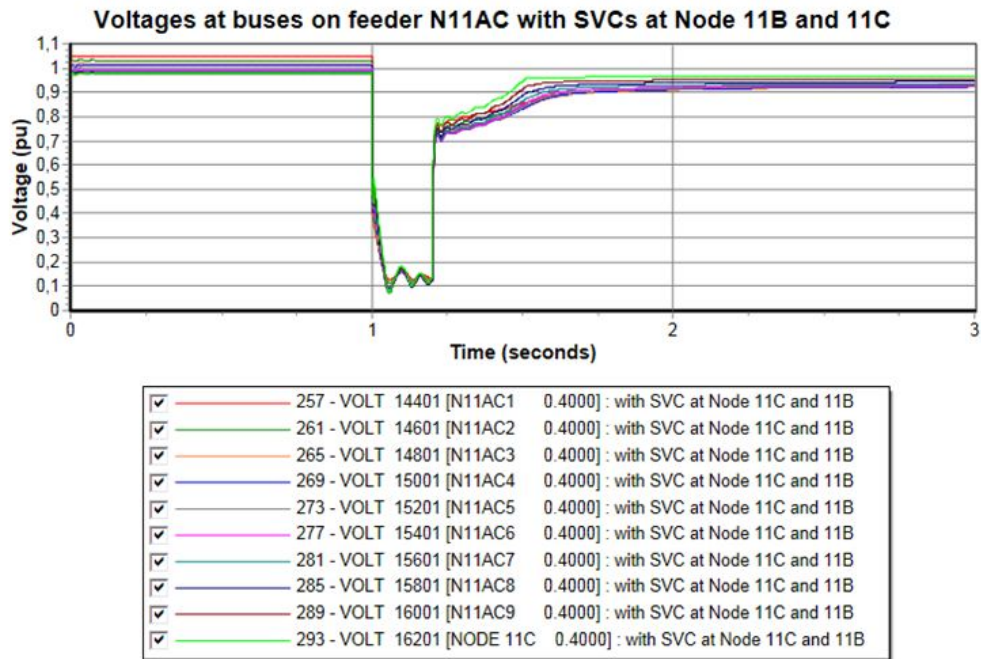


**Figure 6.9:** Voltages at buses on feeder N11AB with SVCs at Nodes 11B and 11C (b)



(c)

**Figure 6.10:** Voltages at buses on feeder N11AC with SVCs at Nodes 11B and 11C (c)

From the simulations, the reactive power output for this case for each SVC is similar to the case shown in Fig. 6.6 where the SVC is connected to Node 11C.

The results presented in the above figures indicated that the improvement in voltage recovery is mostly limited to the two feeders where the SVCs are connected. Next, the study of the Thesis will continue with the connection of the SVC to Node N11AC5.

### 6.1.3 SVC connected to Node N11AC5

In this case, the SVC was connected to bus N11AC5 which is in the middle of feeder N11AC. The results are shown in Fig. 6.11. There is a slightly lower number of buses with voltage below 0.9 pu 1 second after the fault than the case where the SVC is placed at the end of the feeder. However, the improvement is not significant since the voltage on only one additional bus per feeder recovers above 0.9 pu within 1 second compared to the case where the SVC is at the end of the feeder. This is apart from feeder N5AC, N10AB and N10AC where the result is the same for the two cases.

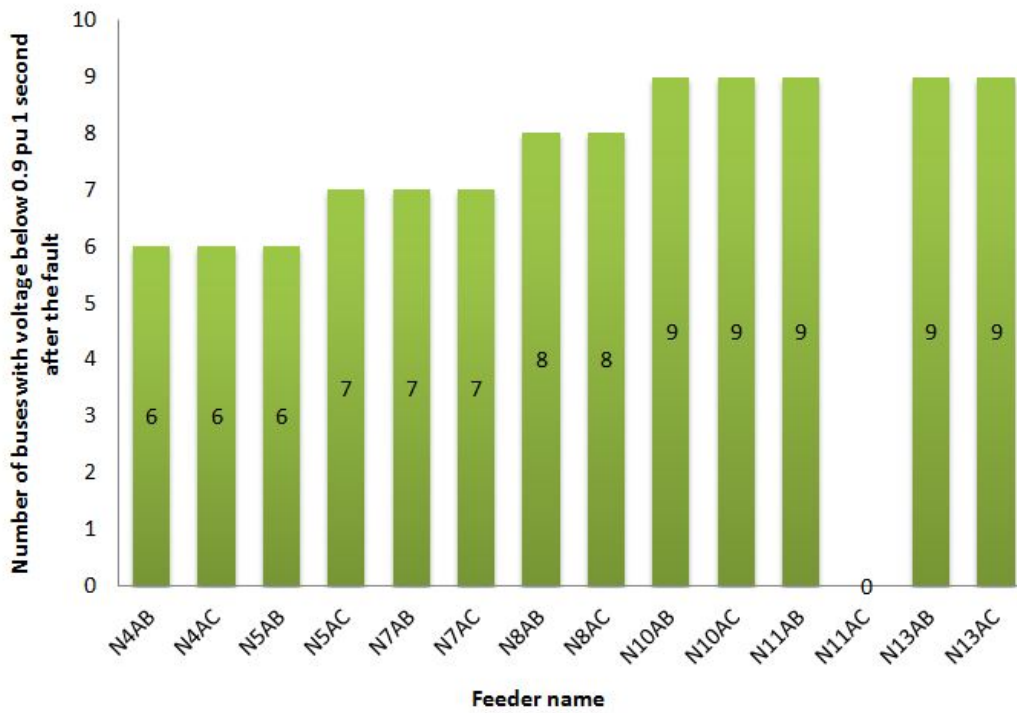
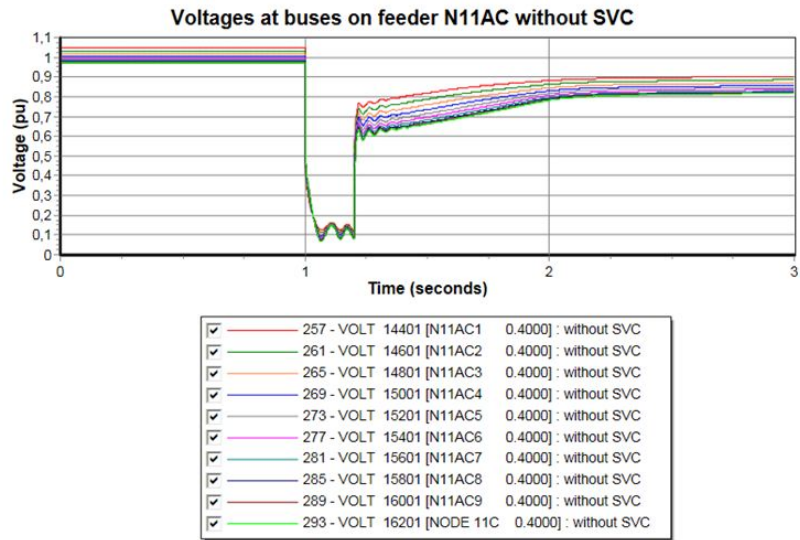


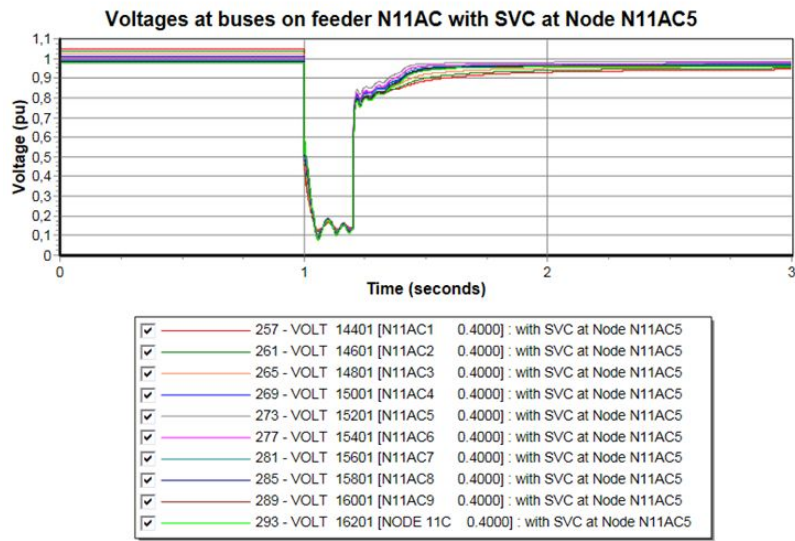
**Figure 6.11:** Number of buses with voltage below 0.9 pu on the various feeders 1 s after initiation of the fault (with SVC at Node N11AC5)

The progression of the voltages at the various buses on feeder N11AC with and without the SVC is shown in Figs. 6.12 and 6.13. From the figure, it can be observed that all the voltages recover above 0.9 pu 1 s after the disturbance with the SVC connected to bus N11AC as opposed to non without the SVC.



(a)

**Figure 6.12:** Voltages at buses on feeder N11AC without SVC (a)



(b)

**Figure 6.13:** Voltages at buses on feeder N11AC with SVC at Node N11AC5 (b)

The SVC output admittance is shown in Fig. 6.14. The maximum admittance output of 0.01 pu on system base (0.5 Mvar when multiplied by system base) is higher than the case where the SVC is connected to the end of the feeder which is 0.006 pu (0.3 Mvar) giving an SVC with a higher rating if it is connected in the middle of the feeder (-0.125/0.5 Mvar compared to -0.1/0.3 Mvar).

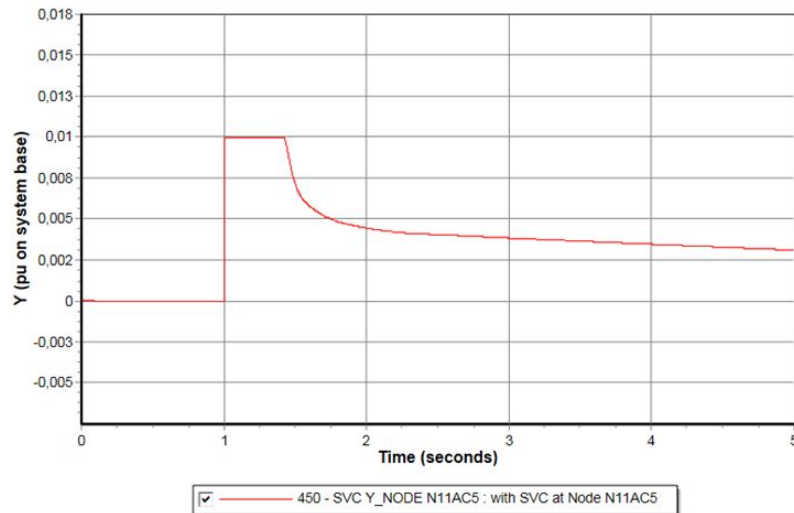


**Figure 6.14:** SVC output admittance (with SVC at Node N11AC5)

#### 6.1.4 SVCs connected to Node 13C, 13B, 11C, 11B, 10C, 10B, 8C, 8B, 7C, 7B, 5C and 5B

SVCs were connected to the end of the 12 feeders (Node 13C, 13B, 11C, 11B, 10C, 10B, 8C, 8B, 7C, 7B, 5C and 5B) according the voltage deviation indices shown in Table 6.3. The feeders with the least deviation indices are feeders N4AB and N4AC. The SVCs were not connected to the two aforementioned feeders. The SVCs were connected at the end of the feeders since the difference in the recovery of the voltages between the case where the SVC is placed at the end of a feeder and the one where it is placed in the middle is not big but the rating is lower for the former case. The results of the simulation are shown in Fig. 6.15. As can be seen, voltages on five buses on feeder N4AB and another five on feeder N4AC still do not recover to 0.9 pu within 1 second after the disturbance.

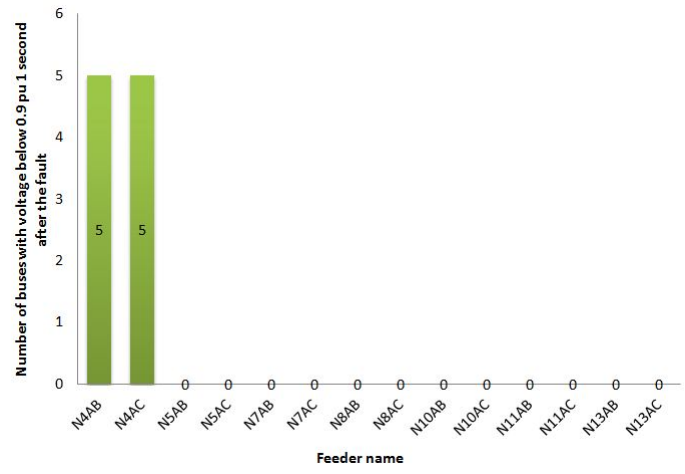


**Figure 6.15:** Number of buses with voltage below 0.9 pu on the various feeders 1 s after initiation of the fault (with SVCs at Node 13C, 13B, 11C, 11B, 10C, 10B, 8C, 8B, 7C, 7B, 5C, 5B)

The output admittances of the SVCs are shown in Fig. 6.16. The maximum output is the same for each SVC. However, there is a slight difference after the clearing of the fault when the outputs start decreasing. This may be explained by the fact that there is more SVC reactive power output at buses where the voltage deviation is higher.

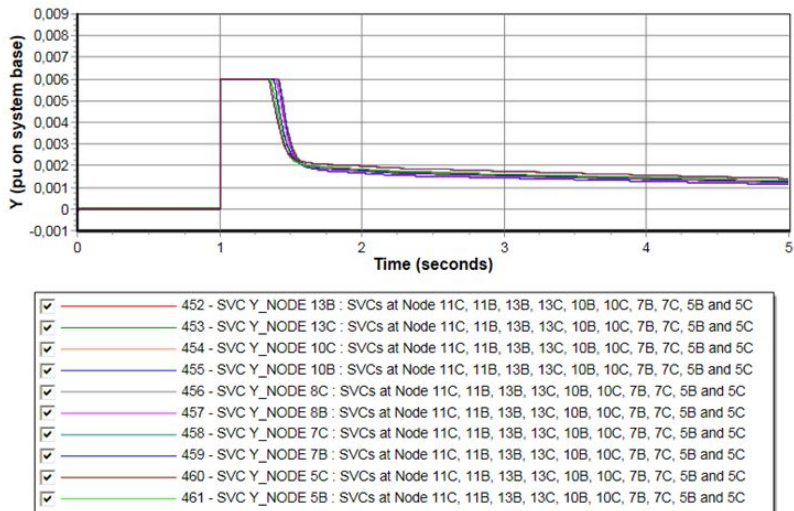


**Figure 6.16:** SVC output admittances (with SVCs at Node 13C, 13B, 11C, 11B, 10C, 10B, 8C, 8B, 7C, 7B, 5C, 5B)

Thus, it follows that an SVC has to be placed on the bus at the furthest point of each feeder in order to have all the voltages in the network recovering to 0.9 pu within one second after the initiation of a fault. This gives a total of 14 SVCs each with a rating of -0.1/0.3 Mvar.

### 6.1.5 SVC placed at Node N11A

An SVC was connected to Node N11A at the beginning of feeders N11AB and N11AC so as to see the effect on the recovery of the voltages following the disturbance. The rating of the SVC is -0.25/1 Mvar. The SVC was placed at this bus because feeders N11AB and N11AC had the highest voltage deviation indices as can be seen in Table 6.3. The results are shown in Fig. 6.17. There is a significant improvement in the recovery of the voltage on the various feeders compared to the case where a smaller sized SVC (-0.1/0.3 Mvar) is connected at the end of either one of the two feeders. The number of buses with voltage below 0.9 pu is much lower and this trend is more uniformly spread with only feeders N8AB and N8AC having one more bus (6 buses) with voltage below 0.9 pu with the other feeders having 5 buses. However, not all bus voltages on feeders N11AB and N11AC fulfil the voltage recovery criterion in this case.

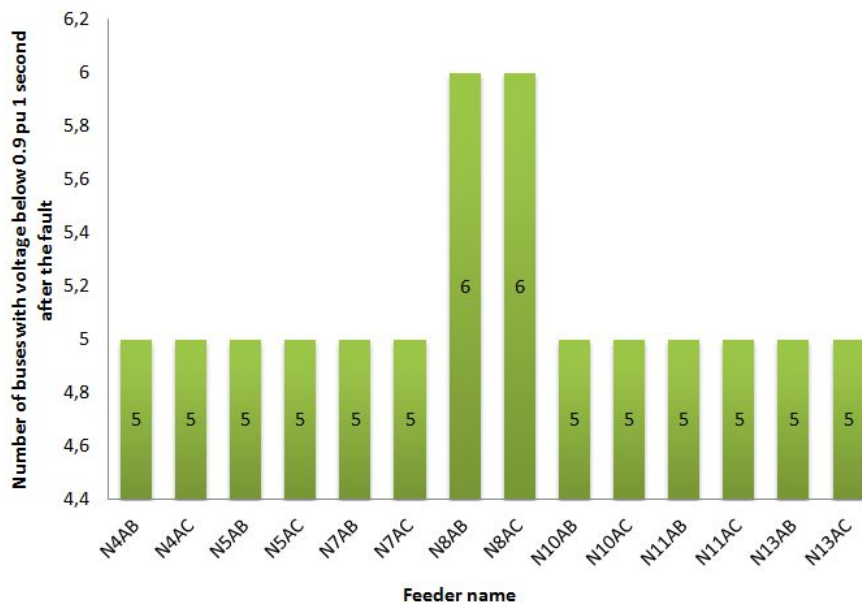
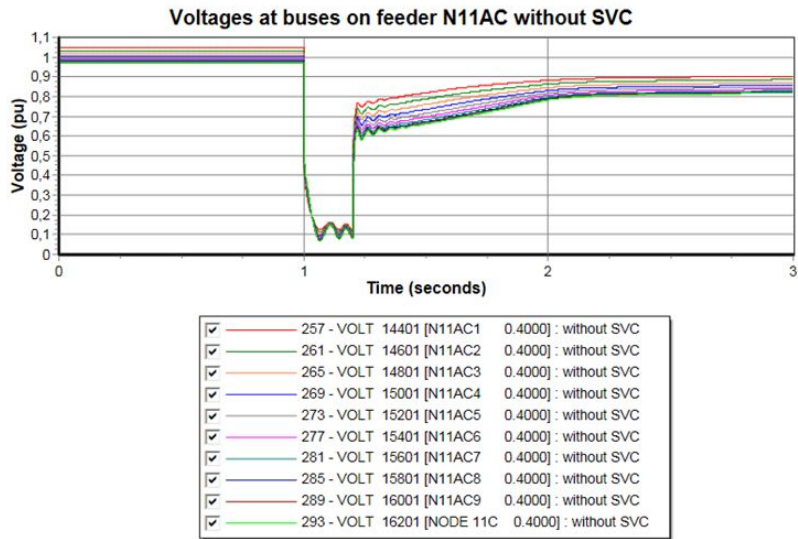


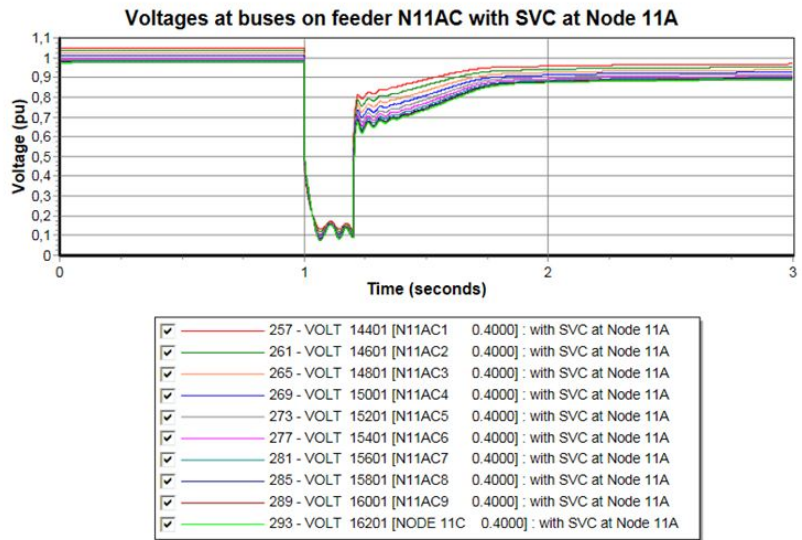
**Figure 6.17:** Number of buses with voltage below 0.9 pu on the various feeders 1 s after initiation of the fault (with SVC at Node 11A)

The progression of the voltages at buses on feeder N11AC is shown in Figs. 6.18 and 6.19 . Not all the voltages at buses on feeder N11AC recover above 0.9 pu in this case. This could be due to the distance from Node N11A where the SVC is connected to the buses at the end of the feeder despite the rating of the SVC being higher. Similar results are obtained for the evolution of voltages on feeder N11AB.



(a)

Figure 6.18: Voltages at buses on feeder N11AC without SVC (a).



(b)

Figure 6.19: Voltages at buses on feeder N11AC without with SVC at Node 11A (b).

The output admittance of the SVC is shown in Fig. 6.20. The maximum output in this case is 0.02 pu on system base (1 Mvar). The initial output admittance is slightly above zero. The possible explanation for this is that the SVC contributes to maintaining the voltage in steady state in the load flow solution with this output. Hence, the same output is maintained in the initial conditions pre-disturbance.

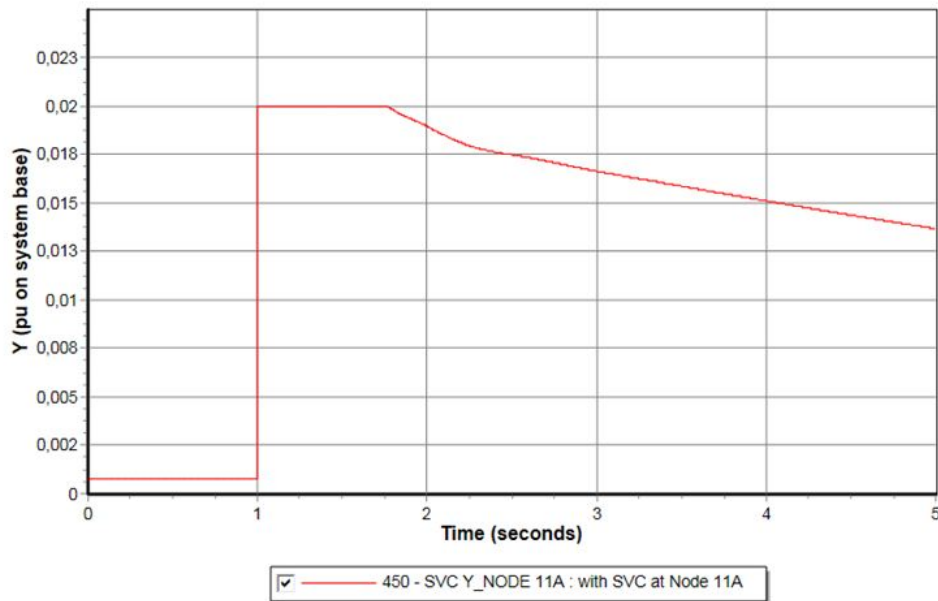


**Figure 6.20:** SVC output admittance (with SVC at Node 11A).

### 6.1.6 SVCs placed at Node 11A and 13A

Since the feeders with the highest voltage deviation indices are feeder N11AB, N11AC, N13AB and N13AC the SVCs were now connected to Node 11A and Node 13A. Node 11A supplies feeder N11AB and N11AC while Node 13A supplies feeder N13AB and N13AC. The results are shown in Fig. 6.21. In this scenario, all the voltages at buses on feeder N10AB, N10AC, N11AB, N11AC, N13AB and N13AC recover above 0.9 pu within 1 s. Most of the voltages at buses on the other feeders also recover within 1 s.

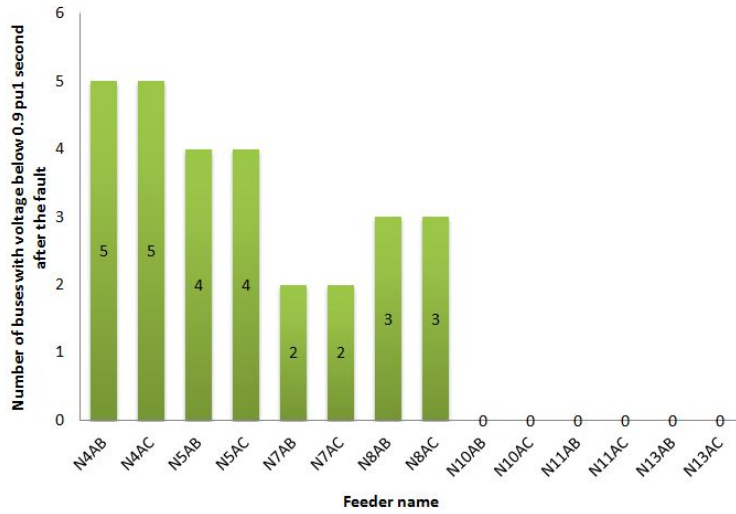


**Figure 6.21:** Number of buses with voltage below 0.9 pu 1 second after the fault on the various feeders (with SVCs at Node 11A and 13A).

The output admittances of the SVCs are shown in Fig. 6.22. The maximum output of both SVCs is 0.02 pu (1 Mvar). However, the reduction in the output is faster for the SVC connected to Node 13A. This is due to the fact that the voltage deviation index for feeder N13AB and N13AC (which are fed from Node 13A) is lower than the one for feeder N11AB and N11AC (which are fed from Node 11A).

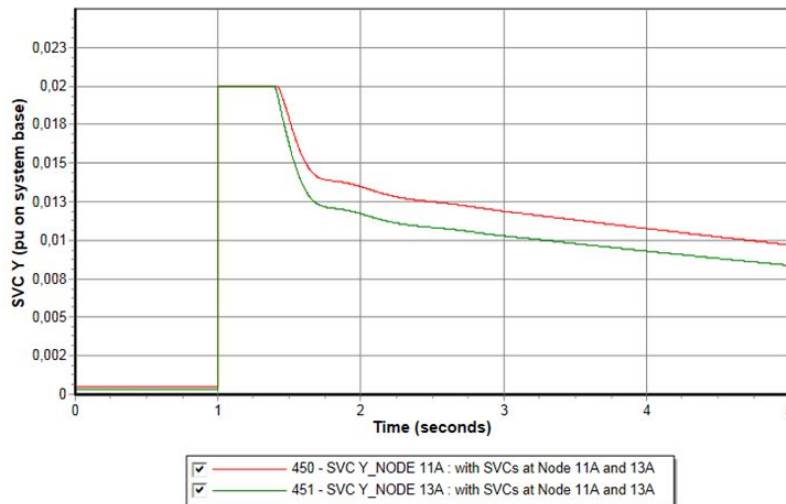


**Figure 6.22:** SVC output admittances (with SVCs at Nodes 11A and 13A).

### 6.1.7 SVCs placed at Node 4A, 11A and 13A

The voltage deviation was re-calculated using the simulation results from the case where the SVCs are connected to Node 11A and Node 13A with the voltage scan API Python syntax enabled. The results are shown in Table 6.4 (see below). It can be seen from the table that feeder N4AB and N4AC have the highest voltage deviation indices. Thus, an SVC is connected to Node 4A as well.

**Table 6.4:** Voltage Deviation on the various LV feeders with SVCs connected to Node 11A and 13A

Feeder Name	Voltage Deviation
N4AB	0.0906
N4AC	0.0906
N5AB	0.08195
N5AC	0.08327
N7AB	0.07388
N7AC	0.07388
N8AB	0.08007
N8AC	0.08007
N10AB	0.06683
N10AC	0.06683
N11AB	0.0645
N11AC	0.06713
N13AB	0.04898
N13AC	0.04898

The results of the simulation with SVCs connected to NODE 4A, 11A and 13A are shown in Fig. 6.23. It can be seen that almost all the voltages at the various buses recover above 0.9 pu within 1 s apart from voltages at a total of 4 buses on feeder N4AB and N4AC (two on each feeder).

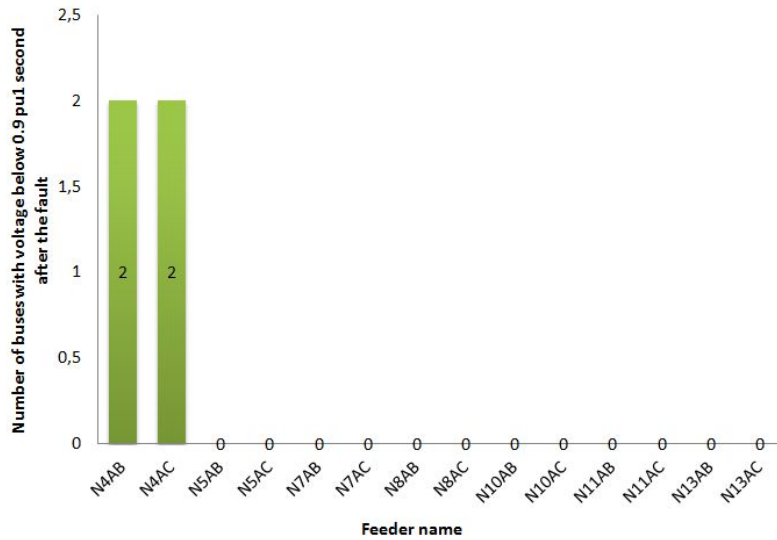


**Figure 6.23:** Number of buses with voltage below 0.9 pu at 2s on the various feeders (with SVCs at Node 4A, 11A and 13A).

The output admittances of the SVCs are shown in Fig. 6.24. The output admittance of the SVC connected to Node 4A is sustained for a longer period of time than the other two SVCs due to the higher voltage deviations on feeders N4AB and N4AC which are supplied from node 4A.

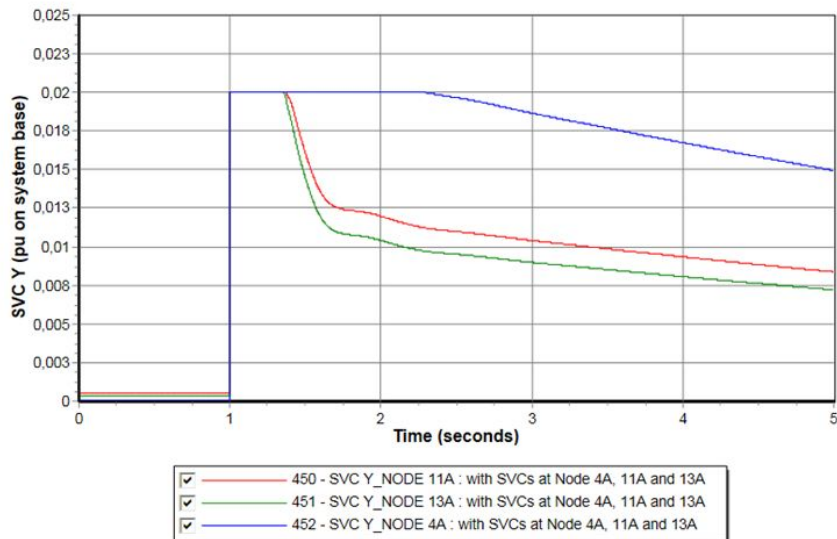


**Figure 6.24:** SVC output admittances (with SVCs at Nodes 4A, 11A and 13A).

### 6.1.8 SVCs placed at Node 4A, 5A, 11A and 13A

The voltage deviation was re-calculated with SVCs connected to Node 4A, 11A and 13A. The results are shown in Table 6.5. The highest deviation is on feeders N4AB and N4AC. However, an SVC is already connected to Node 4A. Increasing the rating of the SVC did not result in all the voltages at buses on feeders N4AB and N4AC to recover to 0.9 pu within 1 s. Therefore, an SVC was connected to the bus that supplies the feeders with the second highest voltage deviation that is Node 5A. The voltages at all the buses in the network recovered above 0.9 pu within 1 s with these four SVCs connected.

**Table 6.5:** Voltage Deviation on the various LV feeders

Feeder Name	Voltage Deviation
N4AB	0.07472
N4AC	0.07472
N5AB	0.06836
N5AC	0.0697
N7AB	0.06202
N7AC	0.06202
N8AB	0.06908
N8AC	0.06908
N10AB	0.05764
N10AC	0.05764
N11AB	0.05647
N11AC	0.05911
N13AB	0.04721
N13AC	0.04721

The output admittances of the SVCs are shown in Fig. 6.25. The output of the SVC connected to Node 4A takes longer than the rest to decrease because feeder N4AB and N4AC (fed by Node 4A) have the highest voltage deviation and thus require higher reactive power support.

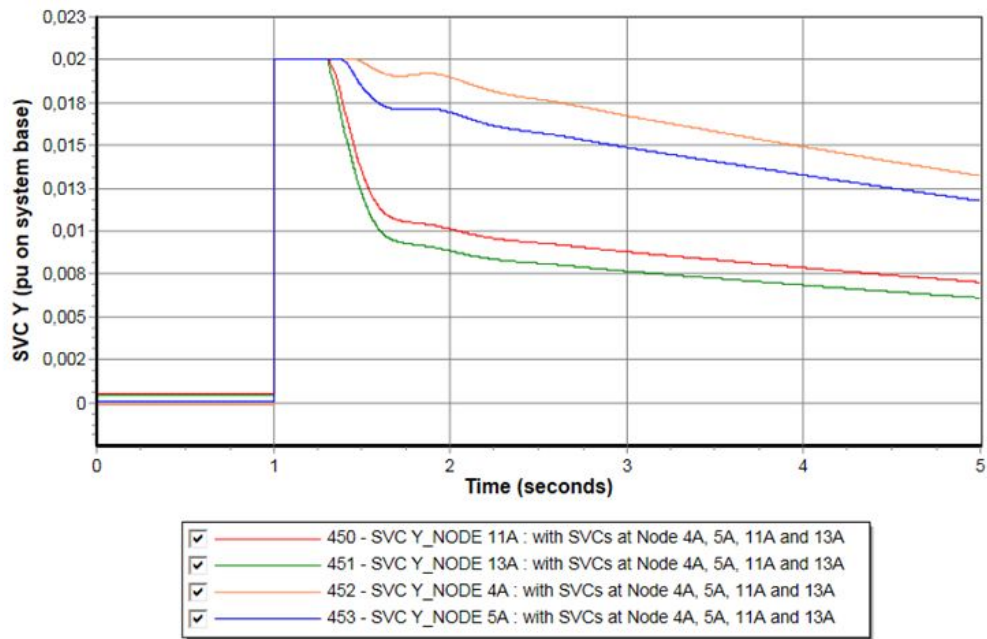


**Figure 6.25:** SVC output admittance (with SVCs at Nodes 4A, 5A, 11A and 13A).

Table 6.7 shows the final locations of the SVCs. The higher rated SVCs are at the beginning of the feeders, which is for one of the cases studied, while the lower rated SVCs are located at the ends of the feeders for the other case. One SVC was connected in the middle of feeder N13AC at bus N13AC5 for one of the cases studied and its rating is midway between the other two (the ones located at the beginning and at the end of the feeders).

**Table 6.6:** Location of SVCs for the various scenarios

Location	Size		
	-0.1/0.3 Mvar	-0.125/0.5 Mvar	-0.25/1 Mvar
Node 13A			X
Node 11A			X
Node 5A			X
Node 4A			X
N13AC5		X	
Node 13C	X		
Node 13B	X		
Node 11C	X		
Node 11B	X		
Node 10C	X		
Node 10B	X		
Node 8C	X		
Node 8B	X		
Node 7C	X		
Node 7B	X		
Node 5C	X		
Node 5B	X		
Node 4C	X		
Node 4B	X		

Using the higher rated SVCs (-0.25/1 Mvar) entails having a total of 4 SVCs connected at the beginning of the LV feeders whilst using the smaller SVCs with a rating of -0.1/0.3 Mvar would require a total of 14. This gives a total of 4 Mvar and 4.2 Mvar for the larger and smaller SVCs respectively. A decision would have to be made to either get a smaller number of the higher rated SVCs or a larger number of the lower rated SVCs. The investment cost would also have to be compared. However, a cost benefit analysis was not done as it is outside the scope of this project. In this case, using 4 SVCs is preferred since the number to be installed is smaller, which may also result in lower maintenance costs.

# 7

## Improvement of voltage stability by combining load interruption with using SVCs

**I**N this chapter, the improvement of voltage stability by a combination of load interruption and using SVCs is investigated. Load interruption alone resulted in a reduction in the number of buses with voltage below 0.9 pu 1 s after a fault on one of the lines between Node 1 and 2. However, not all the voltages recovered to 0.9 pu within the stipulated time even for the case where 80% of the non-motor load is interrupted. This can be seen in Fig. 5.18 where voltages on a total of 108 buses in the network are still below 0.9 pu 1 s after the disturbance for the case where 80% of the load is interrupted. Moreover, reconnecting a large amount of non-motor load also has to be done in steps so as not to introduce transients in the system. The use of SVCs resulted in the voltages at all buses recovering within 1 s thus meeting the criterion. However, the foregoing solution of using SVCs might be an expensive option due to the large number of FACTS devices (SVCs) that are required. A combination of load interruption and the use of SVCs was thus investigated to see the effect on the voltage recovery and to utilize the positive aspects of each solution.

### 7.1 Simulations Results

The case that was used is where 40% of non-motor load is interrupted and only 3% of the motor load is shed. The non-motor load is tripped then reconnected but the motor load is merely disconnected and not reconnected. Initially, the simulation was done without SVCs. The results are shown in Fig. 7.1. From the figure the number of buses with voltage below 0.9 pu 1 s after the fault is applied reduced from 268 without load interruption to 96 when load is interrupted. This is a significant improvement. However,

the number of buses with voltage below 0.9 pu is still high.

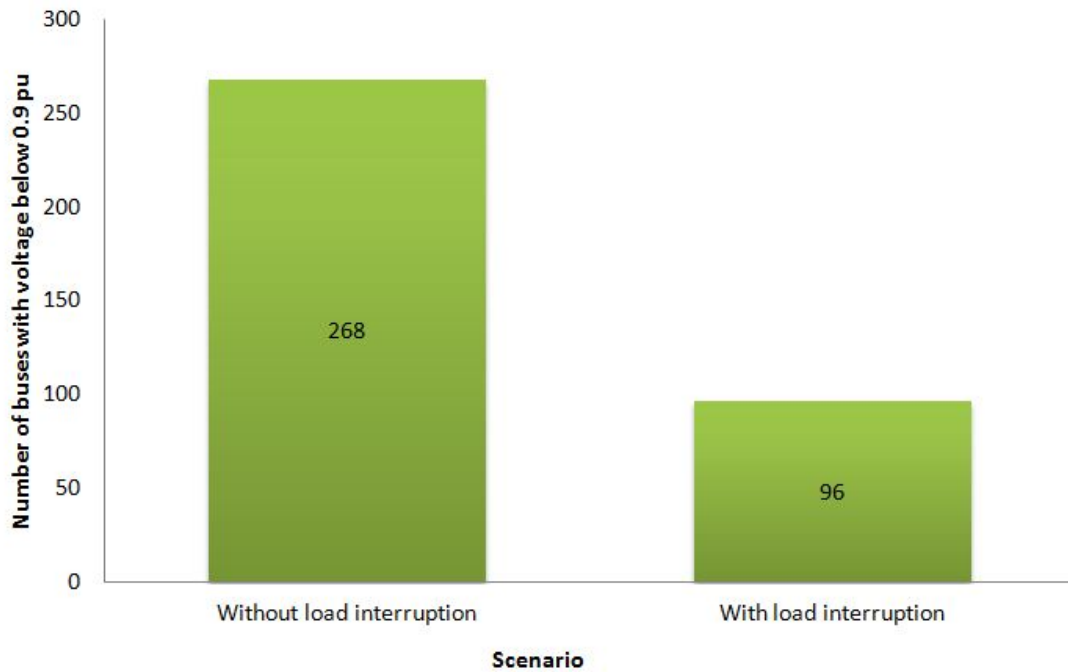


**Figure 7.1:** Comparison between the number of buses with voltage below 0.9 pu 1 s after initiation of a fault with and without load interruption

The voltage deviation index was checked again by running the voltage scan using python during the dynamic simulation with load interruption of 40% non-motor load and 3% motor load. The results are shown in Table 7.1.

**Table 7.1:** Voltage Deviation on the various LV feeders with SVCs connected to Node 11A and 13A

<b>Feeder Name</b>	<b>Voltage Deviation</b>
N4AB	0.1027
N4AC	0.1027
N5AB	0.08817
N5AC	0.1008
N7AB	0.05527
N7AC	0.05014
N8AB	0.06225
N8AC	0.05208
N10AB	0.06112
N10AC	0.07217
N11AB	0.05719
N11AC	0.05959
N13AB	0.05081
N13AC	0.05875

The results shown in Table 7.1 indicate that the feeders with the highest voltage deviation are feeder N4AB and N4AC that are fed from Node 4A followed by feeder N5AB and N5AC that are supplied from Node 5A. Thus, SVCs were connected to Node 4A and Node 5A and the dynamic simulation was run again. The rating of each one of the two SVCs is -0.25/1 Mvar. This time all the bus voltages recovered above 0.9 pu within 1 second as shown in Fig. 7.2.

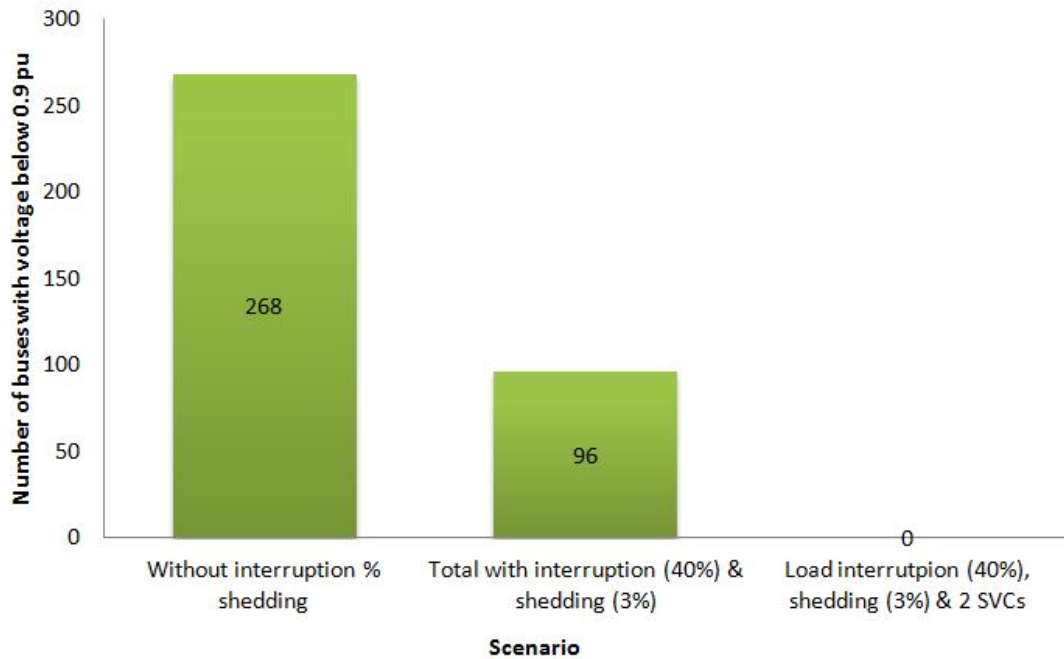


**Figure 7.2:** Number of buses with voltage below 0.9 pu 1 s after initiation of a fault without load interruption, with load interruption and a combination of load interruption and using 2 SVCs.

From the results, it can be deduced that combining load interruption with the use of SVCs results in a reduction of the amount of load that has to be interrupted. In this case, load interruption of more than 40% of the non-motor load and load shedding of more than 3% of the motor load can be avoided. Load interruption can also be done in combination with the use of SVCs without any load shedding at all. Moreover, the number of SVCs required to ensure that all the bus voltages recover within 1 s has been reduced from 4 to 2. This entails a significant saving on the investment capital required since the number of FACTS devices reduces by half. The basic idea that has been observed is that the more the load that is interrupted the less the number of SVCs that are required and vice versa. The proportion of load to be interrupted and the number of SVCs to install can be decided depending on the prevailing situation and the preferred options.

# 8

## Improvement of voltage stability by load shedding using the PSS/E Undervoltage Load Shedding Model Relay

**I**N this chapter the use of an under-voltage load shedding relay is investigated. Load shedding involves only disconnection of loads. The load is not reconnected. In PSS/E load shedding was done using the LVSH under-voltage load shedding relay model. Python was used to automate the dynamic simulations for each case that was studied.

### 8.1 Simulation results

The relay model that was used has three stages for load shedding. In this case, only the first stage was used. In addition, the fraction of load to shed can also be specified. The under-voltage load shedding relay trips both motor and non-motor loads. The voltage at which load shedding commences is also specified as well as the pickup time. The voltage that was specified for the commencement of load shedding is 0.8 pu. The pickup time that was used is 220 ms. The pickup timer at a bus is first started when the voltage is below the threshold that is set for the commencement of load shedding. The pickup timer is reset after being started for a particular bus if voltage at that bus recovers above the threshold value within the set time. The load at a given bus is shed if the voltage remains below the specified threshold value for a time that is longer than the pickup time. This is done automatically by the relay model until the fraction of load specified is shed. Dynamic simulations were done for various scenarios with different proportions of load shed for each case. The case where 42% of the load was shed resulted in voltages at

all buses recovering above 0.9 pu within 1 s after the initiation of the disturbance. This is shown in Fig. 8.1. The voltage evolution at bus 13 C, which is the furthest bus from the source of supply, for the cases where 20%, 30% and 42% of the load is shed is shown in Fig. 8.2. As can be clearly seen in the figure, the voltages recover above 0.9 pu within 1 s after the disturbance for the case where 42% of the load is shed.

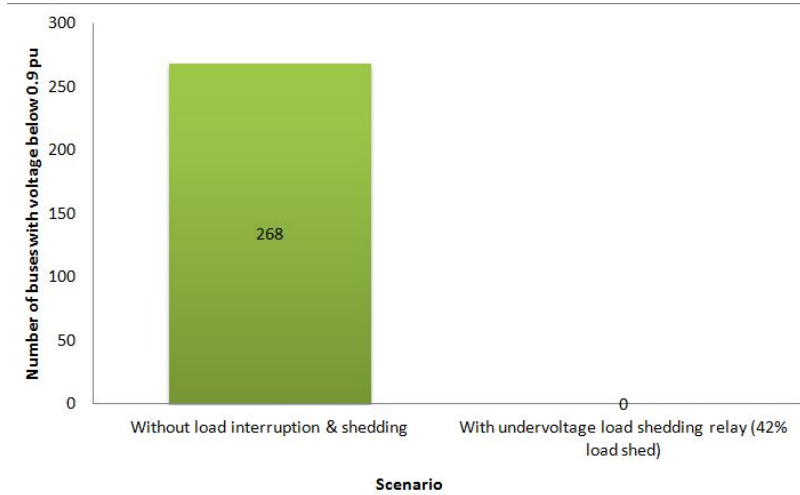


**Figure 8.1:** Number of buses with voltage below 0.9 pu 1 s after initiation of a fault without load interruption and shedding and using the under-voltage relay (with 42% of the load being shed)

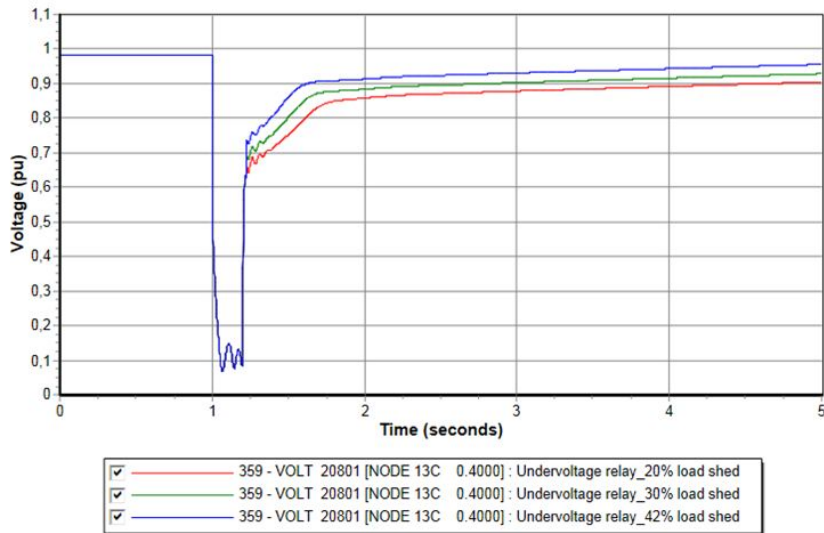


**Figure 8.2:** Evolution of voltage at Node 13C for the cases where 20%, 30% and 42% of the load is shed in the network

Simulations were also done with different pick times. It was observed that as the pickup time, which is essentially the delay time to shedding of the load at a bus, is increased the recovery of the voltage is slower as can be seen in Fig.8.3. This means that the amount of load that should be shed increases as the pickup time is increased to achieve the same result in terms of voltage recovery as the case with a lower pickup time.

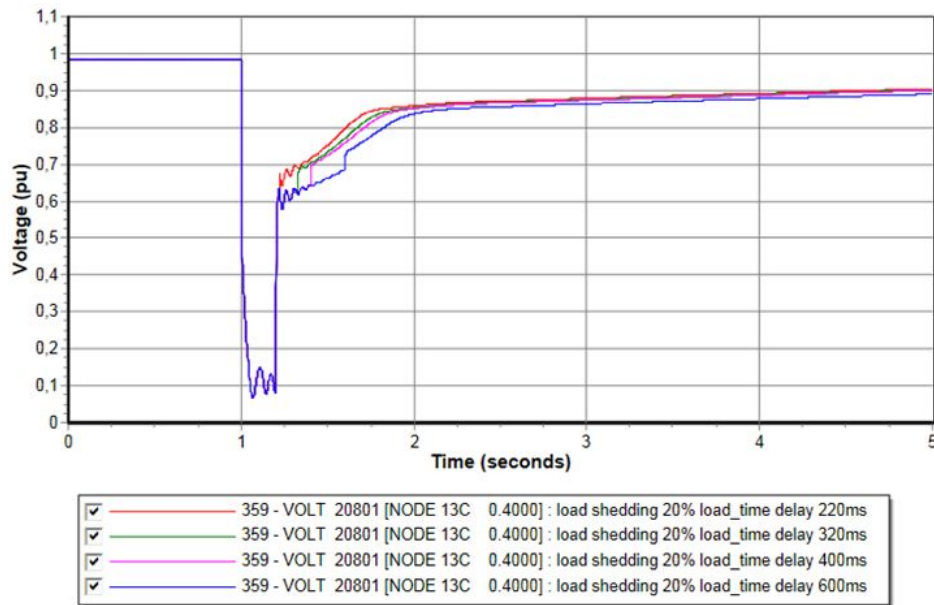


**Figure 8.3:** Comparison of voltage recovery for various pickup times (220ms, 320ms, 400ms and 600ms)

The use of an undervoltage relay resulted in all the bus voltages recovering with load shedding of only 42% of the load. However, the load is not reconnected so this results in losing a big part of the load. The power company would have to compensate the consumers that are off supply. Moreover, consumers would be inconvenienced and some of them would also incur losses.

The final results of all the simulations performed are shown in Fig. 8.4. The figure illustrates that a combination of load interruption and using SVCs gives the best results from the investigations that have been carried out.

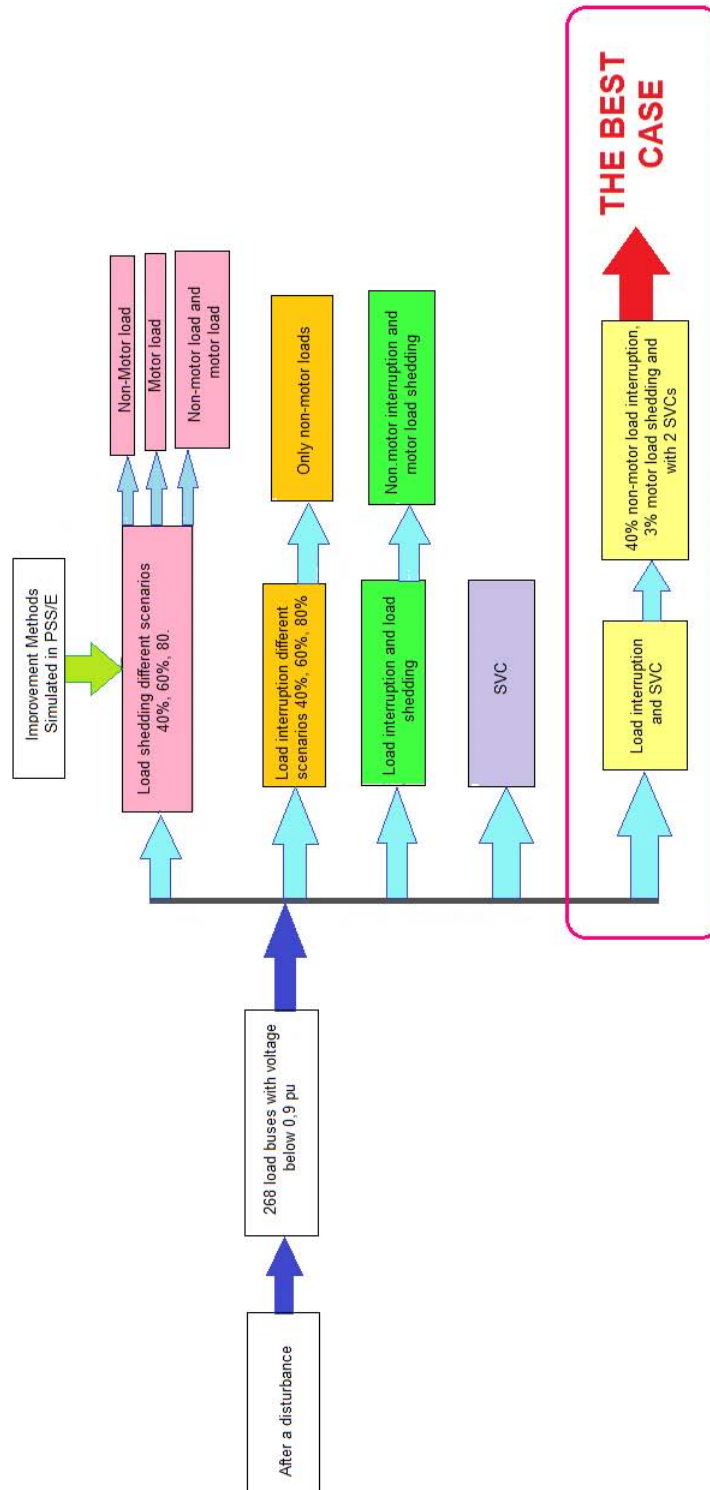


Figure 8.4: Final results of the voltage stability improvement investigations.

# 9

## Conclusions and Future Work

### 9.1 Conclusions

THE presence of low inertia induction motors in a distribution network may lead to voltage instability after a severe disturbance. Therefore, measures have to be implemented to reduce the possibility of voltage collapse and to meet the grid requirements. Studies have to be undertaken to assess the vulnerability of a system to voltage instability. Different methods can be implemented to help the voltage to recover faster following a disturbance. Some of the methods that can be used are load shedding, load interruption, undervoltage relay load shedding and using FACTS devices such as SVCs. A combination of some of these methods can lead to better results.

During this thesis different methods were investigated and implemented on a test network to see their effects regarding the improvement of voltage stability. The results show that the number of load buses with voltages that recovered to 0.9 pu in 1 second are almost the same for load shedding and load interruption of non-motors loads. However, the load is disconnected for load shedding unlike the case for interruption where all the loads are reconnected back to the system after a few seconds. For instance, the amount of load saved for the case where 60% of the non-motor load is interrupted is 84. Load interruption is therefore a good solution but the fraction of load interrupted can be high. It was observed that reconnection of motors is not practical because it introduces a severe disturbance in the system. This could be because of the small inertia constant of the motors which makes them liable to stall within a short time thereby drawing a lot of current and depressing the voltage further if reconnection is attempted.

It was seen that combining load interruption of non-motor loads with load shedding of motors resulted in voltage at more load buses recovering to 0.9 pu within 1 sec. Load shedding therefore aids the voltage recovery but it may be expensive and inconvenient because the loads are not reconnected back. It was observed that SVCs offer fast support

for voltage recovery and all voltages recover above 0.9 pu within 1 second but several devices are required. This might entail huge capital injection. By combining load interruption with the use of SVCs the amount of load interrupted is reduced and the number of SVCs required is also reduced. This leads to a better overall scheme. Therefore, a combination of load interruption and using SVCs is the best solution. The two methods complement each other. Fewer loads are interrupted and the number of SVCs installed to improve the recovery of the voltage can be reduced thereby lowering the investment cost.

## 9.2 Future Work

The following future works are proposed for this project:

- A cost benefit analysis of either using SVCs or load interruption so as to compare the costs of the two methods.
- Further automation of the algorithm for load interruption in Python.
- Performing the simulations using a different software such as DIGSILENT Powerfactory so as to compare the results.
- Investigating the use of different types of FACTS devices such as STATCOM for aiding the voltage recovery.
- Performing simulations on a large transmission system supplying distribution networks with large amounts of motor loads.

# References

- [1] Siemens Industry Inc. *Program Operation Manual*. Siemens Power Technologies International, October 2013.
- [2] T. Van Cutsem, C. Moors, and D. Lefebvre. Design of load shedding schemes against voltage instability using combinatorial optimization. *Power Engineering Society Winter Meeting, IEEE*, 2:848–853, 2002.
- [3] Lecture no. 9 in Power System Operation. *Voltage Stability (part 1)*. Chalmers University of Technology, Gothenburg, 2013.
- [4] NERC Transmission Issues Subcommittee Subcommittee, System Protection, and Control. A technical reference paper fault - induced delayed voltage recovery, May 2014.
- [5] B. Otomega and T. Van Cutsem. Distributed load interruption and shedding against voltage delayed recovery or instability. *PowerTech (POWERTECH), IEEE*, pages 1–6, 2013.
- [6] B. Otomega and T. Van Cutsem. Undervoltage load shedding using distributed controllers. *IEEE Transactions on Power Systems*, 22(4):1898–1907, 2007.
- [7] C.W. Taylor. *Power system voltage stability*. McGraw-Hill Ryerson, Limited, 1994.
- [8] T. Van Cutsem and C. Vournas. *Voltage Stability of Electric Power Systems*. Springer Science & Business Media, 1998.
- [9] C.W. Taylor. Concepts of undervoltage load shedding for voltage stability. *Power Engineering Society Winter Meeting, IEEE*, 7:480–488, 1992.
- [10] Jamal A. Yasin Ismail A. Hamzah. Static var compensators (svc) required to solve the problem of delayed voltage recovery following faults in the power system of the saudi electricity company, western region (sec-wr). Volume:4, 2003.

- [11] IEEE/CIGRE joint task force on stability terms and definitions. Definition and classification of power system stability. *IEEE Transactions on Power Systems*, 19(3):1387–1401, 2004.
- [12] T. Van Cutsem. Voltage instability: phenomena, countermeasures, and analysis methods. *IEEE Proceedings*, 88(2):208–227, 2000.
- [13] and E.H. Camm. V. Stewart. Modeling of stalled motor loads for power system short-term voltage stability analysis. , *IEEE Power Engineering Society General Meeting*, 2:1887–1892, 2005.
- [14] E.G. Potamianakis and C.D. Vournas. Short-term voltage instability: effects on synchronous and induction machines. *IEEE Transactions on Power Systems*, 21(2):791–798, 2006.
- [15] NARAIN G., HINGORANI, and LASZLO GYUGYI. *Understanding FACTS: concepts and technology of Flexible AC Transmission Systems*. Wiley-IEEE Press, 2000.
- [16] RAJ, P.V., and M. SUDHAKARAN. Optimum load shedding in power systems strategies with voltage stability indicators. *Engineering*, 2:12–21, 2010.
- [17] MARAM and . ET. Al. M, D. An optimal load cut policy with event-driven design against voltage stability using theta-particle swarm optimization. *Journal of Basic and Applied Scientific Research*, 3(3):91–100, 2013.
- [18] L. ZHIPENG, FUSHUAN, and LEDWICH G. W. An optimal under-frequency load shedding strategy considering distributed generators and load static characteristics. *International Transactions on Electrical Energy Systems*, 24(1):75–90, 2014.
- [19] P. WANG and BILLINTON R. Optimum load-shedding technique to reduce the total customer interruption cost in a distribution system. *IEE Proc-Genrr. Transm. Distrib.*, 147(1):51–57, 2002.
- [20] L.P. HAJDU, J. PESCHON, W.F. TINNEY, and D.S.: PIERCY. Optimum load-shedding policy for power systems. *International Transactions on Electrical Energy Systems* , *IEEE Trans*, 87(3):784–795, 1968.
- [21] ET.AL MOSTAFA, M.A. Optimal dynamic load shedding using a newton based dynamic algorithm. *Electric Power System Research*, 34(3):157–163, 1995.
- [22] D.K. SUBRAMANIAN. Optimum load shedding through programming techniques. *IEEE Trms*, 90(1):89–94, 1971.
- [23] CHAN and YIP E. S.M. A solution of the transmission limited dispatch problem by sparse linear programming. , *IEEE Trans*, 98:1044–1053, 1979.
- [24] D. DEVARAJ and J.P. ROSELYN. Genetic algorithm based reactive power dispatch for voltage stability improvement. *International Journal of Electrical Power and Energy Systems.*, 32(10):1151–1156, 2010.

- [25] EL ARINI MAHDI. Optimal dynamic load shedding policy for generation load imbalances including characteristics of loads. *International Journal of Energy Research*, 23(1):79–89, 1999.
- [26] MOMOH, ZHU. J.Z. J.A., and S.S. KADDAH. Optimal load shedding study of naval-ship power system using the everett optimization technique'. *Electric Power Systems Research*, 60(3):145–152, 2002.
- [27] VRAKOUPOULU and ANDERSSON G. M. An adaptive load shedding technique for controlled islanding. *To be publish*.
- [28] DING XU and GIRGIS A.A. Optimal load shedding strategy in power systems with distributed generation. *IEEE Power Engineering Society Winter Meeting*, 2:788–793, 2001.
- [29] KARIMI and ET. AL. M. Combination of adaptive and intelligent load shedding techniques for distribution network. *Power Engineering and Optimization Conference (PEDCO) Melaka, Malaysia, 2012 Ieee International*, pages 57–61, 2012.
- [30] A.G. BEVRANI, TIKDARI, and HIYAMA. A.G. Power system load shedding: Key issues and new perspectives. *World Academy Science, Engineering and Technology*, 4:161–166, 2010.
- [31] J. LIU, C.H. XIA, SHROFF, and H.D. N.B., SHERALI. *Distributed Optimal Load Shedding for Disaster Recovery in Smart Electric Power Grids: A second-Order Approach*.
- [32] O. ] ZIAEE and ET. AL. An optimal pricing policy for interruptible load contracts in power markets: A case study for iran. *Energy and Power*, 1(1):14–20, 2011.
- [33] Peter Crossley, Franc Ilar, and Daniel Karlsson. System protection schemes in power networks, 2001.
- [34] Bogdan Cutsem, Thiery Van; Otomega. Distributed load interruption and shedding against voltage delayed recovery or instability. 2013.
- [35] V. Sermanson T. Van Cutsem B. Otomega F. Capitanescu, H. Lefebvre. Prospects of an improved system protection scheme against voltage instability in the rte system. 2008.
- [36] Bogdan Otomega Thiery Van Cutsem. Local vs. wide-area undervoltage load shedding in the presence of induction motor loads, 2009.
- [37] Bogdan Otomega Thiery Van Cutsem. A load shedding scheme against both short- and long-term voltage instabilities in the presence of induction motors. 2011.
- [38] Robert A. Jones Lee Y. Taylor S. Mark Halpin, Keith Harley. Slope-permissive under-voltage load shed relay for delayed voltage recovery mitigation. 2008.

- [39] Venkataramana Ajjarapu Hua Bai. A novel online load shedding strategy fo mitigating fault-induced delayed voltage recovery. Volume:26 , Issue: 1, 2004.
- [40] R; Birsa J; RIggle M.; Takeda M; Teramoto H.; Kono Y.; Temma K; Yasuda S; Wofford K; Attaway P.; Lawson J. Sullivan, D; Pape. Managing fault-induced delayed voltage recorvery in metro atlanta with the burrow county svc. 2009.
- [41] D Vassilis, C.; Costas Vournas. Design strategies for load-shedding schemes against voltage collapse in the hellenic system. Volume:23 , Issue: 2, 2008.
- [42] P. Chen and B. Bak-Jensen. Z. Chen. Comparison of steady-state svc models in load flow calculations. *IEEE Universities Power Engineering Conference*, pages 1–5, 2008.
- [43] FACTS terms, DC definitions task force, FACTS working group, and FACTS sub-committee. Proposed terms and definitions for flexible ac transmission system (facts). *IEEE Transactions on Power Delivery*, 12(4):1848–1853, 1997.
- [44] H. Ambriz-Perez, E. Acha, and C.R. Fuerte-Esquivel. Advanced svc models for newton-raphson load flow and newton optimal power flow studies'. *IEEE Transactions on Power Systems*, 15(1):129–136, 2000.
- [45] R.J. Koessler. Dynamic simulation of static var compensators in distribution networks. *IEEE Transacctions on Power Systems*, 7(3):1285–1291, 1994.
- [46] J.L. MCAVOY. W.K. WONG, D.L. OSBORN. Application of compact static var compensator solves voltage-flactuation problem. *IEEE Transactions on Power Delivery*, 5(2):1113–1120, 1990.
- [47] Task Force No. 2 on SVC. CIGRE Working Group 38-01. Static var compensator. *IEEE Transacctions on Power Systems*, 9(1):229–240, 1994.
- [48] Task Force No. 2 on SVC. CIGRE Working Group 38-01. *Static Var Compensators*. I.A. Erinmez, 1986.
- [49] Stephen J Chapman. *Electric Machinery Fundamentals*.
- [50] Induction motor.
- [51] A Hughes published. *Electric Motors and Drives*.
- [52] Siemens Power Technologies International. *Program application guide Volume 2*.
- [53] Siemens Power Technologies International. *MODEL LIBRARY*.
- [54] Wikipedia, “python (programming language).
- [55] Siemens Power Technologies International. *Program Application Guide Volume 1*.

- [56] L. MUSIRIN and T.K.A RAHMAN. On-line voltage stability based contingency ranking using fast voltage stability index (fvsi). *Transmission and Distribution Conference and Exhibition, 2002*, 2:1118–1123, 2002.
- [57] P. KESSEL and H. GLAVITSCH. Estimating the voltage stability of a power system. *IEEE Transactions on Power Delivery*, 1(3):346–354, 1986.
- [58] M.H. HAQUE. Use of local information to determine the distance to voltage collapse. *Power Engineering Conference*, pages 408–413, 2007.
- [59] M. MOGHAVVEMI. Technique for contingency monitoring and voltage collapse prediction. *Generation, Transmission and Distribution IEE Proceedings*, 145(6):634–640, 1998.
- [60] A. MOHAMED, G.B. JASMON, and S. YUSOFF. A static voltage collapse indicator using line stability factors. *Journal of Industrial Technology*, 7(1):73–85, 1989.
- [61] M. Moghavvemi and O. Faruque. Real-time contingency evaluation and ranking technique. *Generation, Transmission and Distribution IEE Proceedings*, 145(5):517–524, 1998.
- [62] C. REIS and F.C. MACIEL BARBOSA. A comparison of voltage stability indices'. *Electrotechnical Conference*, 21:1007–1010, 2006.

# A

## Distribution Network

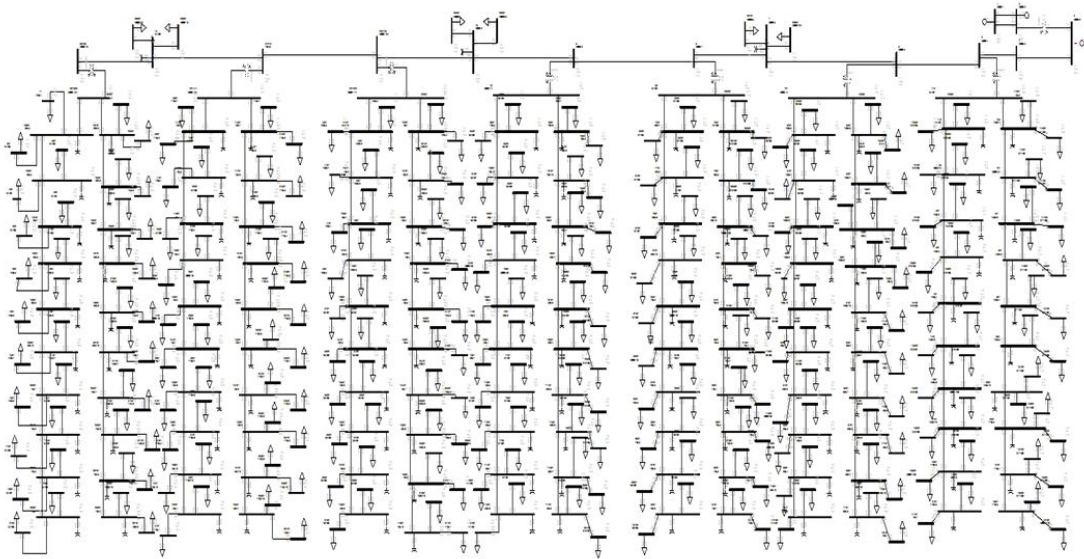


Figure A.1

# B

## Python Scripts

### Python script for dynamic simulations without load interruption or SVCs

```
import os,sys PYTHONPATH = r'C:\Program Files (x86)\PTI\PSSE33 \PSSBIN'
MODELFOLDER = r'C:\Program Files (x86)\PTI\PSSE33\MODELDRW'
sys.path.append(PYTHONPATH)
os.environ['PATH'] += ';' + PYTHONPATH
import psspy
import redirect
#import pssepath
#pssepath.add_pssepath()
#import psspy
# Redirect output from PSSE to Python:
redirect.psse2py()
# Last case:
CASE = r"D:\Base case_without load interruption or SVCs\50% load.sav"
psspy.psseinit(12000)
psspy.case(CASE)
# Convert loads (3 step process):
psspy.conl(-1,1,1)
psspy.conl(-1,1,2,[0,0],[100,0,0,100])
psspy.conl(-1,1,3)
# Convert generators:
psspy.cong()
# Solve for dynamics
psspy.ordr()
psspy.fact()
psspy.tysl()
```

```

# Save converted case
case_root = os.path.splitext(CASE)[0]
psspy.save(case_root + "_C.sav")
# Add dynamics data
psspy.dyre_new(dyrefile="D:\Base case_without load interruption or SVCs\Model pa-
rameters without interruption or SVCs.dyr")
# Add channels by subsystem
# BUS VOLTAGE
psspy.chsb(sid=0,all=1, status=[-1,-1,-1,1,13,0])
# MACHINE SPEED
psspy.chsb(sid=0,all=1, status=[-1,-1,-1,1,7,0])
# Add channels individually
# BRANCH MVA
psspy.branch_mva_channel([-1,-1,-1,1,2], '1')
#set the calculation parameters of dynamic simulation
idef,rdef =psspy.getbatdefaults()
psspy.dynamics_solution_param_2([idef,idef,idef,idef,idef,idef,idef,idef],
[rdef,0.0001,0.0018,rdef,rdef,rdef,rdef,rdef])
# Save snapshot
psspy.snap(sfile="D:\Base case_without load interruption or SVCs\without interruption
or SVCs.snp")
# Initialize psspy.strt(0,outfile="D:\Base case_without load interruption or SVCs\without
interruption or SVCs.out")
# Run to 1 second
psspy.run(0,1.0,1000,1,0)
# 3-phase fault on branch between node 1 and node 2
psspy.dist_branch_fault(ibus=1, jbus=2, id='1')
# Run to 1.2 seconds
psspy.run(0,1.2,1000,1,0)
# Clear fault
psspy.dist_clear_fault(1)
psspy.dist_branch_trip(ibus=1, jbus=2, id='1')
# Check the bus voltages that are higher than 1.1 p.u and lower than 0.8 p.u
psspy.set_vltsn(1,1.1,0.8)
# Run to 5 seconds psspy.run(0,5,1000,1,0)
# Halt psspy.pssehalt_2()

```

## Python script for load interruption dynamic simulations

```
import os,sys
PYTHONPATH = r'C:\Program Files (x86)\PTI\PSSE33\PSSBIN'
MODELFOLDER = r'C:\Program Files (x86)\PTI\PSSE33\MODELDRW'
sys.path.append(PYTHONPATH)
os.environ['PATH'] += ';' + PYTHONPATH
import psspy
import redirect
#import pssepath
#pssepath.add_pssepath()
# Redirect output from PSSE to Python:
redirect.psse2py()
# Last case:
CASE = r"D:\Load interruption\50% load.sav"
psspy.psseinit(12000)
psspy.case(CASE)
# Convert loads (3 step process):
psspy.conl(-1,1,1)
psspy.conl(-1,1,2,[0,0],[100,0,0,100])
psspy.conl(-1,1,3)
# Convert generators: psspy.cong()
# Solve for dynamics psspy.ordr()
psspy.fact()
psspy.tysl()
# Save converted case
case_root = os.path.splitext(CASE)[0]
psspy.save(case_root + "_C.sav")
# Add dynamics data
psspy.dyre_new(dyrefile="D:\Load interruption\Model parameters.dyr")
# Add channels by subsystem
# BUS VOLTAGE psspy.chsb(sid=0,all=1, status=[-1,-1,-1,1,13,0])
# MACHINE SPEED
psspy.chsb(sid=0,all=1, status=[-1,-1,-1,1,7,0])
# Add channels individually
# BRANCH MVA
psspy.branch_mva_channel([-1,-1,-1,1,2], '1')
#set the calculation parameters of dynamic simulation
idef,rdef =psspy.getbatdefaults()
psspy.dynamics_solution_params([idef,idef,idef,idef,idef,idef,idef,idef],
[rdef,0.0001,0.0018,rdef,rdef,rdef,rdef,rdef], "")
# Save snapshot
psspy.snap(sfile="D:\Load interruption\load interruption_60% non-motor load.snp")
```

```

# Initialize
psspy.strt(0,outfile="D:\Load interruption\load interruption_60% non-motor load.out")
# Run to 1 second
psspy.run(0,1.0,1000,1,0)
# 3-phase fault on branch between node 1 and node 2
psspy.dist_branch_fault(ibus=1, jbus=2, id='1')
# Run to 1.2 seconds
psspy.run(0,1.2,1000,1,0)
# Clear fault
psspy.dist_clear_fault(1)
psspy.dist_branch_trip(ibus=1, jbus=2, id='1')
# Check voltages
psspy.set_vltscn(1,1.1,0.9)
# Save output to a file
sys.stdout = open('output 60% non-motor load interruption.txt', 'w')
##Interrupt loads
#Trip loads

psspy.dist_branch_trip(ibus=20801, jbus=2002,id='1')
psspy.dist_branch_trip(ibus=20901, jbus=28001,id='1')
#Reconnect loads after a certain period of time
psspy.run(0,2,1000,1,0)
psspy.bus_data_3(2002, [1,1,1,1], [rdef,rdef,rdef,rdef,rdef,rdef,rdef], '13CL10')
psspy.bus_data_3(28001, [1,1,1,1], [rdef,rdef,rdef,rdef,rdef,rdef,rdef], '13BL10')
psspy.dynamicsmode(0)
psspy.dist_branch_close(ibus=20801, jbus=2002,id='1')
psspy.dist_branch_close(ibus=20901, jbus=28001,id='1')
#Run to 5 seconds
psspy.run(0,5,1000,1,0)
# Halt psspy.psschalt_2()

```

## Python script for dynamic simulations with SVCs connected

```
import os,sys
PYTHONPATH = r'C:\Program Files (x86)\PTI\PSSE33\PSSBIN'
MODELFOLDER = r'C:\Program Files (x86)\PTI\PSSE33\MODELDRW'
sys.path.append(PYTHONPATH)
os.environ['PATH'] += ';' + PYTHONPATH
import psspy
import redirect
# Redirect output from PSSE to Python:
redirect.psse2py()
# Last case:
CASE = r"D:\SVC\SVC Node 13C\50% load with switched shunt SVC.sav"
psspy.psseinit(12000)
psspy.case(CASE)
# Convert loads (3 step process):
psspy.conl(-1,1,1)
psspy.conl(-1,1,2,[0,0],[100,0,0,100])
psspy.conl(-1,1,3)
# Convert generators:
psspy.cong()
# Solve for dynamics
psspy.ordr()
psspy.fact()
psspy.tysl()
# Save converted case
case_root = os.path.splitext(CASE)[0]
psspy.save(case_root + "_C.sav")
# Add dynamics data
psspy.dyre_new(dyrefile="D:\SVC\SVC Node 13C\Model parameters with switched shunt
SVC.dyr")
#Clear all channels
psspy.delete_all_plot_channels()
# Add channels by subsystem
# BUS VOLTAGE psspy.chsb(sid=0,all=1, status=[-1,-1,-1,1,13,0])
# MACHINE SPEED psspy.chsb(sid=0,all=1, status=[-1,-1,-1,1,7,0])
# Plot admittance output of the switched shunt (SVC)
psspy.var_channel([-1, 1576], 'SVC Y_Node 13C')
# Add channels individually # BRANCH MVA psspy.branch_mva_channel([-1,-1,-1,1,2], '1')
#set the calculation parameters of dynamic simulation
idef,rdef =psspy.getbatdefaults()
psspy.dynamics_solution_param_2([idef,idef,idef,idef,idef,idef,idef,idef],
[rdef,0.0001,0.0018,rdef,rdef,rdef,rdef,rdef])
```

```

# Save snapshot
psspy.snap(sfile="D:\SVC\SVC Node 13C\with SVC at Node 13C.snp")
# Initialize
psspy.strt(0,outfile="D:\SVC\SVC Node 13C\with SVC at Node 13C.out")
# Run to 1 second
psspy.run(0,1.0,1000,1,0)
# 3-phase fault on branch between node 1 and node 2 (default bus fault is a 3phase)
psspy.dist_branch_fault(ibus=1, jbus=2, id='1')
# Run to 1.2 seconds
psspy.run(0,1.2,1000,1,0)
# Clear fault
psspy.dist_clear_fault(1)
psspy.dist_branch_trip(ibus=1, jbus=2, id='1')
#Run to 5 seconds
psspy.run(0,5,1000,1,0)
# Halt
psspy.pssehalt_2()

```

### **Python script for load shedding using LVSH undervoltage relay**

```

import os,sys
PYTHONPATH = r'C:\Program Files (x86)\PTI\PSSE33\PSSBIN'
MODELFOLDER = r'C:\Program Files (x86)\PTI\PSSE33\MODELDRW'
sys.path.append(PYTHONPATH)
os.environ['PATH'] += ';' + PYTHONPATH
import psspy
import redirect
# Redirect output from PSSE to Python:
redirect.psse2py()
# Last case:
CASE = r"D:\Load shedding using LVSH model\load shedding 20%\50% load.sav"
psspy.psseinit(12000)
psspy.case(CASE)
# Convert loads (3 step process):
psspy.conl(-1,1,1)
psspy.conl(-1,1,2,[0,0],[100,0,0,100])
psspy.conl(-1,1,3)
# Convert generators:
psspy.cong()
# Solve for dynamics
psspy.ordr()
psspy.fact()
psspy.tysl()

```

```

# Save converted case
case_root = os.path.splitext(CASE)[0]
psspy.save(case_root + "_C.sav")
# Add dynamics data
psspy.dyre_new(dyrefile="D:\Load shedding using LVSH model\load shedding 20%\model
parameters with LVSH.dyr")
# Add channels by subsystem
# BUS VOLTAGE
psspy.chsb(sid=0,all=1, status=[-1,-1,-1,1,13,0])
# MACHINE SPEED
psspy.chsb(sid=0,all=1, status=[-1,-1,-1,1,7,0])
# Add channels individually
# BRANCH MVA psspy.branch_mva_channel([-1,-1,-1,1,2], '1')
#set the calculation parameters of dynamical simulation
idef,rdef =psspy.getbatdefaults()
psspy.dynamics_solution_params([25,idef,idef,idef,idef,idef,idef,idef],
[1,rdef,0.0018,rdef,rdef,rdef,rdef,rdef], "")
# Save snapshot
psspy.snap(sfile="D:\Load shedding using LVSH model\load shedding 20%\load shed-
ding using LVSH model_20# Initialize psspy.strt(0,outfile="D:\Load shedding using
LVSH\load shedding 20%\load shedding using LVSH model_20% loadout") #psspy.run(tpause=0)
# Run to 1 second (s)
psspy.run(0,1.0,1000,1,0)
# 3-phase fault on branch between node 1 and node 2 (default bus fault is a 3phase)
psspy.dist_branch_fault(ibus=1, jbus=2, id='1')
# Run to 1.2 seconds
psspy.run(0,1.2,1000,1,0)
# Clear fault
psspy.dist_clear_fault(1) psspy.dist_branch_trip(ibus=1, jbus=2, id='1')
#Run to 5 seconds
psspy.run(0,5,1000,1,0)
# Halt psspy.pssehalt_2()

```